Spring 5-16-2014

Estimation of Sediment Resuspension and Deposition in Coastal Waters

John E. Filostrat
Environmental Engineering Department, jfilostr@gmail.com

Estimation of Sediment Resuspension and Deposition in Coastal Waters

A Thesis

Submitted to the Graduate Faculty of the
University of New Orleans
in partial fulfilment of the
requirements for the degree of

Master of Science
in
Civil and Environmental Engineering

by

John Edgar Dimitri Filostrat

B.E., Louisiana State University, 2012

May 2014

Dedication

To

My Grandparents

And

St. Joseph of Cupertino

Acknowledgements

The affable patience of Dr. Alex McCorquodale inspires me daily to be an unabashed thinker, and I couldn't be more thankful to this Gulf Coast legend for offering me the opportunity to understand how all meandering ways are ultimately summarized into

$$Q = AV.$$

Dr. LaMotta and Dr. Kura of the University of New Orleans sufficiently introduced and trained me in the fields of water and air engineering, respectively, giving me the confidence to know I can perform any task involving these elements.

My graduate school colleagues, peers, and dear friends ceaselessly invoke my sense of competition, yet always remind me of my stupidity, and will never know how much they influence me to be a better learner.

The research was funded in part by National Science Foundation (NSF) and the Board of Regents of Louisiana as part of the Northern Gulf Coastal Hazards Collaboratory (NG-CHC; http:\\ngchc.org). Additional support was provided by the Louisiana Coastal Protection and Restoration Authority (CPRA, www.coastal.la.gov).

Lastly, as I type this in the dead of night, spring of 2014, I can't ignore the urge to honor the men and women that dedicated their careers to the protection and preservation of my favorite place on earth, though they may seem to be whitewashed as nothing more than a reference in a list at the end of this document.

Table of Contents

List of Tables

List of Figures

Abstract

The Louisiana Gulf Coast is a dynamic system of heavy influence on the cultures that live and prosper around it. Land in this area is in jeopardy of being lost. In 2017, the Coastal Protection and Restoration agency will issue a new State Master and this thesis provides a more intricate way of numerically predicting the behaviors of associated sediments. A model for the estimation of resuspension and deposition is proposed and prepared for integration into the existing model. The silt and clay fractions of the bed sediment and the sediment inflow were modeled by the widely used hydrodynamic models of Delft3D and ECOMSED, using the Young and Verhagen wave properties to obtain orbital velocities and bed shear stress. The critical shear stress for erosion was based on empirical formulas developed by van Rijn.

Keywords: Sediment Distribution. Coastal Restoration, Sediment Diversions, Wave Characteristics, Sediment Transport,

Chapter 1: Introduction

1.1: General Background and Problem Statement

Understanding the behavior of bodies of water like rivers and lakes has been a task common to all humanity since the beginning of civilization, from the Tigris and Euphrates of Mesopotamia, to the Nile of Egypt. Not only did hydrodynamics provide a calendar to model life around, but also imbued human beings with the power to control a permanent residency. Louisiana, the foot of the Gulf Coast and major hub of maritime trade, owes a great deal of her stability to a fundamental awareness of how Lake Pontchartrain, the Mississippi River, and surrounding tributaries behave in regards to the sediment each has control over. On May 22nd, 2012, the Louisiana legislature unanimously approved the 2012 Coastal State Master Plan, adopting it as the blueprint for all coast protection and restoration efforts. Aimed at addressing the most critical problem, coastal erosion, the plan highlighted the 1,880 square miles of land lost in the last 80 years and the 1,750 at risk of being lost in the next 50 years. A large portion of the plan was dedicated to the eco-hydrology mass-balance compartment model, developed by knowledgeable scientists and engineers in the Coastal Protection and Restoration Authority (CPRA, www.coastal.la.gov), which attempted to explain the behavior of various properties of divided subsections, or cells, of the Louisiana coastal region as shown in Figure 1.1.

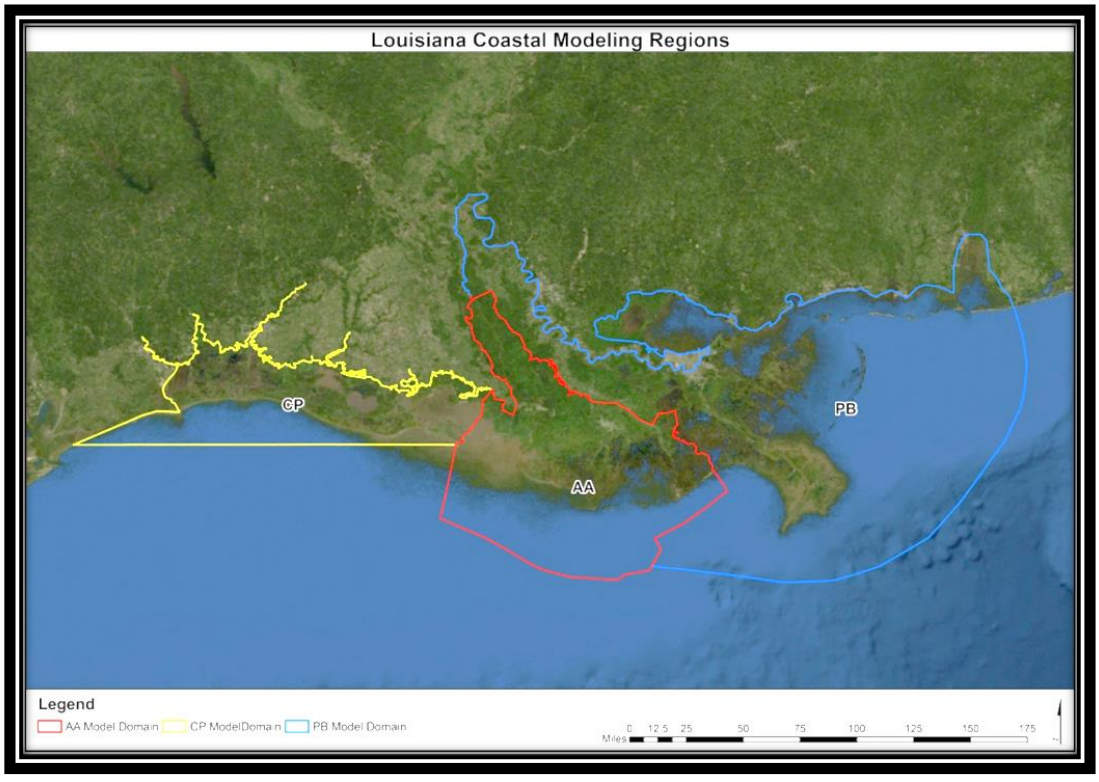

Figure 1. 1. The areas of focus for the 2012 Louisiana State Master Plan

The goal of numerical modeling was to evaluate the performance of potential protection and restoration projects on the coast for the next 50 years, considering factors of each cell, ranging from morphology and vegetation, to water quality and sediment behavior.

The purpose of this study is to compliment the sediment distribution facet of the 2012 Coastal Master Plan (CPRA, Appendix D) and to refine the sediment processes for implementation into the new version of the sediment distribution model in the 2017 Louisiana State Coastal Master Plan.

1.2: Research Objectives

In order to highlight methods used to build the 2012 model, a closer look will be taken into the history of the literature involving sedimentary engineering and sciences, from the early 1900s to the present day. An understanding of the modeling mechanisms will then help build a procedure for better understanding and quantifying the processes describing sedimentary behavior within each cell. The major objectives are:

1. To conduct a literary review, surveying articles offering insight into sedimentary processes,
2. To describe a more physically based method of quantifying the behaviors of four species of sediment (sand, silt, flocculated clay and particulate clay) as regards deposition, resuspension, and flux.
3. To develop a model based on these behaviors,
4. To compare output data of test cells and analyze the reaction of sediments within a water column,
5. To offer suggestions for future studies and refinement of the 2017 State Master Plan.

1.3: Thesis Outline

The following describes the basic structure of the thesis.

Chapter 1 gives a brief introduction, the problem statement, and research objectives.

Chapter 2 provides a literature survey of relevant articles dealing with cohesive and non-cohesive sediment behavior and mechanisms.

Chapter 3 gives the methodology used to formulate model mechanics involving sediment deposition, flocculation, resuspension, and concentration behavior.

Chapter 4 presents the model setup, including definition of constants, variables, and other governing parameters.

Chapter 5 presents results, with discussion, and offers recommendations for future study.

**

Chapter 2: Review of Literature

2.1: General

Three important properties of lake and river sediments are the size of the particles making up the sediment, the composition of the sediment, and bulk characteristics of the sediment mass (USACE, 2002). In this thesis, three main types of sediment will be considered: sand, silt, and clay. Sand and silt is common to all bodies of water throughout the world, but very common to the Mississippi delta is the less understood clay sediment. A clay particle is a mineral whose molecules are arranged in sheets that feature orderly arrays of silicon, oxygen, aluminum, and other elements (Lambe, 1969). Usually these particles are very small and more chemically active than sand. The sheet like materials that make up clay are minerals with a diameter around 0.0039mm (USACE, 2002). The flat surfaces of these particles give clay a large surface area, and when wet is chemically active. Colloidal particles have a surface charge and usually repel one another, but when the charge is neutralized, they are free to collide and aggregation occurs. This produces the cohesive, plastic, and slippery characteristics of its form, which are three classifications that each identify the same material when describing “clay” (USACE, 2002).

Grains of beach sand are quartz, a simpler and less chemically active mineral than clay. It is at least 16 times larger, and in some cases, more than 500 times larger in diameter than the largest clay particle. This causes gravitational forces to play a larger role in behavior than the surface forces exerted by sand grains, which is why they do not stick together, and referred to as non-cohesive (USACE, 2002). Table 2.1 presents several differences between clay and sand.

Table 2. 1. Relations among Three Classifications for Two Types of Sediment (USACE, 2002)

	Bases of Classification		
Name of Sediment	**Usual Composition**	**Size Range, Wentworth**	**Bulk Properties**
Clay	Clay Minerals (sheets of silicates)	Less than 0.0039 mm	Cohesive Plastic under stress Slippery Impermeable
Sand	Quartz (SiO_2)	Between 0.0625 mm and 2.00 mm	Noncohesive Rigid under stress Gritty Permeable

One of the most important characteristics of sediments is the size of the particles, usually defined in terms of its diameter, but because most grains are irregularly shaped, a sieve diameter is more applicable. The sieve diameter is determined by the mesh size of a sieve that will just allow the grain to pass. When performed in a standard manner, sieve experiments provide repeatable results and a more accurate way of grain classification for non-cohesive material (Blatt, 1980). The hydrometry test is used for cohesive material.

A grain’s fall velocity is another way to define its diameter and has the advantage of relating a grain’s diameter to its fluid behavior. This property is very important in

determining the behavior of sediments within a water column and will be closely examined. This concept is the basis for the hydrometry test for cohesive particles.

2.2: Sands

Mineral composition is closely related to other parameters such as sediment density and fall velocity. Quartz is the mineral most commonly found in littoral (the part of a body of water that is closest to the shore) materials because of its resistance to physical and chemical changes, and commonly account for more than 90% of the material on temperate latitude beaches (Krumbein, 1963). Most carbonate sands are formed by organisms (both animal and plant) that make calcium carbonate by changing the local chemical environment to favor carbonate deposition (USACE, 2002). Heavy minerals are other minerals that form a small percentage of beach sands. Their specific gravities are usually greater than 2.87. These minerals are frequently black or reddish and may color the entire beach. The most common of these are: andalusite, apatite, augite, biotite, chlorite, diopside, epidote, garnet, hornblende, hypersthene-enstatite, ilmenite, kyanite, leucoxene, magnetite, muscovite, rutile, sphene, staurolite, tourmaline, zircon, and zoisite (Pettijohn, 1957).

Sediment density is the mass per unit volume of a material, which in SI units, is measured in kilograms per cubic meter (kg/m^3) and is a function of its composition. Densities for minerals usually encountered in coastal engineering include quartz, feldspar, clay minerals, and carbonates, given in table 2.2:

Table 2. 2. Densities of Common Coastal Sediments (USACE, 2002)

Mineral	Density kg/m^3
Quartz	2,648
Feldspar	2,560 - 2,650
Illite	2,660
Montmorillonite	2,608
Kaolinite	2,594
Calcite	2,716
Aragonite	2,931
Dolomite	2,866

The density of a sediment sample may be calculated by adding a known weight of dry sediment to a known volume of water. The change in volume is measured and this is the volume of the sediment.

The specific weight of a material is its density times the acceleration of gravity, g (in SI is 9.807 m/s^2) giving it units (N/m3). The specific gravity of a material is its density divided by the density of water at 4 degrees centigrade, which is 1000.0 kg/m^3, causing specific gravity to be a dimensionless quantity.

Zhou and McCorquodale (1992) derived an equation to describe the relationship of the density of a fluid to temperature, pressure, and mass concentrations in the fluid (Zhou & McCorquodale, 1992):

$$\rho = \rho_{ref} + \left(1 - \frac{1}{S_s}\right) X$$

where Ss is the specific gravity of the particle, X is the mass fraction, and ρ_{ref}, the reference density is

$$\rho_{ref} = [999.8396 + 18.224944T - 0.00792221T^2 - 55.4486 * 10^{-6}T^3 + 14.97562 * 10^{-8}T^4 - 33.32952 * 10^{-11}T^5 + (0.802 - 0.002T)TDS]/[1 + 0.018159725T]$$

TDS= total dissolved solids in kg/m3. T= water temperature in oC.

An almost linear correlation can be seen within the temperature range mostly seen around the Mississippi Delta and Lake Pontchartrain area as shown in Figure 2.1:

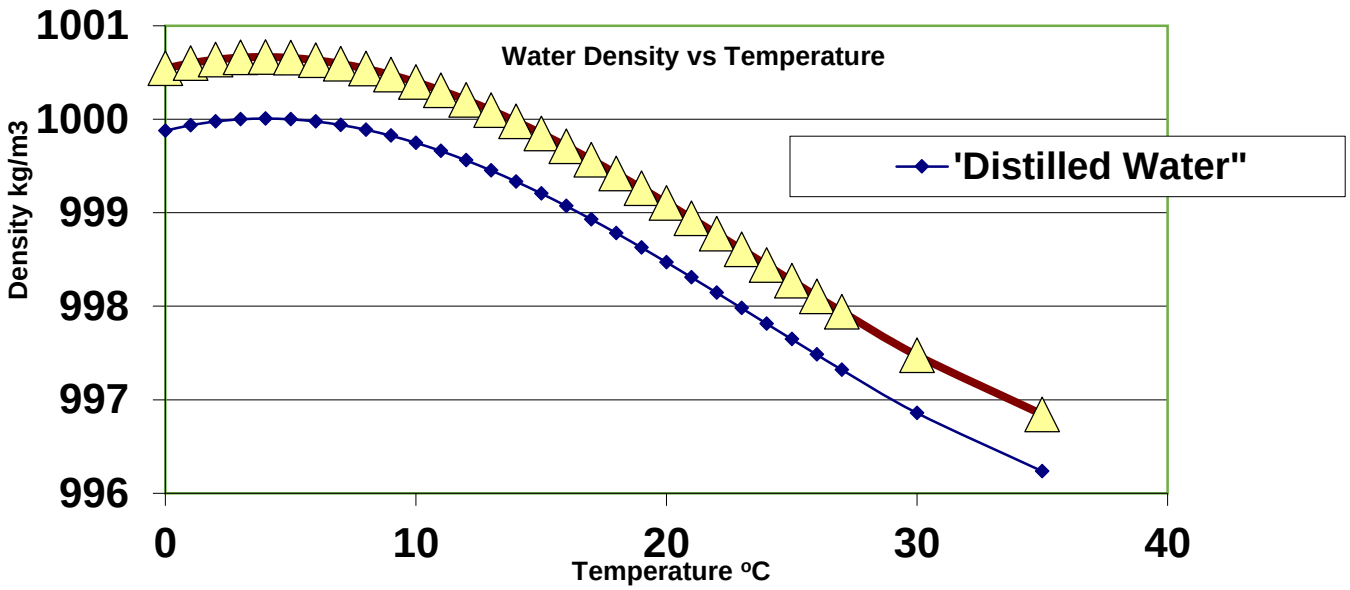

Figure 2. 1. Water density as a function of temperature. Linear results are seen around the 15-25 degree area (Zhou & McCorquodale, 1992)

2.3: Settling Velocity: Sands and Silts

When a particle falls through water, it accelerates until it reaches its fall or settling velocity, which is the terminal velocity that a particle reaches when the drag force on the particle just equals the downward gravitational force (USACE, 2002). Many factors influence a particle's settling velocity, including its size shape and density, and the fluid density and viscosity. For two of the sediment classes examined here, silt and clay particulate, Stoke's Law will provide an adequate measurement of the particle's settling velocity. George Gabriel Stokes derived an expression in 1851 for the drag force

exerted on spherical objects with very small Reynolds numbers in a continuous viscous fluid, making the following assumptions:

- Laminar Flow
- Spherical particles
- Homogeneous material
- Smooth surfaces
- Particles do not interfere with each other

For a single sphere falling in an infinite still fluid, the balance between the drag force and the gravitational force is:

$$C_D \frac{\pi D^2}{4} \frac{\rho w_s^2}{2} = \frac{\pi D^3}{6} (\rho_s - \rho_w) g \quad 2.1$$

And solving for setting velocity,

$$w_s = \sqrt{\frac{4gD_{50}}{3C_D}\left(\frac{\rho_s}{\rho_w} - 1\right)} \quad 2.2$$

where w_s is the settling velocity, C_D is the dimensionless drag coefficient (see Figure 2.2), D_{50} is the 50th percentile grain diameter, ρ_w is the density of water, and ρ_s is the density of the sediment.

Determining the appropriate drag coefficient presents a problem. Laboratory data of Rouse and others shows how the drag coefficient varies as a function of the Reynolds number ($Re = \frac{w_s D}{\nu}$, where ν is the kinematic viscosity).

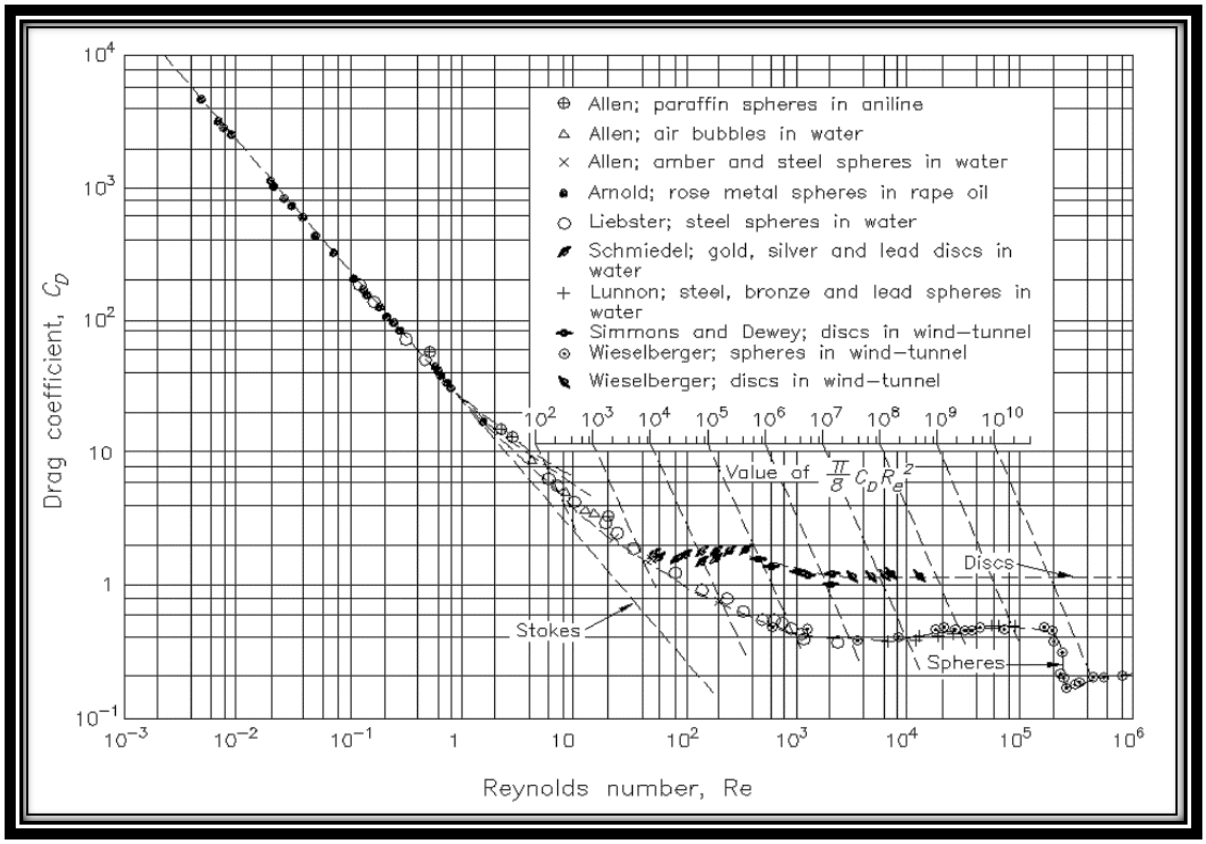

Figure 2. 2. Drag coefficient as a function of Reynolds Number (Vanoni, 1975).

The plot in Figure 2.2 can be divided into three regions. In the first, the Reynolds number is less than about 0.5, and the drag coefficient decreases linearly with the Reynolds number. This is the region of small and light grains gently falling at slow velocities. The drag on the grain is dominated by viscous forces, rather than inertia forces, and the fluid flow past the particle is entirely laminar. The middle range is from about Re>400 to Re<200,000. Here the drag coefficient has the approximately constant value of 0.4 to 0.6. In this range the particles are large and denser, and the fall velocity is faster because the behavior of C_D now dominates the viscous forces, and the wake behind the particle has become turbulent. At about Re=200,000, the drag coefficient decreases abruptly. This is the region of very large particles at high settling velocities. Here, not only is the wake turbulent but the flow in the boundary layer around the particle is turbulent as well. The first region, the region of interest for small particles, Stokes found the analytical solution for drag force as:

$$C_D = \frac{24}{Re} = \frac{24\nu}{w_s D_{50}} \qquad 2.3$$

This line is labeled “Stokes” in Figure 2.2. Substituting equation 2.3 into 2.2 gives the fall velocity is this region as:

$$w_s = \frac{g{D_{50}}^2}{18\nu}\left(\frac{\rho_s}{\rho_w} - 1\right) \qquad 2.4$$

Note that in this region the velocity increases as the square of the grain diameter and is dependent upon the density and kinematic viscosity. Equation 2.2 presents an expression of densities, $\sqrt{\frac{\rho_s}{\rho_w} - 1}$, which can change depending on locations.

For quartz sand grains in fresh water, this factor is about 1.28. For quartz grains in ocean water, this factor reduces to about 1.25 because of the slight increase in density of salt water. For quartz grains in muddy water, the factor will decrease somewhat more. If the suspended mud is present in a concentration of 10 percent by mass, the factor becomes 1.19. Natural increases in water density encountered in most water bodies will decrease the settling velocity of quartz by less than 7 percent (USACE, 2002).

Figure 2.3 illustrates the change in settling velocity in water and air according to temperature and Reynolds number:

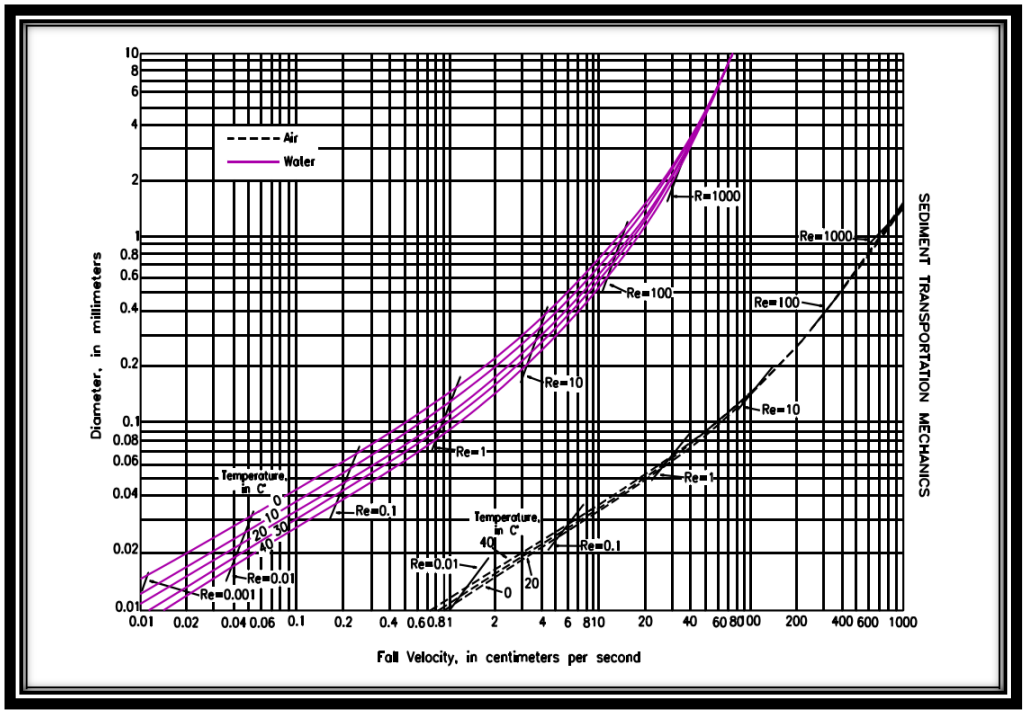

Figure 2. 3. Settling Velocity of quartz spheres in air and water (Vanoni, 1975)

Several other factors affect settling velocity. A floc, or tight clump of grains in an otherwise clear fluid will fall faster than a single grain because the adjacent fluid is partially entrained and the drag on each particle decreases. But if the grains are uniformly distributed in the fluid, each will fall slower because, as each grain falls, replacement fluid must flow upward and this flow impedes other grains. An adjacent wall will also decrease the fall velocity (USACE, 2002).

Porosity, bulk density, and permeability are related bulk properties that arise from the fact that aggregations of sediments have void spaces around each grain. The porosity, *P*, is defined as the ratio of pore space, or voids, to the whole volume. It is related to the

volume concentration, *N,* which is the ratio of the solid volume to the whole number; and to the voids ratio, *e,* which is the ratio of pore space to solid space by:

$$e = \frac{P}{N} \quad 2.6$$

$$N = 1 - P = \frac{1}{1+e} \quad 2.7$$

Porosity is a function of how tightly the grains are packed together, and generally is not constant for a given sediment. As a grain settles to the bed, the effects of gravity plus the effects of the lateral fluid stresses over the bed cause the volume concentration to decrease; meaning, the grains have less opportunity to roll around and find a position of maximum stability, or, the most tightly packed position. Grains in the surf zone are typically compacted to near their maximum volume concentration, while in estuaries they are not. In natural sands, volume concentration is essentially independent of grain size within the sand size range. However, the volume concentration is complicated by the irregular shape and non-uniform size of the grains. In general, an increase in non-uniformity of grain sizes increases the volume concentration (decreases the porosity) because small grains can fit into the pore spaces of the large grains (USACE, 2002). Good porosity data is not often available and the standard assumption in long shore transport computations is that sand has a porosity of 0.40, although there are likely to be significant variations from that figure (Galvin, 1979).

Bulk density refers to a group of particles. Dry bulk density is the mass of an aggregation of grains divided by the volume of the grains (solids) plus the volume of the pore spaces:

$$Dry\ Bulk\ Density = N\rho_s \quad 2.8$$

Saturated bulk density is the mass of an aggregation of grains plus the mass of the interstitial water divided by the volume of the sample:

$$Saturated\ Bulk\ Density = (N\rho_s) + (P\rho) \quad 2.9$$

The dry bulk density is never greater than the grain density, and the saturated bulk density is only greater than the grain density if the interstitial fluid is denser than the grains (if the grains float). Table 2.3 lists typical bulk quantities for several sediments and contains three parts: A-typical engineering data; B-saturated densities of naturally occurring surficial soils, along with porosity information; and C-dry densities of synthetic laboratory soils. Comparison of the two columns of data in C gives an ideal of the consolidation to be expected from settling and a minimum estimate of the bulking of newly placed dry material (USACE, 2002).

Table 2. 3. Soil Densities Useful for Coastal Engineering Computations (USACE, 2002)

A. Typical Engineering Values (from Terzaghi and Peck (1967), Table 6.3)

Material	Dry Bulk Density, kg/m^3	Saturated Bulk Density, kg/m^3
Uniform Sand		
Loose	1,430	1,890
Dense	1,750	2,090
Mixed Sand		
Loose	1,590	1,990
Dense	1,860	2,160
Clay		
Stiff glacial		2,070
Soft, very organic		1,430

B. Natural Surface Soils (from Daly, Manger, and Clark (1966), Table 4-4)

Material	No. of Samples	Mean Porosity, %	Saturated Bulk Density, kg/m^3	Locality
Sand	12	38.9	1930	Cape May sand spits
Loess	3	61.2	1610	Idaho
Fine Sand	54	46.2	1930	CA seafloor
Very Fine Sand	15	47.7	1920	CA seafloor
Sand-Silt-Clay	3	74.7	1440	CA seafloor

C. Laboratory Soils (from Johnson and Olhoeft (1984), Table 4)

Material	Dry Bulk Density "fluffed" kg/m^3	Dry Bulk Density "tapped", kg/m^3
Gravelly Soil	1,660	1,770
Sandy Soil	1,440	1,560
Dune Sand	1,610	1,760
Loess	990	1,090
Peat	270	320
Muck	800	850

Note: Data for loess in Parts B and C are representative of silty material.

Permeability is the ability of water to flow through a sediment bed, and is largely a function of the size and shape of the pore spaces. Flow into and out of the bed is one source of energy dissipation for waves traveling in shallow water (Kajiura, 1957), (Peregrine, 1980). Permeability is also a major factor in determining the steepness of the foreshore. Sediment is carried shoreward during the wave uprush in the swash zone. The permeability of the swash zone helps control how much of this water returns to the sea on the surface (above the bed) and how much returns through the bed. The surface backrush will transport sediment seaward, decreasing the equilibrium foreshore slope (Savage, 1958), (Kirk, 1969), (Packwood, 1983). Just seaward of the breaker zone recent studies have suggested that even small amounts of wave-induced flow passes into and out of the bed and may have a major effect on the bottom boundary layer and the resulting sediment transport (Inman, 1992)

Clays, silts, and muds are usually found as a foundation material or a material to be dredged. The flat topography of coastal plans and the quiet waters of bays and lagoons are often underlain by clay (USACE, 2002). Some older clays are consolidated and can stand with near-vertical slopes when eroded. Many eroding coastal flats contain much clay.

Silt is a classification of particles that falls between sand and clay. After a long period of time, rocks are weathered down into tiny fragments, producing silt. Glaciers can also produce a form of silt called silt flour. Mostly in deltas, estuaries, and glacial lakes, silts make up a significant portion of the sediment examined around the Mississippi. Beaches are driven mostly by waves and have very little silt because it can be forced out more easily as it stays in suspension longer than heavier particles. Unlike clay, silt is chemically inert and does not stick together.

Peat is extremely compressible sediment that is organically bound by the roots of marsh grasses in back bays and tidal wetlands. Field evidence suggests the compression of organic matter by sand causes subsidence on barrier islands (Kraft, 1979). Shore erosion can expose the organically bound sediment to ocean waves which causes erosion and can produce *pillow*, or cobble-shaped fragments of organically bound sediment, often found on barrier island coasts after storms (USACE, 2002).

2.4: Muds

Mud deposits (sometimes referred to as fluid mud) are believed to oscillate with the passage of water waves above them, absorbing energy from the waves and reducing their height.

When clay and silt are mixed with water in equal proportions, mud is formed. Mud also contains small amounts of sand and organic material but still acts more as a fluid than a solid. It often accumulates in dredged channels and sometimes offshore of the coast. This can cause wave modification by absorbing their energy as the mud oscillates with the passing of the wave (Zhao, 1989), (Shen, 1994), (deWit, 1994) . Fluid mud is a suspension of fine-grained sediment in close proximity, slowing down settling but not forming a connected matrix of bonds (McAnally, et al., 2007). It is often associated with a lutocline (a sudden change in sediment concentration with depth) and typically forms in near-bottom layers in lakes and estuaries, but can occur in any water body with enough fine-sediments and periods of low intensity flow. It usually has concentrations of tens to hundreds of grams per liter and bulk densities between 1,080 and 1,200 kg/m^3. It is composed mostly of water, clay, and silt sized particles, typically defined with having a less than 62.5 micron diameter (referring to non-cohesive, or disaggregated grains, not loosely bound flocs).

The amount of water in fluid mud varies. In dredging, fluid mud has been defined as suspension concentrations in the range of about 50-350 kg/m^3 (Teeter, 1992). In naturally occurring fluid mud, 10kg/m^3 has been suggested as a lower limit for fluid mud concentration because this often corresponds to the lutocline at the top of a fluid mud layer (Parker, 1977), (Kineke, Sternberg, Trowbridge, & Geyer, 1996). 250 kg/m^3 has been suggested as an upper limit, as this marks the transition to a framework-supported deposit which is much less likely to be mobile (Kirby, 1986). For fluid mud with low organic content, the range of 10-250 kg/m^3 corresponds to a sediment-induced density increase from 6 to 150 kg/m^3 above that of clear water (McAnally, et al., 2007). For fluid mud with a low organic content, clay-sized particles typically make up 50-70% of the solids, with silt content usually secondary to clay. In energetic environments, larger particles (in the fine sand size fraction) are occasionally caught in fluid mud, but their tendency to rapidly settle downward through it generally keeps the sand component to less than a few percent of a sample. Some example grain sizes of well-studied fluid mud are listed in Table 2.4 (McAnally, et al., 2007).

Table 2. 4. Example Fluid Mud Size Characteristics *(McAnally, et al., 2007)*

Site	Median grain size microns	Clay-size (%)	Silt-size (%)
Amazon, Brazil (Allison et al. 1995, Sternberg et al. 1996)	0.7–0.9	70–80	20–30
Mobile Bay, (Nichols et al. 1978)	3.2	70	30
Giroronde, France (Granboulan et al. 1989)	—	50–60	40–50
Laguna Madre, (Teeter 2001)	4.3	50	50
Eel River Shelf (Wheatcroft and Borgeld 2000)	—	50	50
James River	12	40	60

The mineralogy of fluid mud is usually dominated by platey, cohesive minerals from the class of clays and micas, with the specific minerals depending on the location of the sample. In the Gironde, clays and micas contribute about 60-70% with quartz contributing 20-25% and calcite 5-10% (Granboulan, Feral, & Villerot, 1989). Among the mineral clays and micas in the Gironde fluid mud, about 75% is composed of smectites and illite, with the remainder kaolinite and chlorite. Seasonal river floods introduce new material to the fluid mud, slightly increasing the mean diameter of fluid mud sediment as well as its quartz and feldspar content. Mineralogy of the dredged mud at Mobile Bay was dominated by montmorillonite and kaolinite, whereas illite and chlorite dominated at the James River dredge site (Nichos & Thompson, 1978). Fluid mud deposits on the Amapa mud banks, Brazil, contain unequal quantities (20-40%) of smectite, illite, kaolinite, and quartz, with trace amounts of chlorite, feldspar and iron minerals (Allison, Nittrouer, & Kineke, 1995). Organic matter can influence fluid mud by preventing it to dewater. In highly eutrophic Lake Apopka, Florida, the solids component of the 45cm thick fluid mud layer covering the lake bed is 63% organic matter in association with the accumulation of decomposing algae (Bachmann, Hoyer, & Canfield, 2000). Organic rich fluid muds characteristic of shallow eutrophic lakes in Florida such as Apopka and Okeechobee are highly anoxic (it lacks oxygen) and associated with high levels of phosphorus and nitrogen (Schelske & Kenney, 2001) (Havens, James, East, & Smith, 2003).

In comparison to the relatively stagnant, organic rich fluid muds found in some lakes, fluid muds in subaqueous deltas and estuaries and along high energy coasts tend to contain less organic matter, partly because the loading of inorganic sediment relative to organic matter tends to be much higher. At concentrations over 1 kg/m^3, the suspended solids of the Amazon River contain less than 2% organic matter (Hedges & Keil, 1999). Organic content of suspended solids at high concentration in other estuaries associated with fluid mud, such as the Yangtze and Yellow River Estuaries in China, are similarly

low (Cauwet & Mackenzie, 1993). Fluid mud deposits on the mid-shelf off the Eel River contain only about 1 to 2% organic matter (Leithold & Hope, 1999).

Fine sediment grains tend to bind together (aggregate or flocculate) under some circumstances, and cohesion significantly affects sediment behavior. Cohesion is caused by particle surface electrical charges and body forces, such as the van der Waals force. Smaller grains are more cohesive, with cohesion becoming progressively more important as grain size decreases below about 40μm (Mehta & McAnally, 2002). Biogenic processes also contribute to flocculation, particularly polymeric binding of grains (Tolhurst, Gust, & Patterson, 2002).

Flocculation of fine sediment grains into larger, multiple-grain particles, or flocs, occurs when a collision brings two particles close enough together for mutually attractive forces to overcome repulsive forces, and the two particles bond. If collisions are strong enough, flocs can be broken apart. Aggregation affects the size, shape, density, and strength of the flocs, and thus their settling velocity and accumulation as fluid mud. Figure 2.4 shows photographs taken by a scanning electron microscope in Chesapeake Bay of flocs by (Zabawa, 1978). The platey and rod-like characteristics of individual sediment grains are seen both in the dispersed state and when flocculated into larger aggregates containing hundreds or thousands of grains. Fluid mud consists of a dense suspension of these flocs.

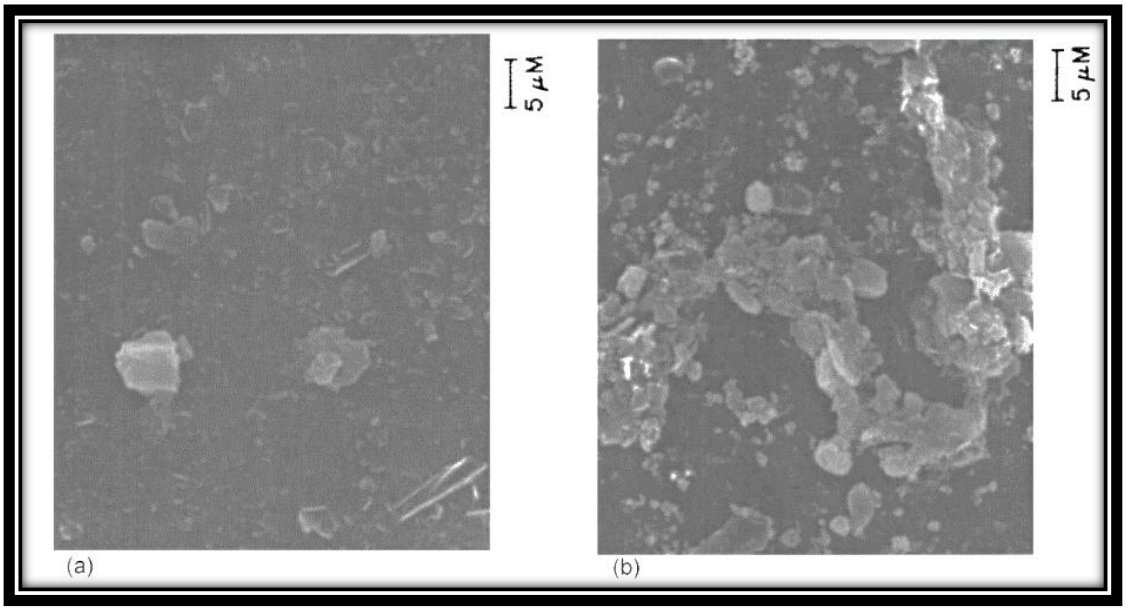

Figure 2. 4. (a) Cohesive sediment in a dispersed state; (b) after flocculation (Zabawa, 1978)

Aggregate settling velocities typically range from 10^{-5} to 10^{-1} m/s, and are a function of size, shape, weight, and surface roughness, along with fluid properties. A general expression for settling velocity given by (Mehta & Li, 1996) divided the settling range into four zones: free settling, flocculation settling, hindered settling, and negligible settling, shown in Figure 2.5 and expressed in equation 2.10:

$$w_{s,floc} = \begin{cases} w_s & C_{floc} < C_1 \\ a\frac{{C_{floc}}^n}{\left({C_{floc}}^2+b^2\right)^m} & C_1 < C_{floc} < C_3 \\ negligible & C_3 < C_{floc} \end{cases} \quad 2.10$$

where C_{floc}=total fine sediment concentration; w_s= free settling velocity; *a, n, b,* and *m*= empirical settling coefficients with *a*=33.38, *b*= 2.537, *n*=1.37, *m*=1.89; C_1=0.1-0.3 kg/m^3, and C_3=2-5 kg/m^3. Values chosen for the coefficients were taken from a study of flocculated sediments from Lake Okeechobee, show in figure 2.6 from (Mehta A. J., 1991).

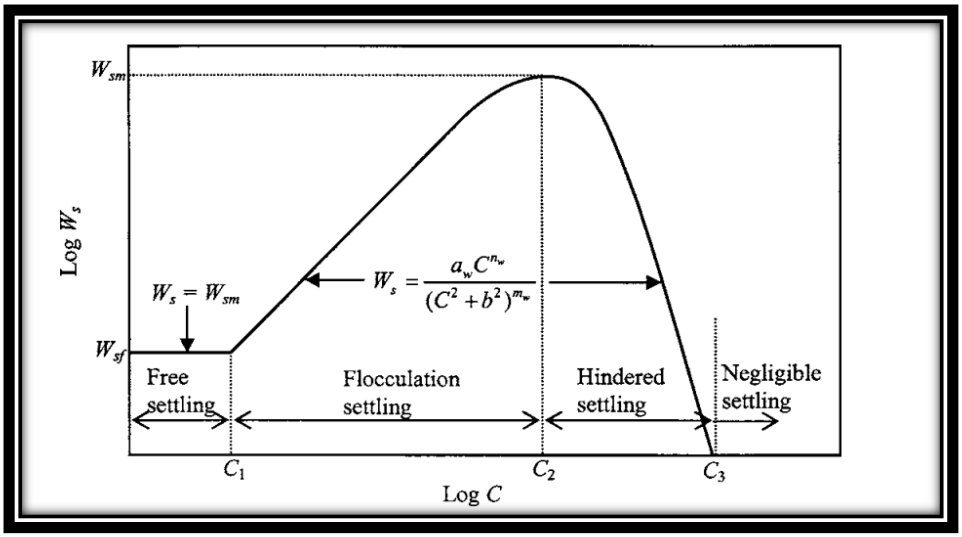

Figure 2. 5. Schematic of average suspension settling velocity dependence on concentration (Mehta A. J., 1991)

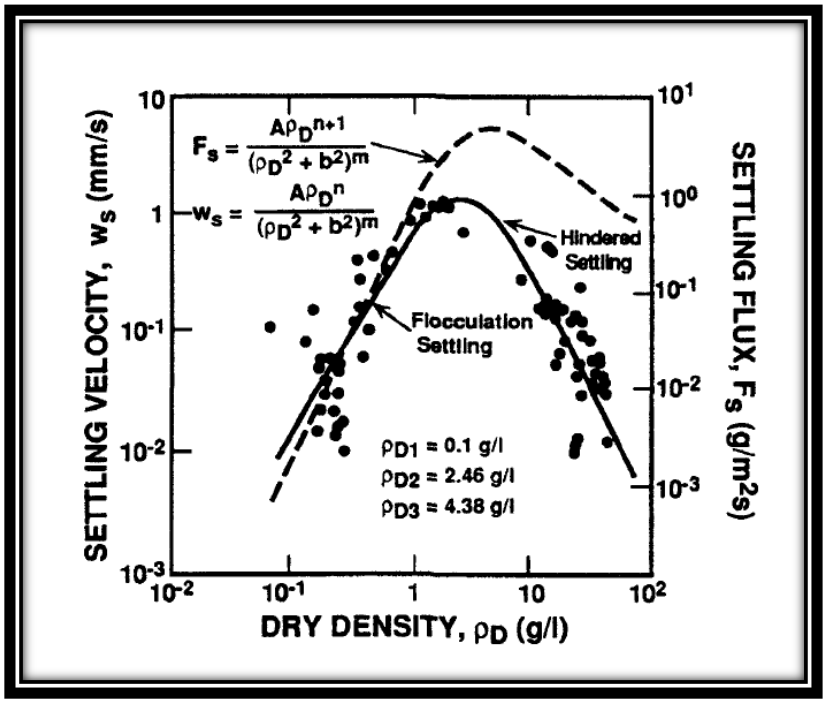

Figure 2. 6. Settling velocities for Lake Okeechobee, as a function of particulate concentration (Mehta A. J., 1991)

Hindered settling of suspended sediment occurs when the suspended sediment concentration increases and inhibits consolidation.

Waves can loosen a cohesive sediment bed and generate fluid mud. The fluidization of a cohesive sediment bottom occurs when the soil matrix is destroyed by excess pore pressure buildup. The upward moving pore fluid exerts a drag force on the sediment aggregates that exceeds the weight of the particles and the strength of higher order inter-aggregate bonds. When the upward pore fluid velocity exceeds a minimum value, aggregates are separated and the sediment becomes fluid supported instead of grain supported, and the sediment is fluidized. When sediment aggregates are supported by the fluid, the water sediment mixture behaves as a fluid with a viscosity 1000 times greater than the viscosity of water (McAnally, et al., 2007).

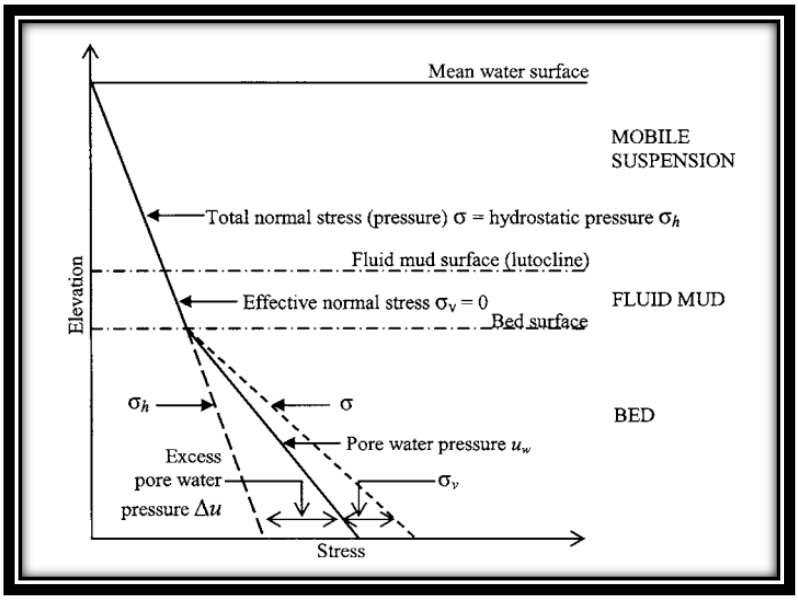

Figure 2. 7. Schematic of instantaneous stress profiles in a water-mud system (Mehta, Lee, & Li, 1994)

2.5: Resuspension

Resuspension is the process in which sediments from the bottom layer of a body of water are re-introduced into the water column by mechanical forces like wave-induced shear stress.

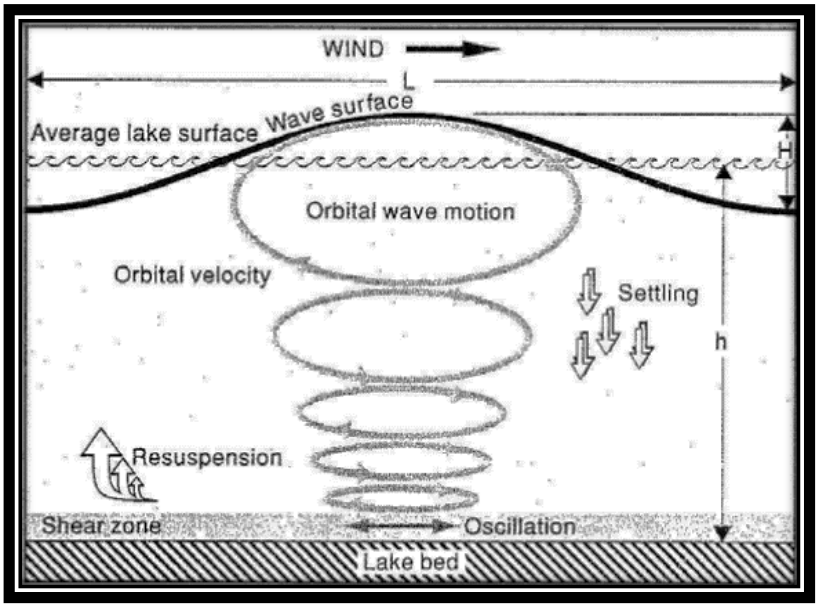

Figure 2. 8. Forces induced by wind that cause resuspension of bed sediment (Laenen & LeTourneau, 1996)

The sediment at the bed and in suspension in most estuaries is typically fine and cohesive in nature (Partheniades, 1965). This is not true of the Mississippi River where the bed is mostly sand; however, the coastal bay areas are generally composed of silt, clay, and organic materials. Surface layers of cohesive sediment beds in estuaries

generally are made of partially consolidated material deposited from flow (Mehta, Parchure, Dixit, & Ariaturai, 1982). These layers have a high water content and low cohesive shear strength, which tends to show a non-uniform variation with depth below the bed surface. The shear strength in this region can be so low, instrumentation have a hard time quantifying it (Partheniades, 1965). The bed can exhibit two modes of failure; surface erosion, involves floc-by-floc rupture and entrainment of the surface sediment. The second, mass erosion, results from a dynamic shear loading of the bed; the plane of failure lies deep in the bed, and results in an almost instantaneous entrainment of the sediment above the plane. In a normal estuarial environment, erosion occurs mostly at the surface. The rate of surface erosion, ε, expressed as the mass of sediment eroded per unit bed area per unit time, is related to the time-rate of change, $\frac{dz}{dt}$, of the depth of erosion, z, below the initial bed surface according to equation 2.11 and 2.12:

$$\varepsilon = h\frac{dC}{dt} \qquad 2.11$$

$$\frac{dC}{dt} = \frac{\rho(z)}{h}\frac{dz}{dt} \qquad 2.12$$

where h= depth of flow, $\frac{dC}{dt}$= time-rate of change of suspended sediment concentration, C, and $\rho(z)$= depth-varying dry density of the bed. Many studies have attempted to measure the variation of $\frac{dC}{dt}$ with time, t, for deposited beds in a closed system and found that, under a constant bed shear stress, τ_b, $\frac{dC}{dt}$ decreases continuously with *t*, beginning with a relatively high value when erosion starts (Mehta, Parchure, Dixit, & Ariaturai, 1982). For a certain range of τ_b, and high time step, ranging from a fraction of an hour to several hundred hours, depending upon the type of fluid-sediment mixture and the magnitude of τ_b, the rate of erosion, ε becomes equal to zero or approaches zero; C becomes constant or approaches a constant value asymptotically (Mehta & Partheniades, 1975). Given the bed density distribution $\rho(z)$, the magnitude of the constant value of C and the rate of approach of C to this value depend upon τ_b, defining the erosive force, and upon parameters which characterize the resistance to erosion.

A series of experiments conducted by Mehta and Partheniades concluded with some very important observations. The rate of surface erosion of stratified, deposited beds continuously decreases with time and can even become zero as the depth of erosion increases for a specific applied shear stress. The erosion rate of uniform beds remains practically invariant. The decrease in the erosion rate of stratified beds occurs because the cohesive shear strength with respect to erosion of the bed increases with depth. Erosion flocs are detached from the bed and entrained, but re-deposition of the entrained sediment does not occur. Erosion stops at a depth where the bed shear stress,τ_b, equals the bed shear strength. This value of τ_b is equal to the critical shear stress, τ_c, of the bed at that depth. An expression for the rate of surface erosion varies exponentially with the normalized excess shear stress, $(\tau_b - \tau_c)/\tau_c$. The critical shear stress in general increases with depth below the initial bed surface and also increases with bed consolidation time. As a result the rate of erosion decreases with increasing consolidation time (Mehta & Partheniades, 1975).

Haralampides (2000(performed a study on Lake Pontchartrain with some focus on resuspension (Haralampides K. , 2000). The following table shows results of calculations of applied bed shear stress for various fetches, depths, and wind speeds over Lake Pontchartrain using the methods proposed by the U.S. Army Corps of Engineers.

Table 2. 5. Shear stress calculation results (Haralampides K. , 2000)

Depth [m]	Fetch [km]	Wind Speed			Shear Stress [N m^{-2}]		
		[mph]	[m/s]	[knots]	shear from waves	shear from currents	total applied shear stress
3.35	36	12	5.36	10.5	0.0004	0.07	0.07
3.35	36	24	10.7	20.9	1.01	0.28	1.29
3.35	36	32	14.3	27.8	5.14	0.64	5.78
4.03	38	12	5.36	10.5	0.00005	0.07	0.07
4.03	38	24	10.7	20.9	0.50	0.28	0.78
4.03	38	32	14.3	27.8	3.60	0.64	4.24
4.31	30	12	5.36	10.5	0.00002	0.07	0.07
4.31	30	24	10.7	20.9	0.36	0.28	0.64
4.31	30	32	14.3	27.8	2.92	0.64	3.56
4.51	26	12	5.36	10.5	0.00001	0.07	0.07
4.51	26	24	10.7	20.9	0.28	0.28	0.56
4.51	26	32	14.3	27.8	2.40	0.64	3.04

A shaker device designed by Lick was used to perform tests regarding resuspension and deposition. Her device simulated orbital currents associated with wave action in Lake Pontchartrain: an increase in the RPM of the machine represented an increase in shear stress generated by higher velocity winds (Haralampides K. , 2000).

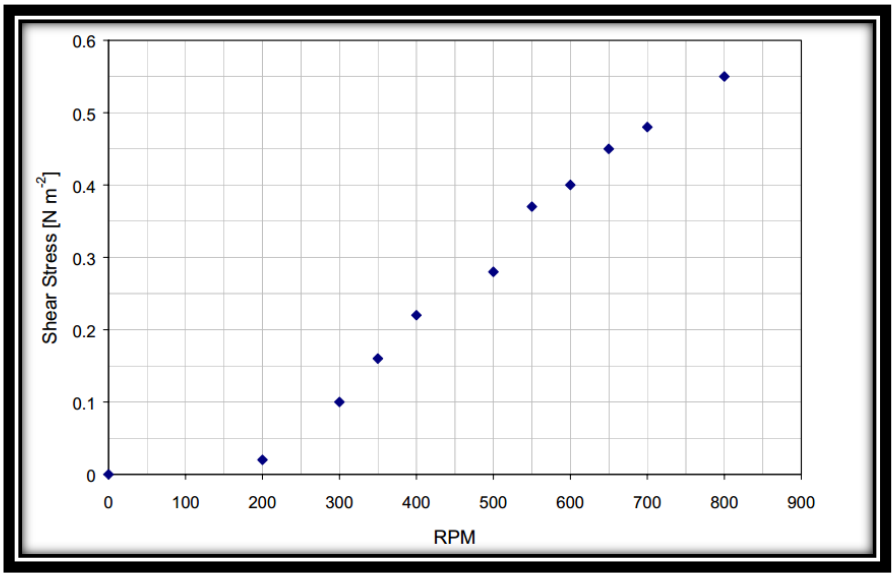

Figure 2. 9. The calibration curve for Lick shaker device shows resuspension of bed material was initiated at 0.1 N/m2 and a rapid increase was seen at 0.16 N/m2 (Haralampides K. , 2000)

Using water samples collected by The Pontchartrain Ecosystem Research and Education Project and wind records obtained from the New Orleans Lakefront Airport, Haralampides (2000) presents a figure helpful for numerical model calibration (Haralampides K. , 2000).

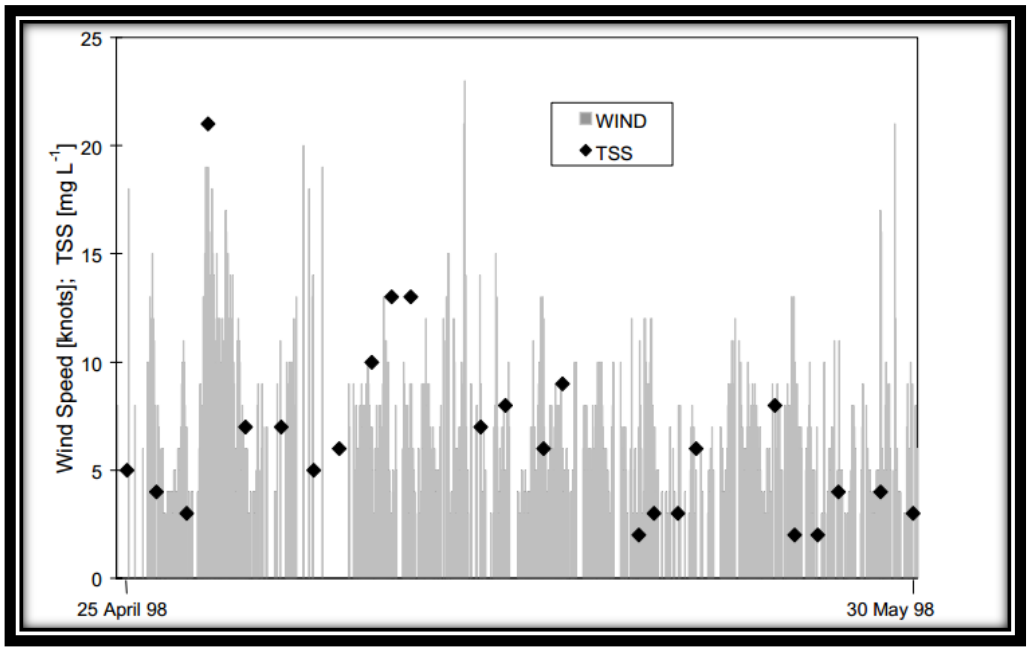

Figure 2. 10. Old Pontchartrain Beach TSS data with hourly wind speeds excluding SSW to SSE winds (Haralampides K. , 2000)

Anderson (1972) observed how resuspension by tidal currents and wind waves contributed to suspended matter (Anderson F. E., 1972). Krone (1966) saw that fine grained sediments were being resuspended from the shallow portions of San Francisco

Bay and transported to deeper areas during the windier summer months (Krone, 1966). Schubel (1968b) observed that wind wave resuspension was an important agent during high wind and rough seas, however, he also noted that high storm concentrations of suspended sediment were dissipated within a few days (Schubel, 1968b). Anderson (1970) felt that wave resuspension of estuarine sediments could cause significant variation in the observed daily cycle of particulate matter flowing through estuaries (Anderson F. E., 1970). His study implies that although shallow water resuspension occurs with low amplitude waves, the sediments usually settle out very rapidly unless the water is rising upward and landward as it does on a flooding tide. In the case of the ebb tide, the water column is settling down and off the tidal flat. This may act to quickly redeposit more of the coarse sediment and weaken the relationship between wave height and resuspension. Therefore there is less resuspension at deeper waters with a given wave height. Suspended sediment concentrations appear to be linearly predictable on the flooding tide for shallow waters and low amplitude waves. In less than 24 hours after wave resuspension most sediment appears to have settled out or have been transported elsewhere (Anderson F. E., 1972).

Chang et. al. (2001) studied sediment resuspension over a continental shelf during hurricanes Edouard and Hortense (Chang, Dickey, & Williams, 2001). They focused on physical processes and optical effects observed during the period 8/22-9/21/96 during the passage of two category 4 hurricanes. An understanding of the processes that control sediment resuspension and transport can be used to help predict and possibly control the fate of sediments as well as pollutants that are introduced onto the shelf at the coastline, offshore, or at the sea surface (Biscaye, 1988). The fate of organic matter on continental shelves is of great interest, especially with regard to the impact on the global carbon budget (Bacon, 1994). Strong atmospheric forcing drives currents and waves that increase bottom turbulence and affect sediment movement over the continental shelf (Twichell, 1987). After the first hurricane passed the study site, sediment was resuspended more than 30m into the water column; the relaxation of sediment concentration to conditions before the first hurricane occurred at about the same time at all depths. The water column temperatures began to restratify roughly 6-7 days after the first hurricane. Wave orbital velocity increased from 2cm s^{-1} to greater than 20 cm s^{-1} during the passage of the first hurricane. Grant (1979), Glenn (1987), and Lynn (1990) and many others have shown that sediment resuspension by waves without strong low-frequency currents is not uncommon (Grant, 1979) (Glenn, 1987) (Lynn, 1990).

Erm et. al. (2011) observed the resuspension of sediment in a semi-sheltered bay due to wind waves and fast ferry wakes (Erm, Alari, & Kask, 2011). They noted how anthropogenic resuspension plays a key role in the western part of Tallinn Bat during relatively calm spring and summer seasons. The near bottom orbital velocities generated daily by fast ferries' wakes are equivalent to those induced by wind waves excited by at least 18m/s southwestern winds and 12m/s northwestern winds. About 400kg of sediment is resuspended and carried away from each meter of coastline annually. Light attenuation also changes with the variations of the concentrations of suspended solids. Alterations in the sediment resuspension regime may also cause changes in the bottom topography. It may be concluded that resuspension of sediment

at the measurement site was due to fast ferry wakes rather than wind waves. Concerning sediment flux, on the average, the seaward flux was 1.3 times as large as the shoreward one. The absolute majority of resuspension events were caused by ship wakes which induced resuspension higher as induced wind waves about 50 times at the .2m level and about 200 times at the .5m level from the sea bed.

Keldeman et. al (2012) studied the sediment dynamics in the shallow Lake Markermeer in The Netherlands (Kelderman, De Rozari, Mukhopadhyay, & Ang'weya, 2012). They reported field and laboratory surveys as well as the first results for a 3-D suspended solids model. Lake Markermeer is about 680 km^2, and 90% of its depth is between 2 and 5 meters. Resuspension rates for the lake were very high, 1,000 g/m^2 day as an annual average, leading to high suspended solids contents, due to the large lake area and its shallowness (high Dynamic Ratio). A 3-D model was set up using Delft 3-D. Sediment characteristics, water depth, and fetch are main determinants for sediment distribution patterns. The research took place over 4 months and comprised of the following: taking an inventory of major sediment characteristics at 50 stations; sediment traps field survey at two permanent stations; preliminary laboratory sediment resuspension experiments; set-up and first results of the 3-D lake water quality SS model. Taken into account were two different layers of bottom sediments: a thin, very “fluffy” layer prone to resuspension under already moderate wind conditions, and a more compact sediment layer. Sediment yield of 995g/m^2 day was derived. Sediment resuspension started off at .5-.7 cm/s. For higher near-bed currents, an exponential increase could be observed with values up to 500-3,500 mg SS/L for a velocity of 1.3 cm/s. An exponential relationship between SS content (mg/L) and near-bed velocity C (cm/s) was estimated: $SS=27 \times e^{3.4*C}$ (with an $R^2=.96$) . Using the 3-D model, a reduction of more than 80% of SS contents, and 30-50% reduction of near bed currents was found in the case of placing artificial wetlands near the center of the lake. This reduced wind fetches by a factor of 2. Another possible measure for SS reduction would be the construction of large deep pits in the lake serving as final sedimentation basis for resuspended sediment material. They concluded that a substantial reduction in lake water turbidities can only be brought about by reducing effecting wind fetches, thus reducing near-bed currents

Blom and Aalderink (1998) reported on the calibration of three resuspension and sedimentation models from Blom, Lick and Partheniades and Krone (Blom & Aalderink, 1998). They were evaluated on data from flume experiments with sediments from Lake Ketal and in situ suspended solids measurements. Phosphorous has a strong tendency to associate with particulate material and large pools tend to accumulate in lake bottoms. Wind induced waves usually are the dominant driving force for sediment resuspension. Many models for resuspension and sedimentation are empirical but this study focuses on models which are largely theoretically based. In these models, the resuspension flux is directly related to the forces at the water-sediment interface, caused by wind-induced waves. The sedimentation flux is equal or proportional to the fall velocity of the particles and the suspended solids concentration. Resuspension is either related to the orbital velocity at some distance near the sediment-water interface or the shear stress at the bottom surface; another view was that sedimentation is described as a function of the bottom shear stress or related to the concentration and

fall velocity only. Parameter values in resuspension and sedimentation models are related to particle size and density (distribution) and sediment characteristics (cohesiveness). When horizontal transport by advection and dispersion can be neglected and vertical gradients in the suspended solids concentration are absent, the suspended solids dynamics can be described with:

$$\frac{\delta C}{\delta t} = h^{-1}(\Phi r - \Phi s) \quad 2.13$$

in which C is the depth averaged suspended solids concentration (gm^{-3}), h is the depth (m), Φr is the resuspension flux ($gm^{-2}s^{-1}$) and Φs is the sedimentation flux ($gm^{-2}s^{-1}$)

Three models are discussed and presented:

Blom: in this model the resuspension flux is a function of the orbital velocity:

$$\Phi r = K_B\left(u_b - u_{b,cr}\right); if\ u_b > u_{b,cr} \quad 2.14$$

$$\Phi r = 0; if\ u_b \leq u_{b,cr} \quad 2.15$$

K_B is a resuspension constant (gm^{-3}), $u_b$is the maximal orbital velocity induced by waves (ms^{-1}) directly above the sediment surface and $u_{b,cr}$ is the minimal (critical) orbital velocity required for resuspension (ms^{-1})

Lick (a):

$$\Phi s = w_s(C - C_b) \quad 2.16$$

which w_s is the fall velocity (ms^{-1}) and C_b is a “background” concentration of non settling suspended material (gm^{-3}). The fall velocity of particles is a function of their size and density

Lick (b):

$$\Phi r = \frac{K_L\left(\tau_b - \tau_{b,cr}\right)}{\tau_{b,cr}}; if\ \tau_b > \tau_{b,cr} \quad 2.17$$

$$\Phi r = 0; if\ \tau_b \leq \tau_{b,cr} \quad 2.18$$

in wich K_L is the resuspension constant ($gm^{-2}s^{-1}$), τ_b is the maximal bottom shear stress induced by the orbital velocity (Pa), and $\tau_{b,cr}$ is the minimal (critical) bottom shear stress.

Partheniades and Krone: in this model the sedimentation flux is a function of the bottom shear stress. It is constrained by a maximal (critical) bottom shear stress, which is by definition, lower than the critical shear stress for resuspension of sediments. Thus resuspension and sedimentation cannot occur simultaneously:

$$\Phi s = w_s\left(1 - \tau_b/\tau_{cr,s}\right) * (C - C_b)\ ; if\ \tau_b \leq \tau_{cr,s} \quad 2.19$$

$$\Phi s = 0\ ; if\ \tau_b > \tau_{cr,s} \quad 2.20$$

in which $\tau_{cr,s}$ is the maximal (critical) shear stress for sedimentation (Pa). The maximal orbital velocity near the bottom was obtained from (Philips, 1966) calculated from the bottom shear stress formula:

$$\tau_b = 0.5\rho_w C_f {u_b}^2 \quad 2.21$$

in which C_f is a dimensionless friction factor, taken here as 0.004 used in (Sheng & Lick, 1979). ρ_w is the density of water (kgm^{-3}). All three models produce, after calibration, a good reconstruction of the data set from the flume experiment. Although the differences in the model fit are not significant, Lick's model resulted in the best fit.

Lee et. al (2005) did a sensitivity analysis of sediment resuspension parameters in coastal area of southern Lake Michigan (Lee, Schwab, & Hawley, 2005). Model sensitivity analysis was performed to identify and compare quantitatively the important resuspension parameters in the coastal area of southern Lake Michigan. A one-dimensional resuspension and bed model capable of dealing with the type of mixed sediments (fine-grained+sand) common in the coastal area was developed and utilized to compare with measured suspended sediment concentration. Results show the most sensitive parameters in the model are the fraction of fine-grained materials and sediment availability. Other resuspension parameters such as settling velocity, critical shear stress, and erosion rate constant are also found to be important. Among these, the absolute magnitude of settling velocity is most crucial in controlling the first order prediction. A one-dimensional resuspension model capable of dealing with mixed sediments was developed to simulate time series of suspended sediment concentrations locally resuspended by waves and currents. The model consisted of two parts: sediment dynamics model and bed model. The sediment dynamics model includes entrainment, deposition, and flocculated and non-flocculated settling of mixed sediments. The depth-averaged sediment dynamics model is described as:

$$h\left(\frac{dC}{dt}\right) = F_R - F_D + F_A + F_L \quad 2.22$$

where h is the water depth, C is the depth-averaged suspended sediment concentration, Fr is the resuspension flux, Fd is the deposition flux, Fa is the net advection flux, and Fl is the lateral flux from the bluff erosion and tributaries. C is totally controlled by the difference of Fr, Fd, Fa, and Fl, by assuming small horizontal diffusion. The effect of Fa was not included in the numerical model. The combined wave and current bed shear stress is calculated simply by the sum of a wave and current bed shear stress since the consideration of nonlinear interaction did not improve results in the their study:

$$\tau_{cw} = [\tau_{wm}^2 + \tau_c^2]^{(1/2)} \quad 2.23$$

where τ_{cw} is the combined shear stress, $\tau_{wm}$is the maximum wave shear stress, and τ_c is the current shear stress.

$$\tau_{wm} = (\tfrac{1}{2})\rho f_w u_{ub}^2 \quad 2.24$$

where f_w is the wave friction factor and $u_{wb}$is the maximum near-bottom wave velocity

$$\tau_c = (\frac{1}{2})\rho C_d U^2 \quad 2.25$$

where C_d is the drag coefficient, taken to be .005, and U is the depth-averaged current velocity.

In many modeling studies, the fraction of fine-grained sediment estimated from a regression curve (f_{cs}) is set to a constant over the study area and the critical shear stress is used as a calibration parameter to control the resuspension rate, which often results in unrealistic critical shear stress (τ_c) values and incorrect prediction. Fortunately, f_{cs} is much easier to measure than τ_c, therefore it is important to use the measured f_{cs} as model input data. The spectrum of settling velocity has a less significant effect, except for the prediction of the lingering small particles right after a large event.

Miller et. al. (2005) monitored bottom sediment resuspension and suspended sediments in shallow coastal waters (Miller, McKee, & D'Sa, 2005). They found the corresponding high concentration of total suspended matter directly influences water quality, benthic and phytoplankton productivity and the redistribution and transport of pollutants and materials. The use of remote sensing technology to map suspended sediment concentration is well documented, but there are numerous reasons why remote sensing may not be employed operationally in studies of coastal systems. The most common limitation is the sensor's spatial or ground resolution. Sensors also cannot adequately capture the temporal dynamics of coastal waters. Airborne systems have the advantage that the user can define the deployment characteristics (time flown, area covered, spatial resolution), but airborne systems are typically expensive to operate and process data. Few studies have examined the coupling between bottom sediment resuspension and the surface expression of resuspension through remotely sensed imagery.

Booth et. al. (2000) present a model to determine wind-induced resuspension in coastal waters (Booth, Miller, McKee, & Leathers, 2000). The basis of their model is the full derivation of wind induced waves developed by the US Army Corps of Engineers Coastal Engineering Research Center (USACE, 2002):

$$\frac{gT}{U_a} = .2857(\frac{gF}{U_A^2})^{1/3} \quad 2.26$$

where U_A is a wind stress factor. The parameter critical wind speed U_c is the threshold wind speed at which resuspension is expected to occur is given as:

$$U_C = [1.2\{4127\left(\frac{T_C^3}{F}\right)\}^{.813}] \quad 2.27$$

where T_C, the critical wave period, is calculated as

$$T_C = (\frac{4\pi d}{g})^{1/2} \quad 2.28$$

Therefore, the model requires input point measurements of wind speed, wind direction, and water depth to provide corresponding point estimates of the occurrence of bottom sediment resuspension or *resuspension potential* (RP). RP was defined as the difference of average daily wind speeds and derived critical wind speed. Bottom

sediment resuspension occurs when RP is positive. An additional parameter, *resuspension intensity* (RI), is introduced to represent the magnitude of the difference between measured wind speed and derived critical wind speed. That is, RP indicates areas where resuspension is predicted to occur and RI provides an index of the intensity of bottom sediment resuspension. They then examine bottom sediment resuspension and suspended sediment transport in Lake Pontchartrain using the numerical model and remote sensing approach. Trzaska (2002) reported that independent of wind direction, resuspension occurs in Lake Pontchartrain, except close to shore in the proximal areas of wind direction, when wind speeds exceed 4 m/s (Trzaska, Miller, McKee, & Powell, 2002). Although resuspension intensity provides a relative index of the amount of wind energy that impacts the bottom, the depth to which sediment is mixed or affected depends in part on sediment grain size and consolidation of bottom sediments. Although the general relationship between resuspension and remotely sensed images of SS is complex, this article demonstrated that an integrated approach that incorporates both a simple wind-driven resuspension model and moderately high resolution images can provide unique insight into sediment dynamics in coastal waters.

In order to evaluate long term performance measures of coastal restoration projects, a mathematical model was developed for the 2012 State master plan which combined many of the above properties. For resuspension of cohesive sediments, E_{res}, a model from ECOMSED (HydroQual, 2002) was used:

$$E_{res} = \frac{a_c}{T_{res} T_{con}^m} \left(\frac{\tau_{bed}}{\tau_{cr}} - 1\right)^n \qquad 2.29$$

where a_c is a constant varying with bed properties, usually between 100 and 100,000; T_{res} is the response time of the bed, typically assumed to equal 1 hour; T_{con} is the time since deposition of sediment; *m* and *n* are calibration constants; $\tau_{bed}$is the bed shear stress; and τ_{cr} is the critical shear stress which will result in resuspension for the class of sediment. The distribution of silt and clay particles in a coastal environment is determined by the transporting currents and the net result of resuspension and depositional fluxes, S_r, .e. a source term defined by equation 2.12:

$$S_r = E_{res} - V_d \qquad 2.30$$

where E_{res}, is the sediment resuspension flux (mass per unit area per unit time) for silt and clay, and V_d= the depositional velocity (McCorquodale, Roblin, Georgiou, & Haralampides, 2009)

Ghose-Hajra et. al. (2014) developed a series of geotechnical laboratory tests on multiple dredged sediments from different geographic locations along the gulf coast to observe the effects of salinity and particle concentration on sediment hydrodynamics and critical bed shear stress for erosion of fine grained sediments used in wetland restoration projects (Ghose-Hajra, McCorquodale, Mattson, Jerolleman, & Filostrat, 2014). Table 2.5 presents the properties of the samples used:

Table 2. 6. Geotechnical properties of dredged slurry samples (Ghose-Hajra, McCorquodale, Mattson, Jerolleman, & Filostrat, 2014)

Sample ID	Source	Liquid Limit (%)	Plasticity Index (%)	Organic Content (%)	Specific Gravity	pH	% coarse	% fines	Salinity (ppt)	Initial Solids Concentration (g/L)
2013-2	Galveston, TX	67	39	2.3	2.64	4.66	9.8	90.2	4.66	179.63
2013-3	Galveston, TX	67	39	2.3	2.64	--	9.8	90.2	31	199.31
2013-4	Cameron, LA	79	50	3.8	2.48	7.54	2.2	97.8	0.402	51.29
2013-5	Cameron, LA	79	50	3.8	2.48	7.72	2.2	97.8	0.62	98.41

The rate and nature of sedimentation of the dredged slurry was monitored for 15 days during each experiment; Figure 2.11 shows the settling curves which represent two distinct settlement phases: zone settling and compression settling. The nature of the settling curve depends on the grain size distribution, salinity of the slurry, as well as on the initial solids particle concentration in the slurry. A higher initial solids concentration generally corresponds to lower sedimentation rates. The nature of the settling curve was not greatly affected by change in slurry salinity; however, there are insufficient data to establish a relationship between salinity and settling velocity (Ghose-Hajra, McCorquodale, Mattson, Jerolleman, & Filostrat, 2014).

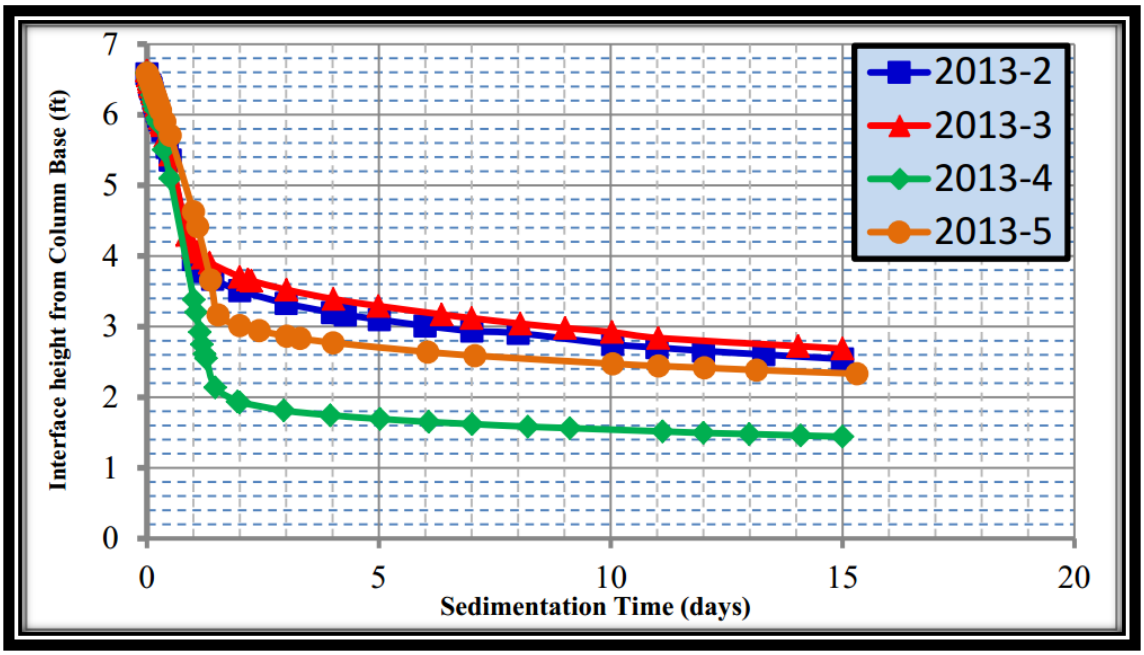

Figure 2. 11. Settling curves for samples 2013-2, 2013-3, 2013-4, and 2013-5 (Ghose-Hajra, McCorquodale, Mattson, Jerolleman, & Filostrat, 2014)

From here, the critical bed shear stress (τ_{cr}) was estimated from the resuspension tests using the frequency of oscillation of the disk and corresponding total suspended solids values. A graph was generated because each sample was run under a different consolidation time and a relationship was derived between critical bed shear stress and consolidation time in days (Figure 2.8):

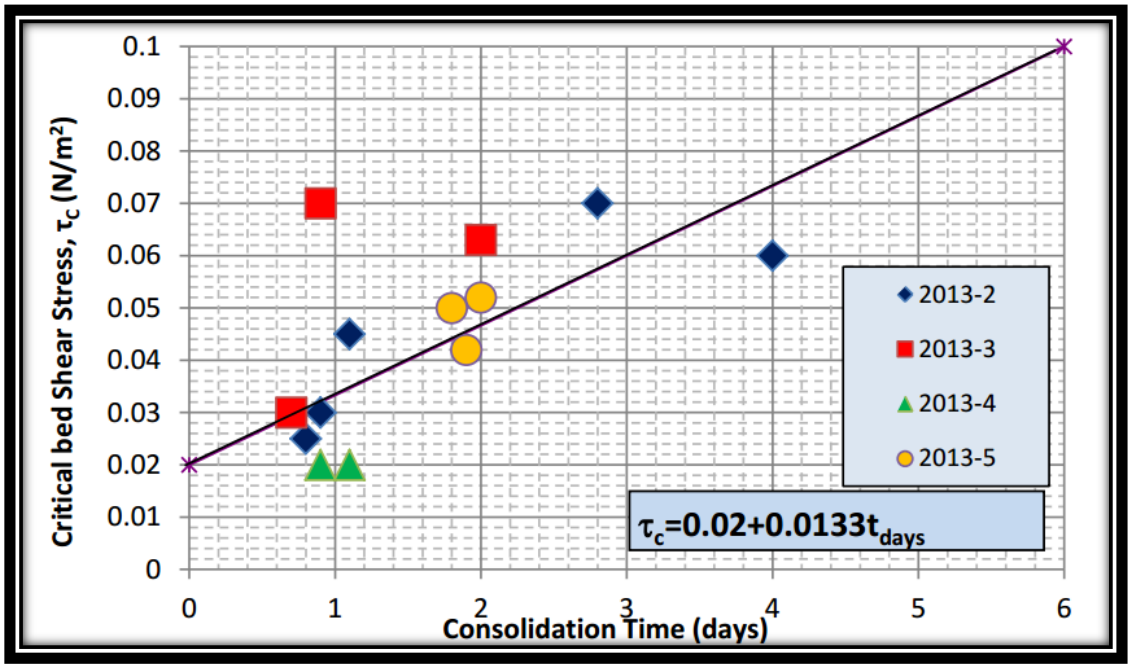

Figure 2. 12. Variation of Critical Bed Shear stress with consolidation time (Ghose-Hajra, McCorquodale, Mattson, Jerolleman, & Filostrat, 2014)

Preliminary results of a study done by (Lo, Bentley, & Xu, 2014) with fine sediments in the Mississippi River show a concentration-dependent exponential decline of consolidation rate versus time, implying that edibility is greatly dependent on the consolidation state.

Van Rijn pioneered new mechanical approaches to the resuspension of sand particles, using similar values of critical shear stress (van Rijn, 1993). First, initial particle motion needs to be determined before water column concentrations can be analyzed. Particle movement will occur when the instantaneous fluid force on a particle is just larger than the instantaneous resisting force related to the submerged particle weight and the friction coefficient. The driving forces are strongly related to the local near-bed velocities; in turbulent flow conditions, the velocities are fluctuating in space and time, thus making initiation of motion not only a deterministic phenomenon but a stochastic process also (Zanke, 2003). Initiation of motion in steady flow is defined to occur when the dimensionless bed-shear stress, ϑ (eq.2.13), is larger than a threshold value, ϑ_{cr}(equation 2.16a and 2.16b):

$$\vartheta = \frac{\tau_{cr}}{(\rho_s - \rho_w) g D_{50}} \qquad 2.31$$

Where τ_{cr}= critical bed shear stress of cohesion less particles; ρ_s= sediment density; ρ_w=fluid density (let s-ρ_s/ρ_w=relative density); g=gravitational acceleration; and D_{50}= median sediment diameter (van Rijn, 2007a).

The critical threshold value, ϑ_{cr}, depends on the hydraulic conditions near the bed, the particle shape, the particle position relative to the other particles, and other factors (van Rijn, 2007a). The hydraulic conditions near the bed can be expressed by the Reynolds number,

$$Re = \frac{u^* D}{\nu}, \quad 2.32$$

Where u^* is the velocity, D is the particle diameter, and ν is the kinematic viscosity coefficient. The viscous effects can also be represented by a dimensionless particle size, D_*:

$$D_* = D_{50}[\frac{(s-1)g}{\nu^2}]^{\frac{1}{3}} \quad 2.33$$

thus making ϑ_{cr} a function of the Reynolds number (van Rijn, Unified View of Sediment Transport by currents and waves. 1: Initiation of Motion, Bed Roughness, and Bed-Load Transport, 2007a).

Many experiments have been performed to determine the ϑ_{cr} values as a function of Re or D_*. The experimental results of Sheilds (1936) related to a flatbed surface are most widely used to represent the critical conditions for initiation of motion (Shields, 1936). The Shields curve represents a critical stage at which only a minor part (1-10%) of the bed surface is moving (sliding, rolling, and colliding) along the bed (van Rijn, 2007a). The Shield's curve is not very accurate for fine sand beds, so, based on the data of Miller et. al. (1977), the critical shear stress can be best represented by (Miller, McCave, & Komar, 1977) (van Rijn, 1993):

$$\vartheta_{cr} = .115(D_*)^{-0.5} \quad \text{for: } D_* < 4 \quad 2.34a$$

$$\vartheta_{cr} = .14(D_*)^{-0.64} \quad \text{for: } 4 \leq D_* < 10 \quad 2.34b$$

Figure 2.9 shows the critical bed-shear stress for particle sizes in the ranges of 4-250 μm (based on equations 2.34 a and b); it decreases from .183 to 0.025 N/m^2 for particle sizes decreasing from 250 to 4μm. The two data points in the silt range taken from Zanke (2003) show that this cohesion less behavior is realistic for pure quartz particles (Zanke, 2003).

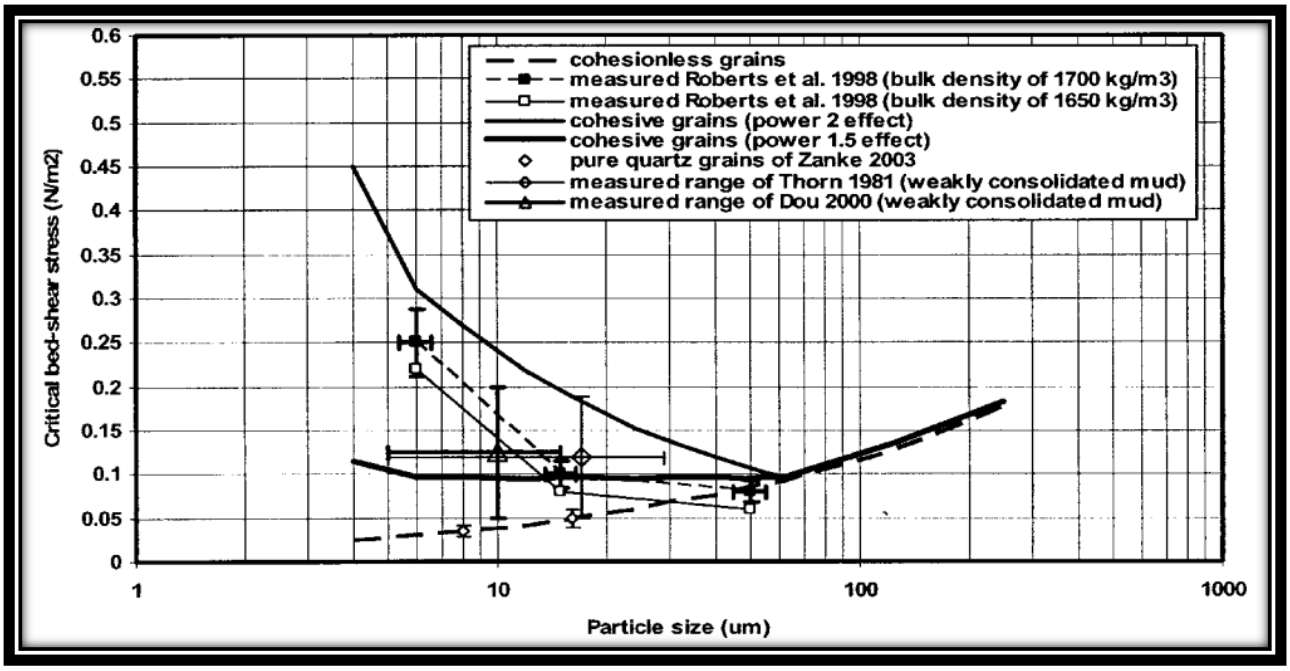

Figure 2. 13. Effect of cohesive force on critical bed-shear stress of fine sediment beds (submerged, weakly consolidated beds for particles <62 μm (van Rijn, 2007a)

The transport of particles by rolling, sliding, and saltating is called the bed-load transport, which, in the lower regime, is strongly related to the migration of bed forms (ripples and dunes). In the upper regime, a thin high-concentration sheet flow layer is present just above the bed, in which the sediment concentrations vary from the maximum (around 1,500 kg/m^3) to about 10 kg/m^3 over a thickness of the order of .01 (van Rijn, 2007a).

For suspended sand transport above the bed, van Rijn derives his formula

$$q_{s,c} = \int_a^h ucdz \qquad 2.35$$

Where c= concentration profile, u=velocity profile including wave-current interaction effects (van Rijn, 1993). The simplified suspended load transport formula for steady flow proposed by van Rijn was extended to coastal flow (waves) as equation 2.36, with equations 2.37-2.41 (van Rijn, 1984b) (van Rijn, 2013):

$$q_s = \alpha_s \rho_s u D_{50} {M_e}^{2.4} {D_*}^{-0.6} \qquad 2.36$$

$$M_e = \frac{(u_e - u_{cr})}{\sqrt{gD_{50}\left(\frac{\rho_s}{\rho_w} - 1\right)}} \qquad 2.37$$

$$u_e = u + \gamma u_{orb} \qquad 2.38$$

$$u_{cr} = \left(\frac{u}{u+u_{orb}}\right) u_{cr,c} + \left(\frac{u}{u+u_{orb}} - 1\right) u_{cr,w} \qquad 2.39$$

$$u_{cr,c} = \begin{cases} 0.19{D_{50}}^{0.1} \log\left(\frac{12d}{3D_{90}}\right) & 0.1\ mm < D_{50} < 0.5\ mm \\ 8.5{D_{50}}^{0.6} \log\left(\frac{12d}{3D_{90}}\right) & 0.5\ mm < D_{50} < 2\ mm \end{cases} \quad 2.40$$

$$u_{cr,w} = \begin{cases} 0.24\left[\left(\frac{\rho_s}{\rho_w} - 1\right) g\right]^{0.66} {D_{50}}^{0.33} T^{0.33} & 0.1\ mm < D_{50} < 0.5\ mm \\ 8.5\left[\left(\frac{\rho_s}{\rho_w} - 1\right) g\right]^{0.57} {D_{50}}^{0.43} T^{0.14} & 0.5\ mm < D_{50} < 2\ mm \end{cases} \quad 2.41$$

Where *u* is the depth-averaged velocity for each time step (considering all flow forcings), α_s is a coefficient ranging from 0.008 to 0.012, γ is a coefficient which is either 0.4 for irregular waves or 0.8 for regular waves, D_{90} is the 90th percentile particle diameter, *T* is the wave period, and all other variables are defined above (van Rijn, 2013). Table 2.6 gives a summary of laboratory and field data presented by van Rijn (van Rijn, 2007a):

Table 2. 7. Summary of Laboratory and Field Data of Coastal Sediment Transport (only Current-related suspended transport; Longshore Suspended Transport) (van Rijn, 2007a)

Case	Water depth h (m)	Longshore velocity u_L (m/s)	Cross-shore velocity u_c (m/s)	Significant wave height H_s (m)	Peak wave period T_p (m)	Angle between current and wave direction [φ (degree)]	Sediment size d_{10} (μm)	Sediment size d_{50} (μm)	Sediment size d_{90} (μm)	Temperature T (°C)	Salinity (parts per thousand)	Near-bed concentration at z (m)	Near-bed concentration at z (kg/m³)	Suspended transport (kg/s/m)
DUT628	0.52	—	0.093	0.121	2.5	0	140	205	300	17	0	0.34	0.017	0.00048
DUT630	0.51	—	0.22	0.123	2.6	0	140	205	300	17	0	0.35	0.019	0.002
DUT632	0.51	—	0.44	0.119	2.5	0	140	205	300	17	0	1.15	0.017	0.027
DUT635	0.5	—	0.107	0.146	2.4	0	140	205	300	17	0	0.59	0.019	0.00086
DUT637	0.51	—	0.22	0.151	2.4	0	140	205	300	17	0	0.81	0.022	0.0051
VB832	0.42	—	0.245	0.105	2.2	90	75	100	130	12	0	1.24	0.027	0.021
VB834	0.42	—	0.13	0.133	2.2	90	75	100	130	12	0	2.26	0.026	0.0122
VB835	0.42	—	0.256	0.139	2.3	90	75	100	130	12	0	3.26	0.024	0.047
VB836	0.42	—	0.317	0.137	2.2	90	75	100	130	12	0	4.0	0.024	0.098
DF87-2B	2.1	—	0	0.3	5.1	0	155	210	280	7	0	0.42	0.035	—
DF87-2C	2.1	—	0	0.4	5.1	0	155	210	280	7	0	1.1	0.03	—
DF87-2E	2.1	—	0	0.75	5.1	0	155	210	280	7	0	1.8	0.05	—
DF87-2F	2.1	—	–0.1	1.1	5.1	0	155	210	280	7	0	0.7	0.03	—
DF87-2G	2.2	—	–0.2	0.75	5	0	155	210	280	7	0	1.25	0.05	—
DF87-2H	1.41	—	–0.3	1.1	5.4	0	155	210	280	7	0	0.96	0.05	—
DF87-2I	1.13	—		1.1	5.4	0	155	210	280	7	0	2.53	0.05	—
DF97-1A	4.55	—	0	1	5	0	135	330	800	18	0	1.2	0.065	—
DF97-1B	4.55	—	0	1.25	5	0	135	330	800	18	0	1.55	0.065	—
DF97-1C	4.5	—	0	1	5	0	85	160	300	18	0	0.8	0.065	—
DF97-1D	4.5	—	0	1.25	5	0	85	160	300	18	0	1.3	0.065	—
DF97-1E	4.5	—	0	1.6	5	0	85	160	300	18	0	1.47	0.065	—
M73-0301	2.9	0.07	0	0.41	2.9	15	89	140	300	10	30	0.04	0.1	0.0011
M73-0302	3.15	0.24	0	0.42	3.1	15	89	140	300	10	30	0.1	0.1	0.016
M73-1301	3.03	0.135	0	0.42	3.2	15	89	140	300	10	30	0.174	0.1	0.0094
M73-1904	2.9	0.335	0	0.9	3.2	15	89	140	300	10	30	0.9	0.1	0.435
M73-2401	2.80	0.035	0	0.75	3	15	89	140	300	10	30	0.97	0.1	0.01
M73-2403	3.2	0.085	0	0.75	3.1	15	89	140	300	10	30	0.43	0.1	0.015
BP77-1	4.8	0.21	0	0.45	7.2	150	140	250	450	7	30	0.025	0.08	0.0024
BP77-2	5	0.42	0	0.55	6.7	150	140	250	450	7	30	0.076	0.1	0.022
BP77-3	4.9	0.24	0	0.95	6.8	150	140	250	450	7	30	0.43	0.08	0.055
BP77-4	5	0.3	0	1	6.6	150	140	250	450	7	30	0.84	0.05	0.08
BP77-5	5.3	0.4	0	1.05	6.5	150	140	250	450	7	30	1.05	0.05	0.3
E89-3C	1.1	0.24	–0.1	0.33	3.3	90	150	300	600	10	30	0.52	0.057	0.012

Figure 2.14 shows van Rijn's findings of the relationship between transport and depth-averaged velocity (u):

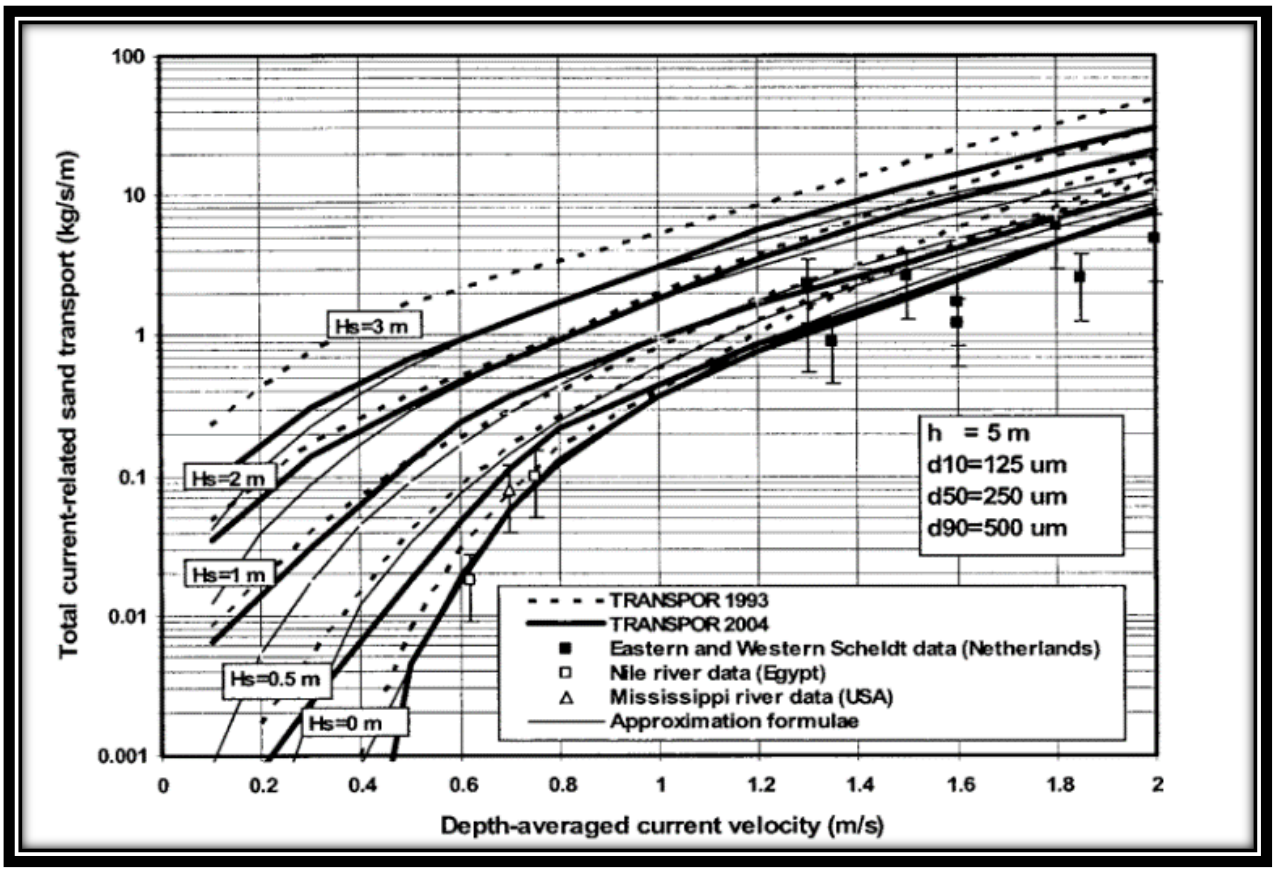

Figure 2. 14. Total sand transport for combined wave-current conditions, h=5m, d50=250 μm (van Rijn, 2007a)

2.6: Bed Shear Stress

In order to develop an appropriate bed shear stress, methods from the Army Corps of Engineers and work by Young and Verhagan (Young & Verhagen, 1996a) will be considered.

With the assumption that the atmospheric pressure, or, the pressure on the free surface is constant, a simplification of the bed shear stress made by Keulegan derived from a series of partial differential equations can be expressed as (Keulegan, 1951):

$$\tau_{bed} = C_f \rho_w {U_{bed}}^2 \qquad 2.42$$

where C_f is a constant approximately equal to 0.0025 (USACE, 2002), ρ_w is water density, and U_{bed} is the bed velocity, to be calculated as:

$$U_{bed} = \mathrm{U} + U_{tide} + U_w + U_{orb} \qquad 2.41$$

($\mathrm{U} + U_{tide}$), the compartment's flow velocity, will be determined from the flows in and out of the open water compartment:

$$(\mathrm{U} + U_{tide}) = \frac{\{\sum|Q_{in}|+\sum|Q_{out}|\}}{2A_x} \quad 2.42$$

where $\sum|Q_{in}|\ and\ \sum|Q_{out}|$ is the magnitude of the sums of the flows in and out, respectively; A_x is the effective cross-section of the open water cell (the effective cell width by depth). The cell width will be assigned in the cell attributes and the depth is computed in the hydrodynamic simulation.

Haralampides (2000) conducted a study on the Lake which monitored its compartment flow velocity (Haralampides K. , 2000). The results of the survey are presented in Figure 2.15.

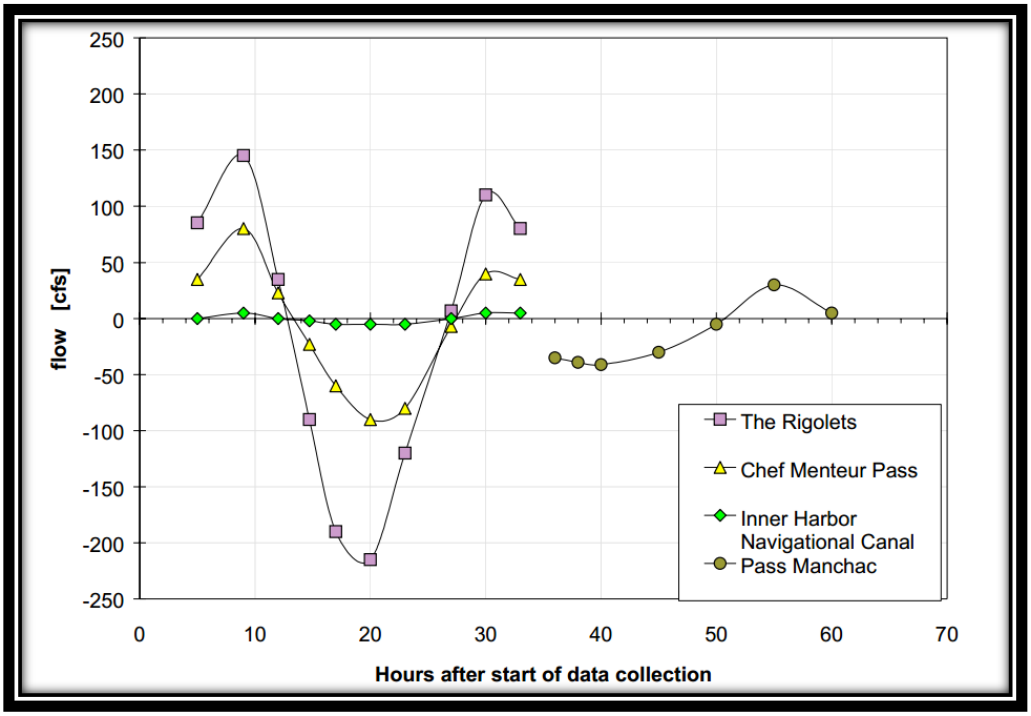

Figure 2. 15. Tidal flow survey results (Aug 27th to 29th, 1997) (Haralampides K. , 2000)

The wind induced currents, U_w, (Ekman, 1905), (Keulegan, 1951), (Rossby & Montgomery, 1935) will be estimated from wind speed, U_{wind} (or U_{10}), by:

$$U_w = k_a U_{wind} \quad 2.43$$

where k_a is in the range 0.023 to 0.032.

The orbital velocity, U_{orb}, will be estimated from linear wave theory:

$$U_{orb} = \frac{gH_s T \cosh\left(\frac{2\pi z}{L}\right)\cos\theta}{2L\cosh\left(\frac{2\pi d}{L}\right)} \quad 2.44$$

The orbital velocity is to be calculated at the bed therefore the height above the bed, z, will equal zero. Equation 2.44 will be calculated for a maximum orbital velocity, which will occur at a wave phase of θ=0, reducing the equation to:

$$U_{orb} = \frac{gH_sT}{2L\cosh\left(\frac{2\pi d}{L}\right)} \quad 2.45$$

where *g* is gravitational acceleration, H_s is significant wave height, *T* is wave period, *L* is wavelength, and *d* is water depth (Demirbilek & Vincent, 2002).

Wavelength can be iteratively solved from depth and wave period (eq.2.30).

$$L = \frac{gT^2}{2\pi}\tanh\left(\frac{2\pi d}{L}\right) \quad 2.46$$

However, a reasonably accurate (±10%), non-iterative approximation correction for wavelength can be used for simplicity, equation 2.47 (Demirbilek & Vincent, 2002).

$$L \approx L_o \tanh\left(\frac{2\pi d}{L_o}\right) \quad 2.47$$

$$L_o = \frac{gT^2}{2\pi} \quad 2.48$$

Period (*T*), Significant wave height (H_s), and depth (*d*) are all required for the above equations. Depth was the only variable calculated in the 2012 Master Plan open water components, therefore, the Young and Verhagan wave model will be incorporated into the open water calculations in order to find the other two parameters needed for bed shear calculations.

Young and Verhagen conducted a fetch limited wind wave growth experiment in water of finite depth, similar to that of Lake Pontchartrain, involving measurements of wind wave spectra, wind speed, and direction at eight stations along the fetch (Young & Verhagen, 1996a). To simplify the data, three non-dimensional variables were taken, represented in the following equations:

$$\epsilon = \frac{g^2E}{u^4} \quad 2.49$$

$$\nu = \frac{f_p u}{g} \quad 2.50$$

$$\mathrm{X} = \frac{gx}{u^2} \quad 2.51$$

where ϵ is the non-dimensional energy, ν the non-dimensional frequency, and X the non-dimensional fetch; g is the gravitational acceleration, E is the total wave energy or variance of the wave record, f_p is the frequency of the spectral peak, x is the depth, and u is a characteristic wind velocity (U_{10}). From the observed data sets, presented in the Figures 2.16 and 2.17, (Young & Verhagen, 1996a) simplified equations 2.49-2.51 into two integrated formulas using empirical formulations:

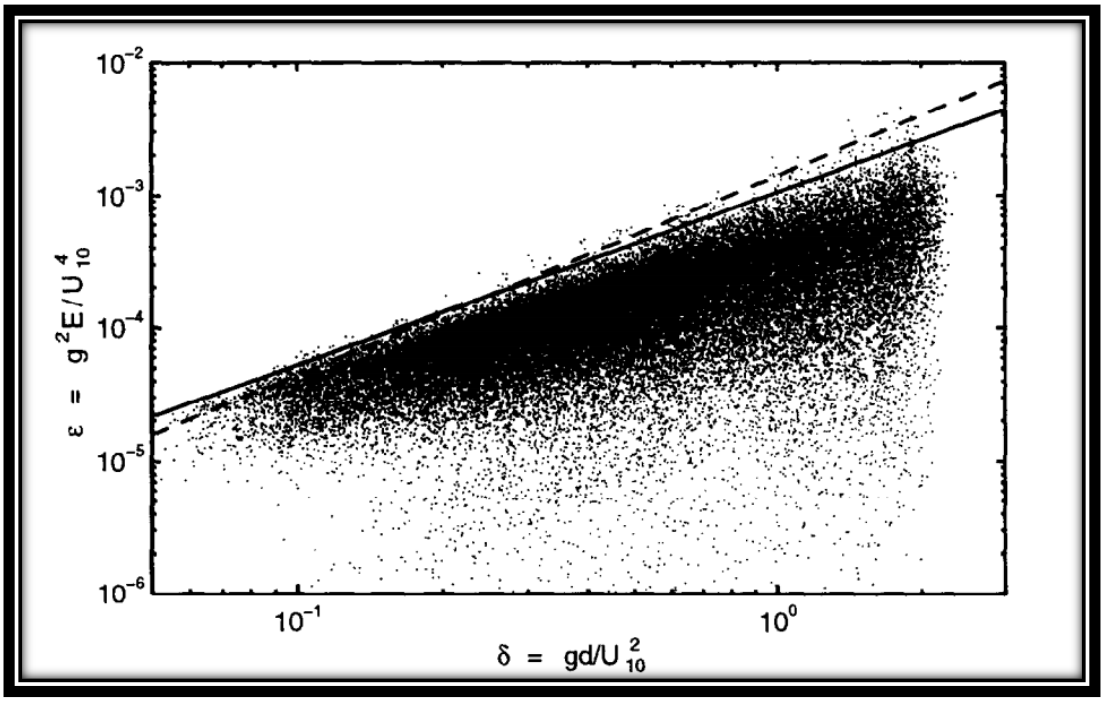

Figure 2. 16. A scatter plot of non-dimensional energy ϵ against non-dimensional depth δ. The full data set of approximately 65,000 points is shown (Young & Verhagen, 1996a).

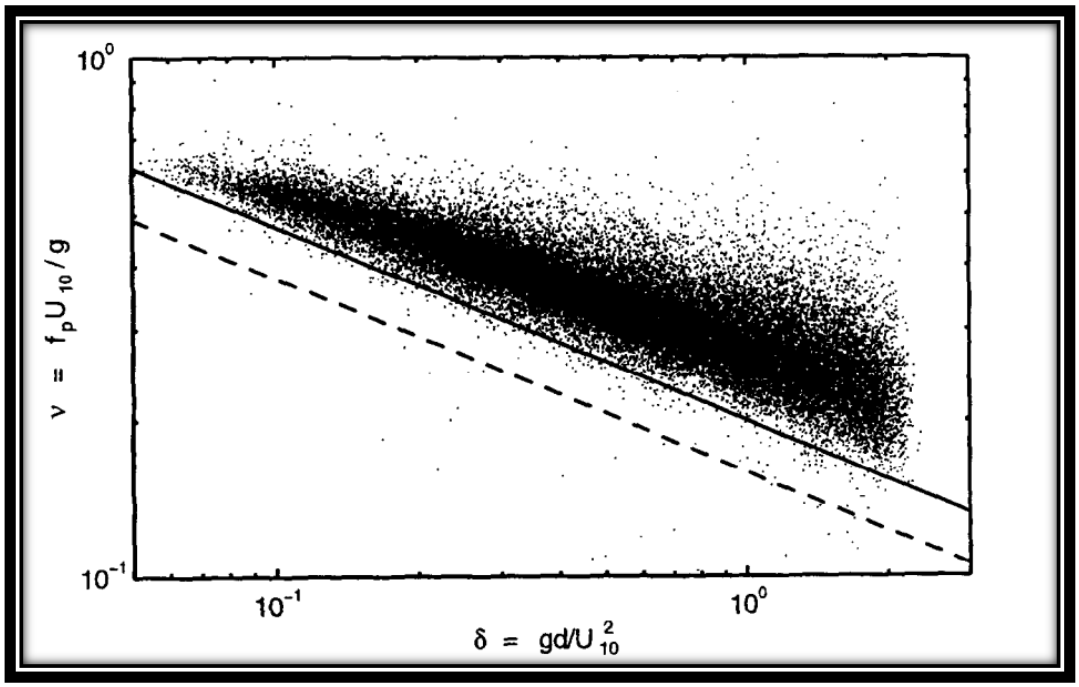

Figure 2. 17. A scatter plot of non-dimensional peak frequency ν against non-dimensional depth δ . The full data set of approximately 65,000 points is shown (Young & Verhagen, 1996a).

$$\epsilon = 3.64 * 10^{-3}\left\{\tanh A_1 \tanh\left(\frac{B_1}{\tanh A_1}\right)\right\}^n \qquad 2.52$$

$$\nu = 0.133\left\{\tanh A_2 \tanh\left(\frac{B_2}{\tanh A_2}\right)\right\}^m \quad 2.53$$

$$A_1 = 0.493 * \delta^{0.75} \quad 2.54$$

$$B_1 = 3.13 * 10^{-3} * \chi^{0.57} \quad 2.55$$

$$A_2 = 0.331 * \delta^{1.01} \quad 2.56$$

$$B_2 = 5.215 * 10^{-4} * \chi^{0.73} \quad 2.57$$

Values for the coefficients *n, m*, E_{lim}, V_{lim}, originally proposed, are *n=1.74, m= -0.37,* E_{lim}*=.00364, and* V_{lim}*=0.133* (Young & Verhagen, 1996a).

Wave period, T, is the reciprocal of wave frequency and significant wave height, Hs, can be estimated according to Young and Verhagen (1996), as:

$$H_s = 3.8\sqrt{E} \approx 4\sqrt{E} \quad 2.58$$

Comparing the Young and Verhagen wave heights with the Corps of Engineers Shore Protection Manual (USACE, 2002), good agreement for shallow water bodies are found, as indicated in Figures 2.18 and 2.19.

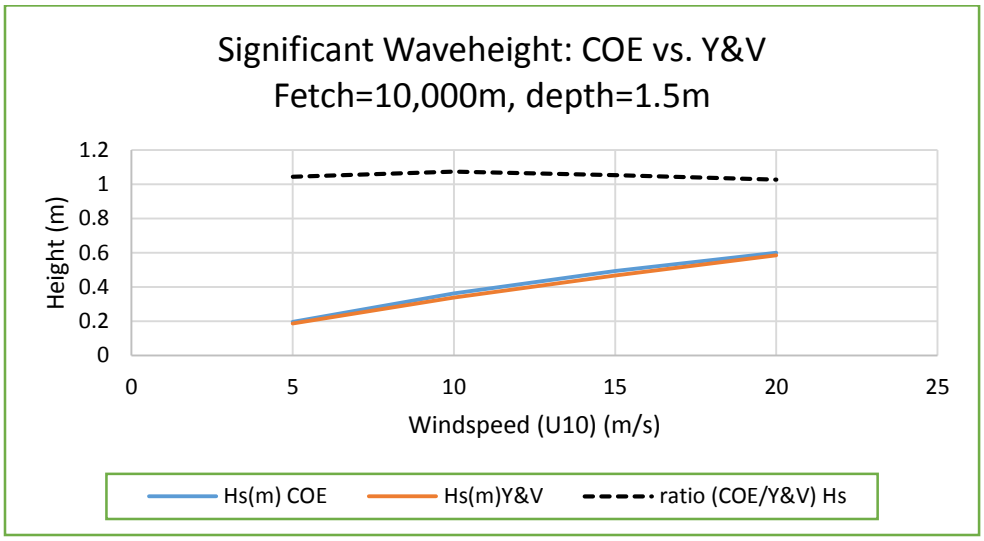

Figure 2. 18. Comparison of significant wave heights from the Corps of Engineers and Young and Verhagen

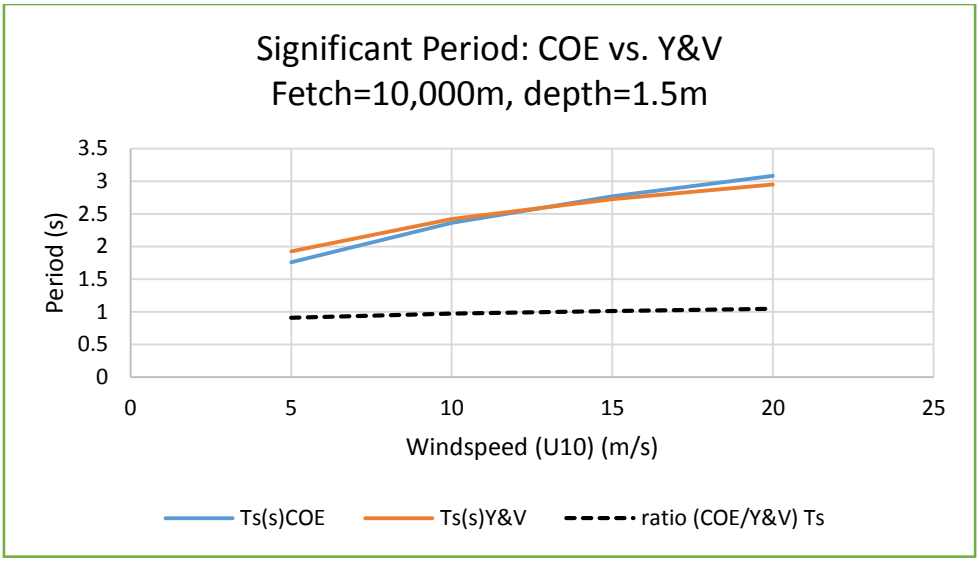

Figure 2. 19. Comparison of significant periods from the Corps of Engineers and Young and Verhagen

Chapter 3: Methodology

3.1: Deposition of Suspended Sediments: Silt and Clay Particulate

A sediment deposition rate (m/s) for each open water compartment will be calculated from the settling velocity of suspended sediments in the water column. Total suspended solids (TSS) will be assumed constant throughout the water column because each compartment is taken to be fully mixed. The 2012 Master Plan used a single settling velocity for suspended sediments, calculated as a function of the (TSS) concentration. For the updated 2017 Master Plan, four size classes will be considered, each requiring its own form of settling velocity. Settling of sands will be considered differently within its resuspension formula, to be discussed later. The settling velocity, w_s, will be calculated for 2 classes, silt and clay particulate, from Stoke's law (eq. 3.1):

$$w_s = \sqrt{\frac{4gD_{50}}{3C_D}\left(\frac{\rho_s}{\rho_w} - 1\right)} \qquad 3.1$$

Where D_{50} is the median diameter of the particle (m), ρ_s and ρ_w are the densities of the particle and water, respectively, g is the acceleration due to gravity (m^2/s), and C_D is a dimensionless drag coefficient (USACE, 2002). Because C_D is a function of the Reynold's number, itself being a function of the settling velocity, the drag coefficient for small particles like silts and clay particulates with slow settling velocities will be estimated by (eq. 2):

$$C_D = \frac{24\nu}{w_s D_{50}} \qquad 3.2$$

where ν is the kinematic viscosity, given by (White, 1978) to be a function of temperature, T (degrees Celsius) in (eq. 3):

$$\nu = \frac{1.79*10^{-6}}{1+.03369T+.000221T^2} \qquad 3.3$$

Substituting equation 3.1 into equation 3.2 gives a settling velocity for silt and clay particulate, (eq. 4)

$$w_s = \frac{g{D_{50}}^2}{18\upsilon}\left(\frac{\rho_s}{\rho_w} - 1\right) \qquad 3.4$$

Equation 3.4 can be used for small sediments with a Reynold's number less than 0.5, but is not applicable to particles such as sand, to be considered later.

Figure 3.1 illustrates the sensitivity of silt's settling velocity to the average temperature of water.

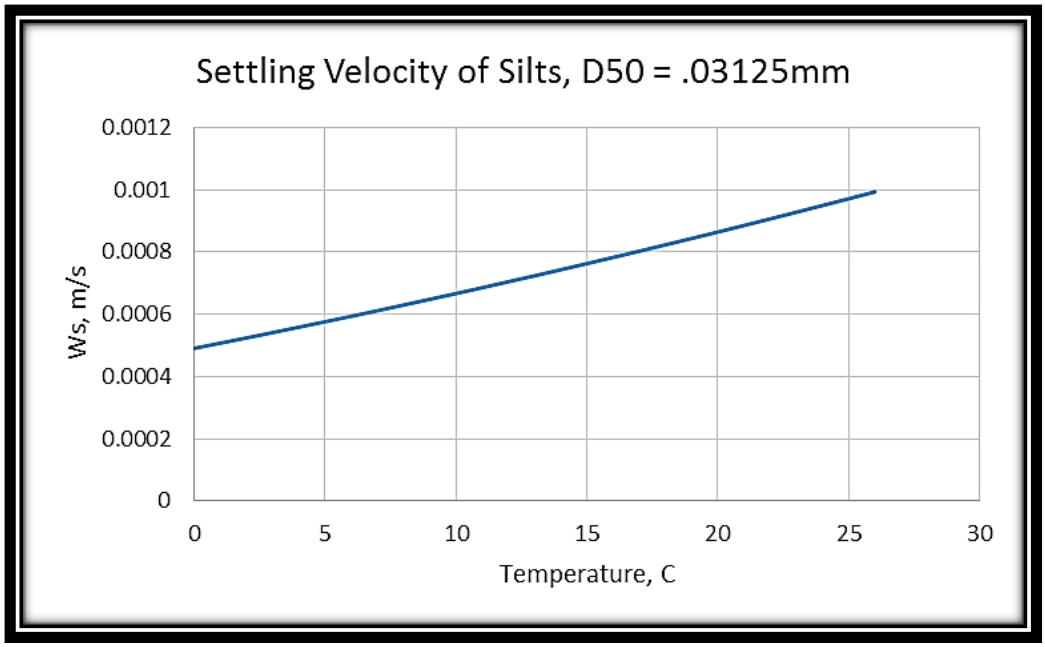

Figure 3. 1. Illustrates the sensitivity of a silt particle's settling velocity to the average temperature of water.

Due to its larger diameter, silts have a much higher settling velocity than clay particulates, causing silt to deposit quicker.

3.2: Deposition of Suspended Sediments: Clay Flocculent

Flocculation is a complex process, but for the sake of these calculations, two factors will be taken into account: sediment concentration and salinity. To estimate the fraction of clay particles that will form floc,P_{floc}, the following inequalities will be used, with salinity concentration governing the function:

$$P_{floc} = \begin{cases} \frac{P_{floc,max}}{C_{sal,max}} C_{sal} & C_{sal} < C_{sal,max} \\ P_{floc,max} & C_{sal} \geq C_{sal,max} \end{cases} \quad 3.5$$

where $P_{floc,max}$is an upper limit to the fraction able to flocculate, C_{sal} is the salinity concentration, and $C_{sal,max}$ is the salinity threshold. Any concentration above $C_{sal,max}$ will not produce any more clay floc; 5 parts per thousand (ppt) was used in the 2012 Master Plan and in Lake Pontchartrain modeling efforts, based on (Kotylar, Sparks, & Schutte, 1996). A salinity of 5 ppt is demonstrated by Kotylar to be a sufficient threshold as the rapid response to salinity peaks at that point, as presented in Figure 3.2.

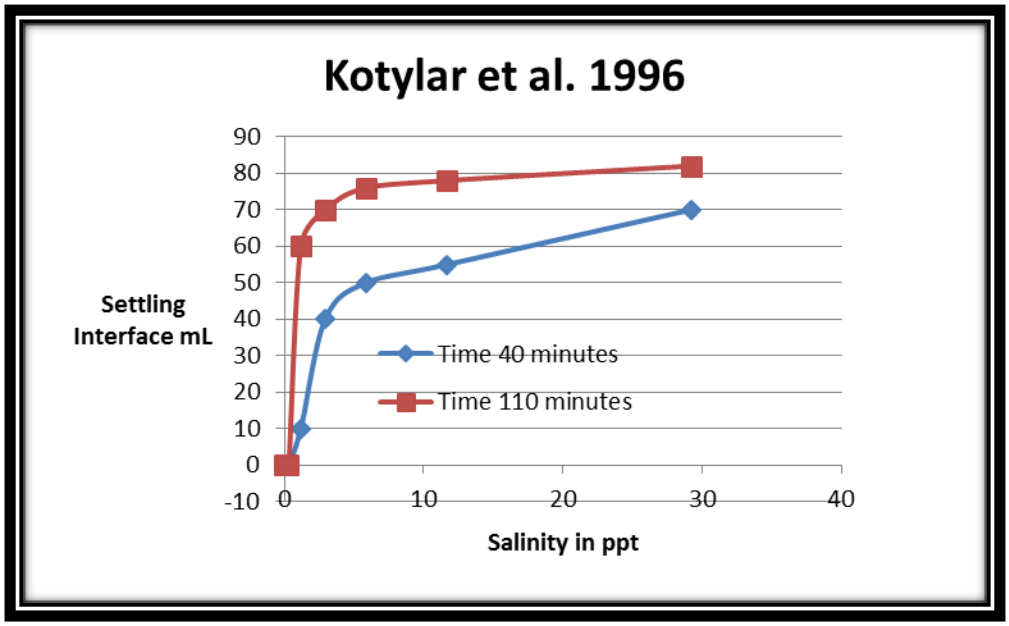

Figure 3. 2. Salinity effect on interface settling (Kotylar, Sparks, & Schutte, 1996)

Simplifying the approach of Deltares (Deltares, 2013), a linear relationship presented between P_{floc} and C_{sal} was chosen due to the nearly linear equation used in the Delft3D-FLOW model, adjusting flocculated settling velocities as a function of salinity.

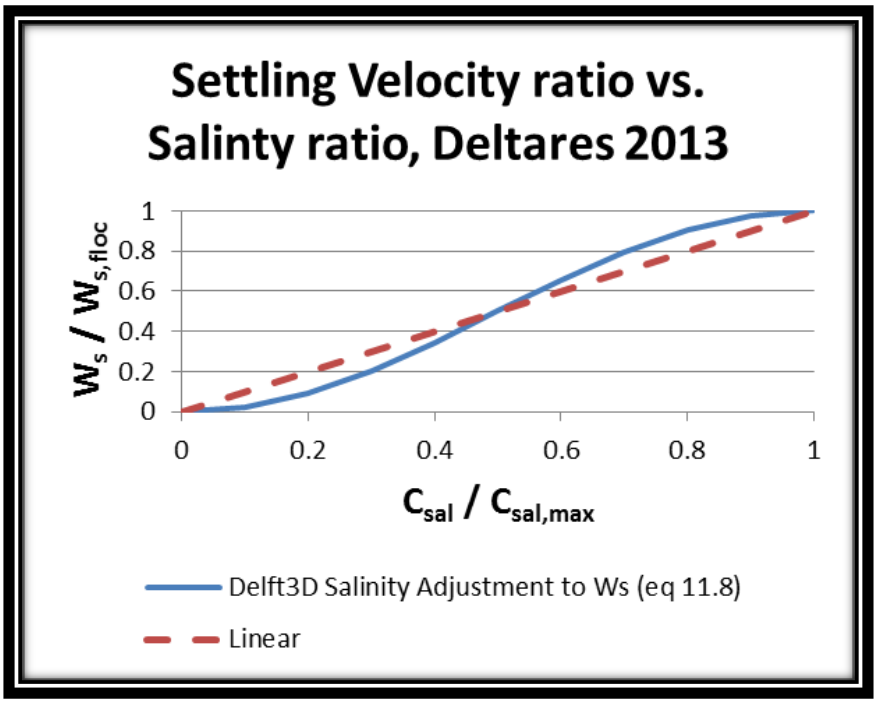

Figure 3. 3. Salinity adjustment to settling velocity for flocculated particles used in Delft3D (Deltares, 2013)

Once the clay sediments are divided into two fractions, a settling velocity for the flocculated particles can be calculated. At first, the settling velocity of flocculated particles will increase with an increase in P_{floc}, but at a certain threshold the settling

velocities will decrease (McAnally, et al., 2007). The dynamics of flocculated settling velocities, depicted in Figure 3.4, will be incorporated into the sediment distribution routine by calculating clay flocculent as:

$$w_{s,floc} = \begin{cases} w_s & C_{floc} < C_1 \\ a\frac{{C_{floc}}^n}{\left({C_{floc}}^2+b^2\right)^m} & C_1 < C_{floc} < C_3 \\ negligible & C_3 < C_{floc} \end{cases} \quad 3.6$$

where C_{floc} is the floc concentration, a=33.38, b=2.537, n=1.83, m=1.89, C1=.1kg/m^3, and C3= 4.38 kg/m^3. The constant values were chosen from a study of flocculated sediments from Lake Okeechobee, as shown in figure 3.5 (Mehta A. J., 1991):

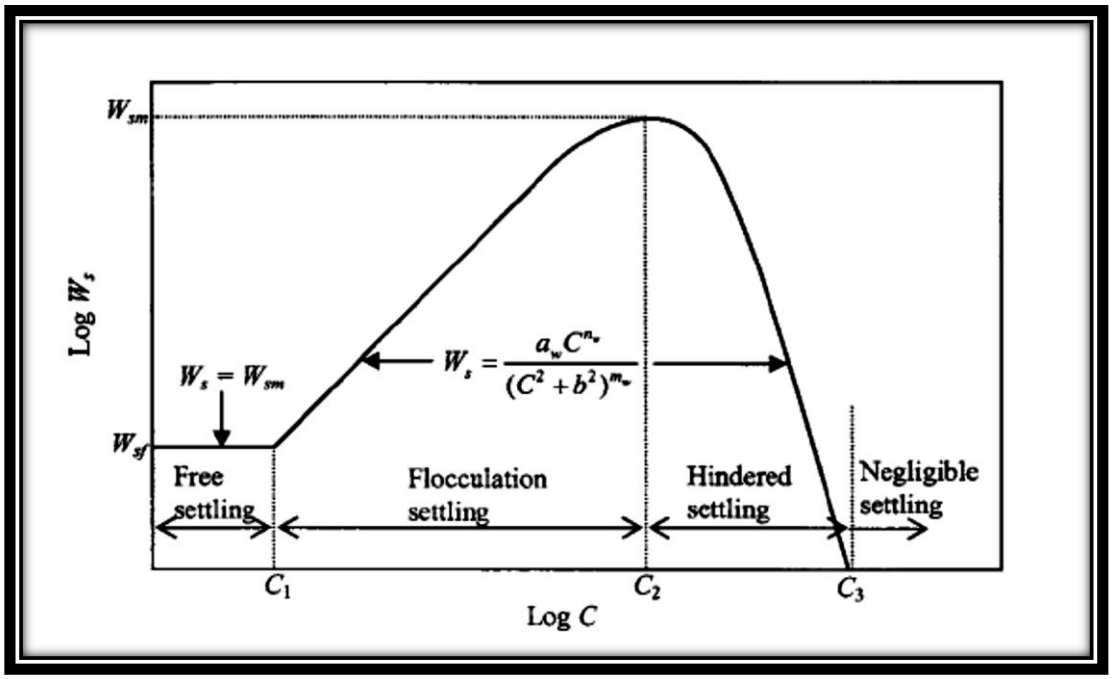

Figure 3. 4. Dynamics of settling velocities of flocculated particles (McAnally, et al., 2007)

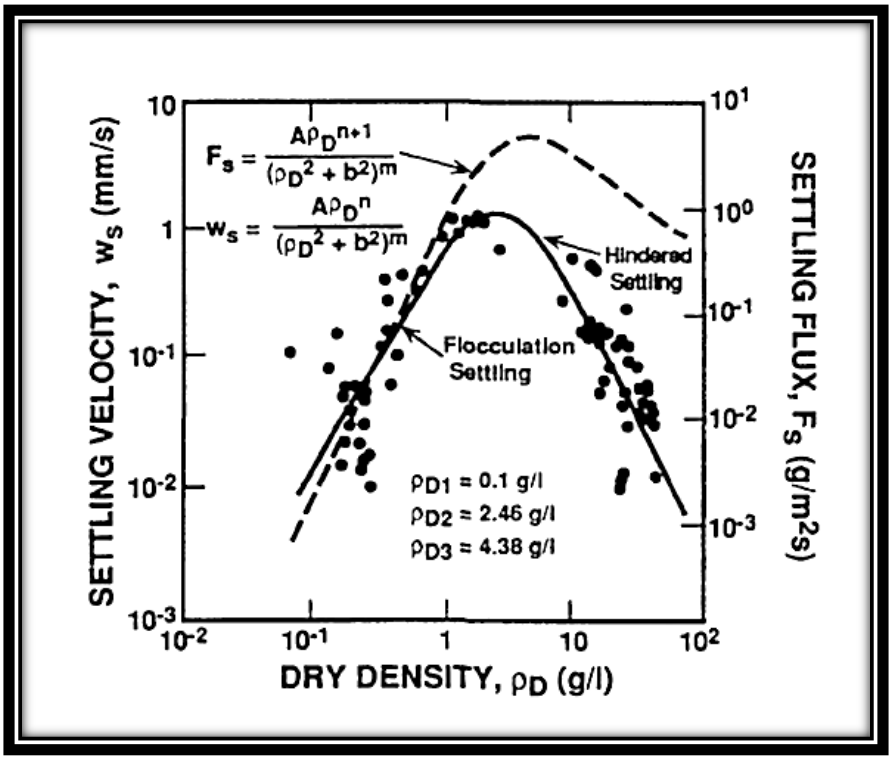

Figure 3. 5. Settling velocities for Lake Okeechobee, as a function of particulate concentration (dry density= particle dry mass/suspension volume) (McAnally, et al., 2007)

The coefficients in equation 3.6 are presented as initial values and can be treated as calibration parameters if required. Possible ranges for C1 = .1-.3 kg/m^3; C3 = 2-5 kg/m^3 (McAnally, et al., 2007). An alternative calculation, to avoid a flocculated fraction, P_{floc}, is to directly include salinity concentration into equation 3.6 by replacing C1 with Csal.

The flocculent settling velocity was found to be approximately 8 m/day in Lake Pontchartrain at a TSS concentration of 40 to 300 mg/L and a salinity of 5 ppt (Roblin, 2008) (Haralampides K. , 2000)

The depositional velocity, $V_{d,k}$, of cohesive sediment (e.g. silt, clay floc, and clay particulate) is related to the settling velocity by the Krone formula (Krone, 1962) (Krone, 1966):

$$V_{d,k} = w_{s,k}(1 - \frac{\tau_{bed}}{\tau_{d,k}}) \qquad 3.7$$

where $w_{s,k}$ is the settling velocity of class, k; τ_{bed} is the bed shear stress; and $\tau_{d,k}$ is the critical velocity for initiation of deposition of class k. Equation 3.7 is applicable only when τ_{bed}>$\tau_{d,k}$. Because there is insufficient field data to distinguish between these two parameters, the depositional critical shear will be equated to the erosional critical shear.

3.3: Resuspension of Sediments: Silts and Clays

3.3.1: Critical Shear Stress

Besides settling, sediment resuspension will be calculated in the 2017 Coastal Master Plan model. Because cohesive and non-cohesive sediments vary in their properties, two resuspension models will be included: one for silt, flocculated clay, and particulate clay, and another for sands.

The main difference in the sediment resuspension calculation of the 2012 Plan and the new one is the method of determining bed shear stresses. The 2012 Plan used wind statistics as a proxy, but this Plan will use a model proposed by Young and Verhagan (1996a) to estimate the bed shear stress (Young & Verhagen, 1996a). Sediment resuspension,E_{res}, in grams per meter squared per second, will be calculated for silt and clay as:

$$E_{res} = \frac{a_c}{T_{res}T_{con}^{m}}\left(\frac{\tau_{bed}}{\tau_{cr}} - 1\right)^{n} \qquad 3.8$$

where a_c is a constant varying with bed properties, usually between 100 and 100,000; T_{res} is the response time of the bed, typically assumed to equal 1 hour; T_{con} is the time since deposition of sediment; *m* and *n* are calibration constants; $\tau_{bed}$is the bed shear stress; and τ_{cr} is the critical shear stress which will result in resuspension for the class of sediment (see table 3.1). To simply this equation, the coefficients a_c, T_{res}, T_{con}, and *m* can be lumped together into a single calibration parameter, while also taking *n* to equal between 1 and 3. This approach has been widely used for resuspension in hydrodynamic models like Delft3D (Deltares, 2013) and ECOMSED (HydroQual, 2002).

Typical values for critical shear stresses for various sediment classes are provided above in Table 3.1 (van Rijn, 2007a).

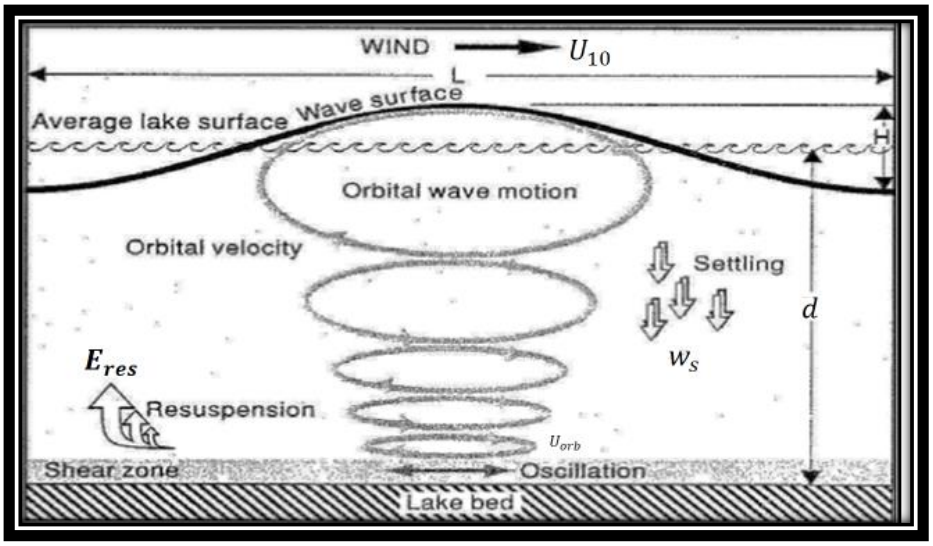

Figure 3. 6. Forces induced by wind that cause resuspension of bed sediment (Laenen & LeTourneau, 1996)

Table 3. 1. Typical values for critical shear stresses for various sediment classes (van Rijn, 2007a)

Particle Size	τ_{cr}	Notes
6 μm	0.25 N/m^2	Quartz particles in cohesive beds with bulk densities of 1,600-1,900 kg/m^3
50 μm	0.08 N/m^2	Quartz particles
8-62 μm	0.1 N/m^2	Weakly consolidated, fine sediments
>200 μm	0.2-0.4 N/m^2	Sand
	0.5 N/m^2	Default value used in Delft3D-Flow

Bed shear stress will be calculated from the Young and Verhagan wave model and linear wave theory, to be discussed in Section 3.3.2.

Ghose-Hajra et. al. (2014) used the Lick Shaker Test (Sheng & Lick, 1979); (Haralampides K. , 2000) to measure the critical shear stress for erosion of cohesive marsh bed sediments as a function of consolidation time, displayed in Figure 3.7 (Ghose-Hajra, McCorquodale, Mattson, Jerolleman, & Filostrat, 2014).

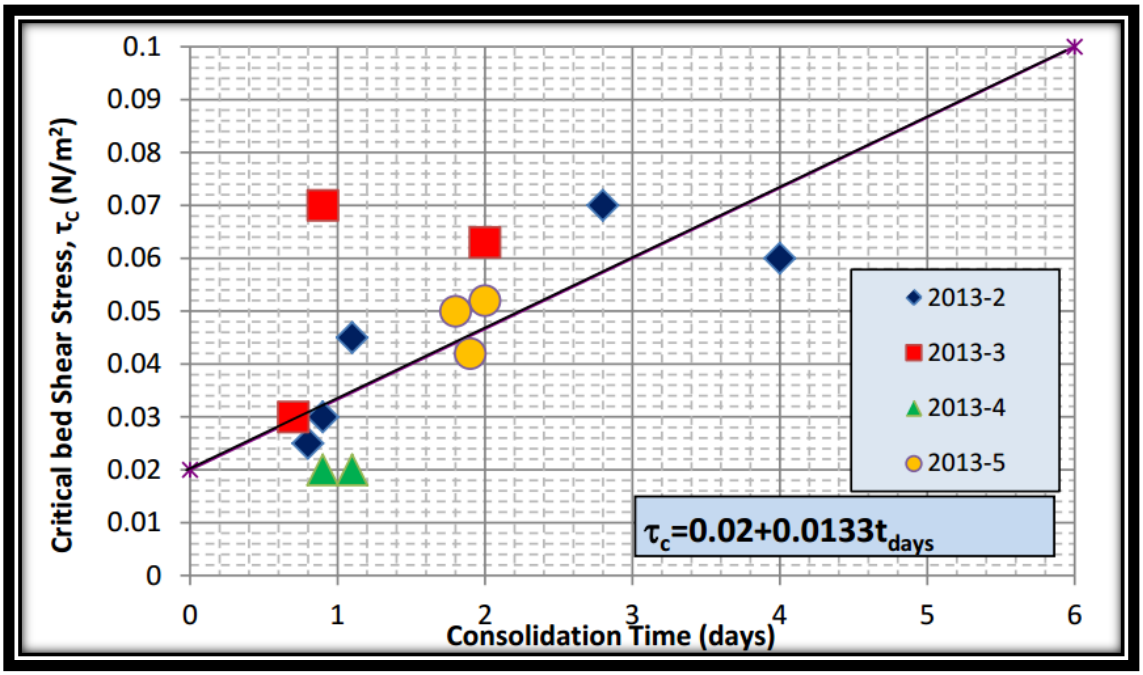

Figure 3. 7.Variation of Critical Bed Shear stress with consolidation time (Ghose-Hajra, McCorquodale, Mattson, Jerolleman, & Filostrat, 2014)

Results show that the critical shear stress increases nearly linearly from approximately 0.02 Pa to 0.1 Pa in 6 days. Because the inter-storm period is roughly 6 days, the critical shear stress of 0.1 Pa in Table 3.1 appears to be justified for the sediment classes being treated here.

3.3.2: Bed Shear Stress

A critical component of the sediment distribution calculation described above is the bed shear stress which will be calculated from the following equation:

$$\tau_{bed} = C_f \rho_w {U_{bed}}^2 \qquad 3.9$$

where C_f is a constant approximately equal to 0.0025 (USACE, 2002), ρ_w is water density, and U_{bed} is the bed velocity, to be calculated as:

$$U_{bed} = \mathrm{U} + U_{tide} + U_w + U_{orb} \qquad 3.10$$

The compartment's flow velocity, $\mathrm{U} + U_{tide}$ will be determined from the flows in and out of the open water compartment:

$$(\mathrm{U} + U_{tide}) = \frac{\{\sum|Q_{in}| + \sum|Q_{out}|\}}{2A_x} \qquad 3.11$$

where $\sum|Q_{in}|\ and\ \sum|Q_{out}|$ is the magnitude of the sums of the flows in and out, respectively; A_x is the effective cross-section of the open water cell (the effective cell width by depth). The cell width will be assigned in the cell attributes and the depth is computed in the hydrodynamic simulation.

The wind induced currents, U_w, (Ekman, 1905), (Keulegan, 1951), (Rossby & Montgomery, 1935) will be estimated from wind speed, U_{wind} (or U_{10}), by:

$$U_w = k_a U_{wind} \quad (3.12)$$

where k_a is in the range 0.023 to 0.032.

The orbital velocity, U_{orb}, will be estimated from linear wave theory:

$$U_{orb} = \frac{gH_s T \cosh\left(\frac{2\pi z}{L}\right)\cos\theta}{2L\cosh\left(\frac{2\pi d}{L}\right)} \quad (3.13)$$

The orbital velocity is to be calculated at the bed therefore the height above the bed in equation 3.13, z, will equal zero. Equation 3.13 will be calculated for a maximum orbital velocity, which will occur at a wave phase of θ=0, reducing the equation to:

$$U_{orb} = \frac{gH_s T}{2L\cosh\left(\frac{2\pi d}{L}\right)} \quad (3.14)$$

where *g* is gravitational acceleration, H_s is significant wave height, *T* is wave period, *L* is wavelength, and *d* is water depth (Demirbilek & Vincent, 2002).

Wavelength can be iteratively solved from depth and wave period (eq. 3.15).

$$L = \frac{gT^2}{2\pi}\tanh\left(\frac{2\pi d}{L}\right) \quad (3.15)$$

However, a reasonably accurate (±10%), non-iterative approximation correction for wavelength (eq. 3.16) can be used for simplicity, equation 3.17 (Demirbilek & Vincent, 2002).

$$L \approx L_o \tanh\left(\frac{2\pi d}{L_o}\right) \quad (3.16)$$

$$L_o = \frac{gT^2}{2\pi} \quad (3.17)$$

Equations 3.13-3.17 require three input variables: Period (*T*), Significant wave height (H_s), and depth (*d*). Depth was the only variable calculated in the 2012 Master Plan open water components, therefore, the Young and Verhagen wave model will be incorporated into the open water calculations in order to find the other two parameters needed for bed shear calculations.

By fitting established wave spectrum equations to observed datasets (See Ch. 2), Young and Verhagen developed empirical relationships for wave energy, *E*, and frequency, *V*, from depth, *d*, fetch, *F*, and wind speed, U_{10}. A non-dimensional energy, ϵ, and non-dimensional peak frequency, ν is developed below (Young & Verhagen, 1996a):

$$\epsilon = 3.64 * 10^{-3}\left\{\tanh A_1 \tanh\left(\frac{B_1}{\tanh A_1}\right)\right\}^n \quad (3.18)$$

$$\nu = 0.133\left\{\tanh A_2 \tanh\left(\frac{B_2}{\tanh A_2}\right)\right\}^m \quad (3.19)$$

$$A_1 = 0.493 * \delta^{0.75} \quad (3.20a)$$

$$B_1 = 3.13 * 10^{-3} * \chi^{0.57} \quad (3.20b)$$

$$A_2 = 0.331 * \delta^{1.01} \quad \text{3.21a}$$

$$B_2 = 5.215 * 10^{-4} * \chi^{0.73} \quad \text{3.21b}$$

$$\delta = g * \frac{d}{U_{10}^2} \quad \text{3.22a}$$

$$\chi = g * \frac{F}{U_{10}^2} \quad \text{3.22b}$$

Values for the coefficients *n and m*, originally proposed by Young and Verhagen, are *n=1.74 and m= -0.37.*

Solving for energy, E, and peak frequency, f_p, and from these, significant wave height, Hs, and Period, T:

$$E = \frac{\epsilon * U_{10}^4}{g^2} \quad \text{3.23a}$$

$$H_{rms} = \sqrt{8 * E} \quad \text{3.23b}$$

$$H_s = \sqrt{2} * H_{rms} \quad \text{3.23c}$$

$$f_p = \frac{\nu * g}{U_{10}} \quad \text{3.23d}$$

$$T = 1/f_p \quad \text{3.23e}$$

Comparing the Young and Verhagen wave heights with the Corps of Engineers Shore Protection Manual (USACE, 2002), good agreement for shallow water bodies are found, as indicated in Figures 3.8 and 3.9.

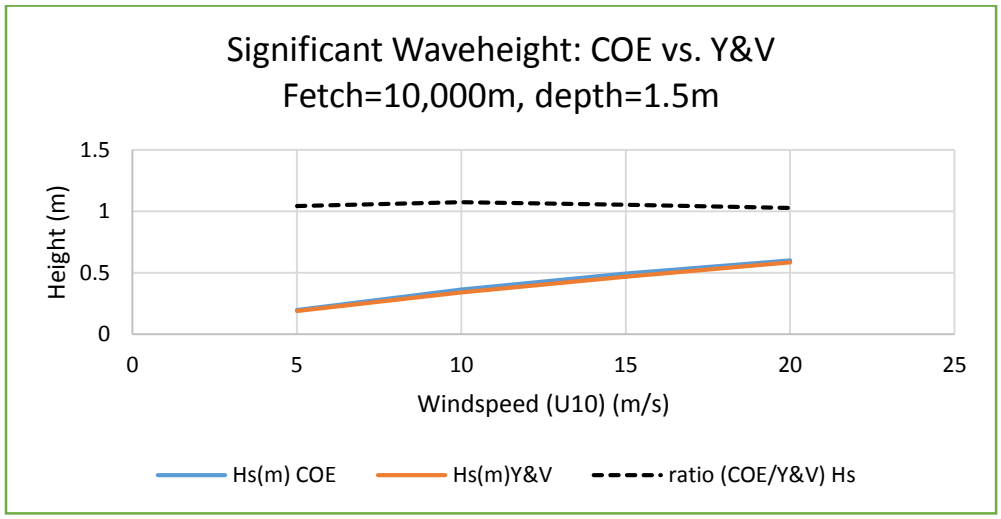

Figure 3. 8. Comparison of significant wave heights from the Corps of Engineers and Young and Verhagen

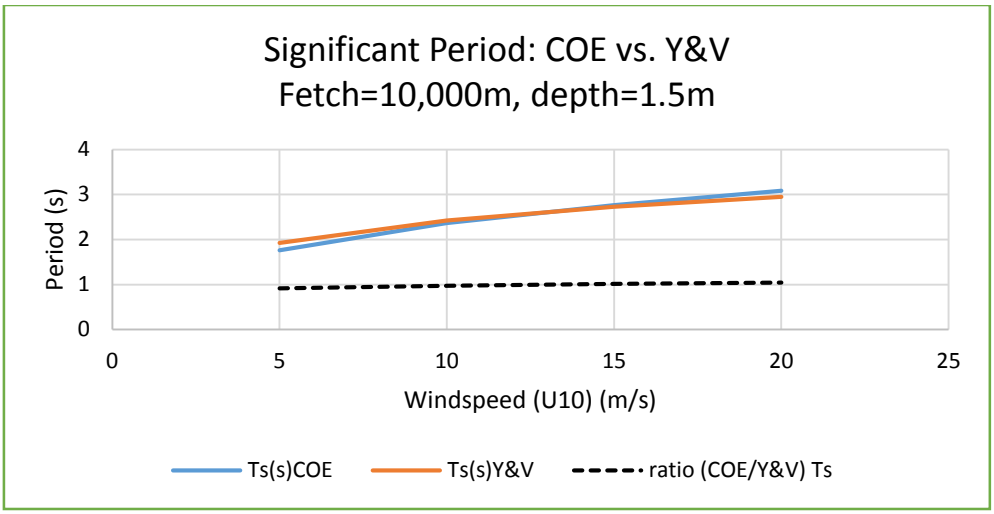

Figure 3. 9. Comparison of significant periods from the Corps of Engineers and Young and Verhagen

3.4: Resuspension of Sediments: Sand

There are have been ways to quantify the resuspension of sands, but the method to be used in this thesis was developed by van Rijn (van Rijn, 2007a)which provides the mechanics in channelized flow. Sand particles will be resuspeneded into the water column if the dimensionless shear stress, ϑ, is greater than the dimensionless critical shear stress which defines the initiation of motion for sand particles, ϑ_{cr},

$$\vartheta = \frac{\tau_{cr}}{(\rho_s - \rho_w) g D_{50}} \tag{3.24}$$

Typical values for the critical shear stress, τ_{cr}, are provided in 3.1, and all other variables have been defined above. Empirical values for critical shear stress for initiation of motion of sand particles, ϑ_{cr}, have been developed by van Rijn (van Rijn, 2007a),

$$\vartheta_{cr} = \begin{cases} 0.115 {D_*}^{-0.5} & D_* < 4 \\ 0.14 {D_*}^{-0.64} & 4 \leq D_* < 10 \end{cases} \tag{3.25}$$

$$D_* = D_{50} \left[\frac{g\left(\frac{\rho_s}{\rho_w} - 1\right)}{\upsilon^2} \right]^{1/3} \tag{3.26}$$

If $\vartheta > \vartheta_{cr}$, the potential rate of sediment, in particularly sands, transport in kg/s/m can be calculated by combining the following equations 3.27-3.32:

$$q_s = \alpha_s \rho_s u D_{50} {M_e}^{2.4} {D_*}^{-0.6} \tag{3.27}$$

$$M_e = \frac{(u_e - u_{cr})}{\sqrt{g D_{50}\left(\frac{\rho_s}{\rho_w} - 1\right)}} \tag{3.28}$$

$$u_e = u + \gamma u_{orb} \tag{3.29}$$

$$u_{cr} = \left(\frac{u}{u+u_{orb}}\right) u_{cr,c} + \left(\frac{u}{u+u_{orb}} - 1\right) u_{cr,w} \quad (3.30)$$

$$u_{cr,c} = \begin{cases} 0.19{D_{50}}^{0.1} \log\left(\frac{12d}{3D_{90}}\right) & 0.1\ mm < D_{50} < 0.5\ mm \\ 8.5{D_{50}}^{0.6} \log\left(\frac{12d}{3D_{90}}\right) & 0.5\ mm < D_{50} < 2\ mm \end{cases} \quad (3.31)$$

$$u_{cr,w} = \begin{cases} 0.24\left[\left(\frac{\rho_s}{\rho_w} - 1\right) g\right]^{0.66} {D_{50}}^{0.33} T^{0.33} & 0.1\ mm < D_{50} < 0.5\ mm \\ 8.5\left[\left(\frac{\rho_s}{\rho_w} - 1\right) g\right]^{0.57} {D_{50}}^{0.43} T^{0.14} & 0.5\ mm < D_{50} < 2\ mm \end{cases} \quad (3.32)$$

where *u* is the depth-averaged velocity for each time step (considering all flow forcings), α_s is a coefficient ranging from 0.008 to 0.012, γ is a coefficient which is either 0.4 for irregular waves or 0.8 for regular waves, D_{90} is the 90th percentile particle diameter, *T* is the wave period, and all other variables are defined above (van Rijn, 2013).

3.5: Development of time step formulas

In order to successfully integrate the above formulations into the new State Master Plan code, a one cell example will be explored here.

Three inputs are needed from each cell: its depth, fetch, and wind speed for each time step. Consider the following cell taken from the south west section of Lake Pontchartrain:

Figure 3. 10. South West section of Lake Pontchartrain (Google Maps, 2014)

This cell, from here on referred to as cell j, possesses a constant depth, and a distance for the directions that the wind can blow, i.e. a fetch; in this case 16 fetches are specified as shown in Figure 3.11 (USGS, 2014).

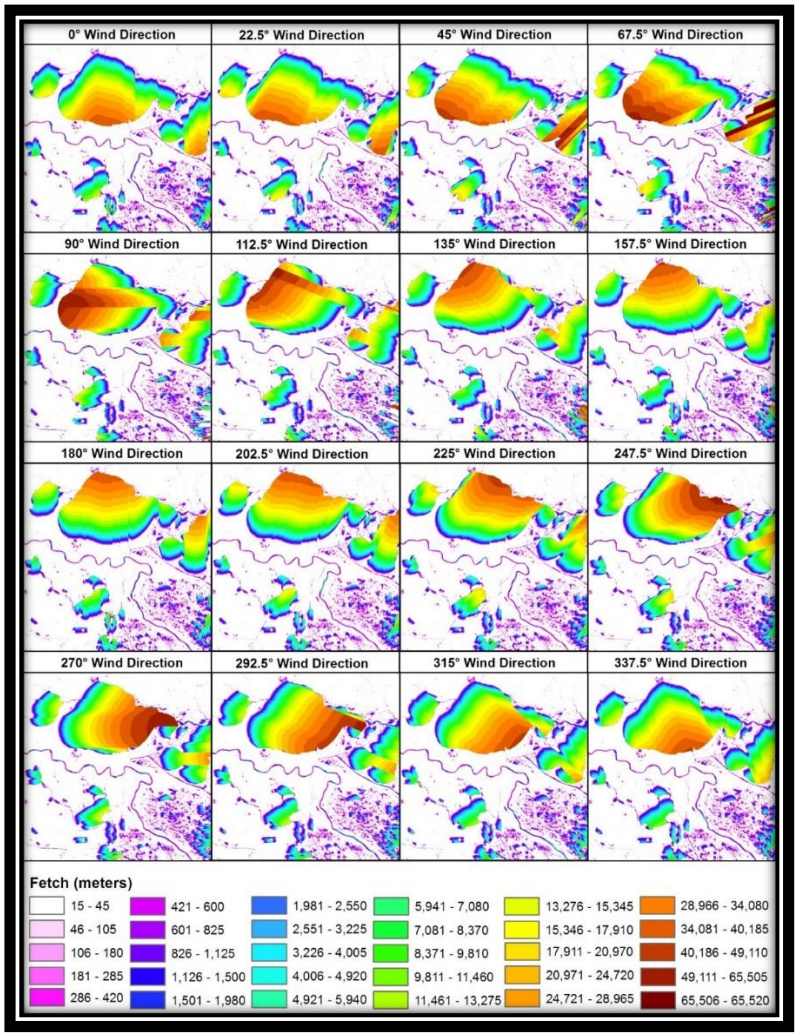

Figure 3. 11. Lake Pontchartrain Fetch Map (USGS)

Recorded daily metadata, collected from various locations around the lake and river give the daily wind speed and direction in which it is blowing, in degrees. Because FORTRAN does not recognize a zero integer, these data are normalized to match a corresponding bin (16 total. See Figures 3.12-3.14).

Windspeed (m/s)	Direction (degrees N)
5.3	19.55
5.2	50.4
5.3	75.81
5.4	72.2
5.4	72.5
5.5	63.44
5.4	92.36
5.2	56.7
5.1	69.33
5	91.89

Figure 3. 12. Metadata of a daily time step, with wind speed and direction

+1	Degrees Integer
20.55	20
51.4	51
76.81	76
73.2	73
73.5	73
64.44	64
93.36	93
57.7	57
70.33	70
92.89	92

Figure 3. 13. Each value for direction is normalized into an integer.

From Map		
4th quad, lake Pontchartrain		
Bin	Degrees	Fetch
1	348.76-11.25	20971
2	11.26-33.75	16000
3	33.76-56.25	17910
4	56.26-78.75	27721
5	78.76-101.25	9811
6	101.26-123.75	7081
7	123.76-146.25	5940
8	146.26-168.75	4921
9	168.76-191.25	5941
10	191.26-213.75	8370
11	213.76-236.25	15346
12	236.26-258.75	24721
13	258.76-281.25	35000
14	281.26-303.75	37000
15	303.76-326.25	29000
16	326.26-348.75	27000

Figure 3. 14. Each normalized direction is placed into a bin of 1-16 representing a fetch

From these data inputs, a fetch, wind speed, and depth can be taken to satisfy the equations that require them. This will then produce a significant wave height, period, orbital velocity, and bottom shear stress.

With each sediment class' settling velocity pre-determined, a resuspension term can be found for each time step. Figure 3.15 summarizes the process.

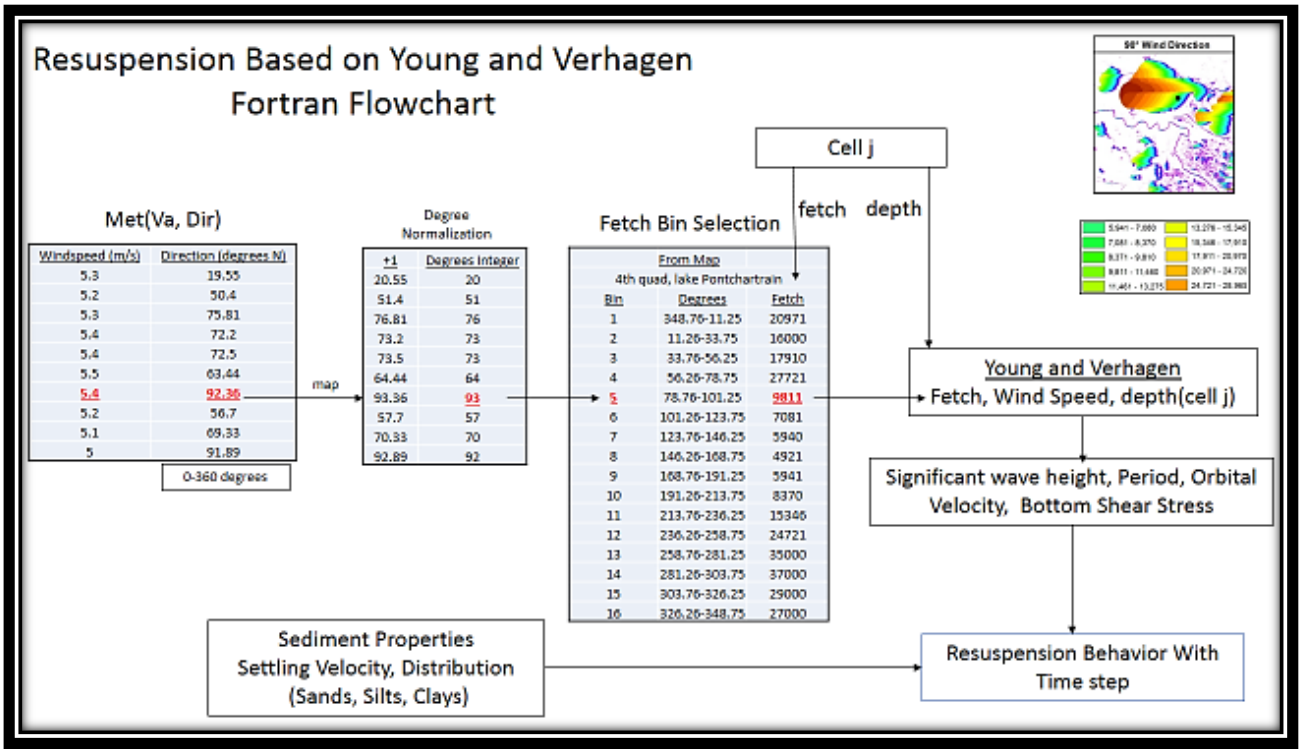

Figure 3. 15. Summary of parameter selection process

Now with a value of resuspension for each sediment class and time step, and a calculated value for settling velocity, a differential equation for concentration in the water column can be developed:

$$\frac{dm_k}{dt} = (V_{res_k} - W_{s_k} C_k) A_s \quad 3.33$$

$$C_k = \frac{m_k}{\forall} \quad 3.34$$

where $\frac{dm_k}{dt}$ is the change of mass (m_k) of sediment class, k, over time; V_{res_k} is the value for resuspension for sediment class, k; $W_{s_k}$is the settling velocity for sediment class, k; C_k is the concentration of sediment class k; A_s is the surface area of the water column, and ∀ is the volume of the water column ($A_s * h$)

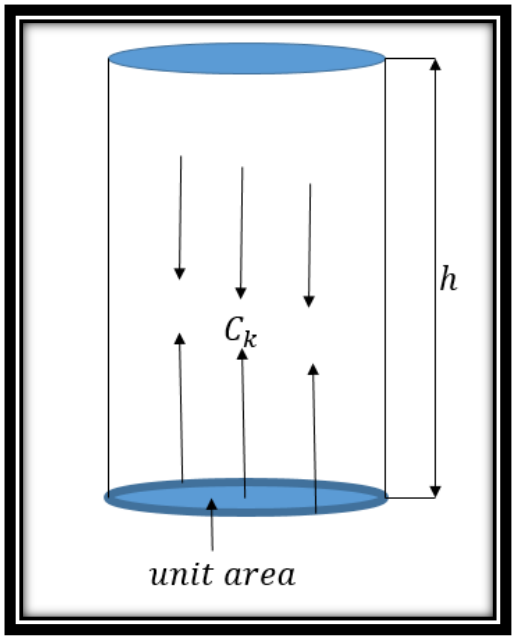

Figure 3. 16. Water column with height, h, and surface area, As

From equation 3.33, it can be said:

$$m_k^{n+1} = m_k^n + \left(V_{res_k} - W_{s_k} C_k\right) \Delta t A_s \quad 3.35$$

Solving for concentration of sediment class k by dividing the mass by the volume of the water column, or cell, a time step function for concentration is developed.

In the case of a diversion, three scenarios must be considered:

I. $(u + u_w) < u_{cr},\ q_s = 0;\ therefore\ deposition\ rate = Q_{s_{in}}$ 3.36a

II. $(u + u_w) > u_{cr}\ and\ Q_{s_{in}} > bq_s;\ Q_{s_{out}} = bq_s;\ therefore\ deposition\ rate = Q_{s_{in}} - bq_s$ 3.36b

III. $(u + u_w) > u_{cr}\ and\ Q_{s_{in}} < bq_s;\ Q_{s_{out}} = bq_s;\ therefore\ erosion\ rate = bq_s - Q_{s_{in}}$ 3.36c

where u the depth is averaged velocity, u_w is the adjusted wind velocity (eq. 3.12), q_s is the rate of sediment resuspension for sand (eq. 3.27), $Q_{s_{out}}$ and $Q_{s_{in}}$ is the flow of sediments in and out, and b is the width. Possible ways to estimate b, proposed by (McCorquodale, 2014), is

$$b = F_{cal} * \sqrt{A_s} * (Aspect\ Ratio) \quad 3.37$$

where F_{cal} is a calibration factor; A_s is the open water surface area; and $Aspect\ Ratio$ is the ratio of (open water width)/(open water length). These parameters would be provided as a cell attribute.

$Q_{s_{out}}$ is dependent on the wind velocity inequalities, but $Q_{s_{in}}$ can be written as:

$$Q_{s_{in}} = C_s(u * b) \quad 3.38$$

and,

$$\frac{\Delta Deposition}{day} = \left(\frac{W_k C_k - V_{res}}{d}\right) * \Delta t$$

Potential instabilities can be resolved with the central difference solution method. Consider equation 3.39:

$$\frac{dC_k^{n+1}}{dt} = \frac{Q}{As}\left(\frac{C_{in} - C_{cell}^n}{d}\right) + \left(\frac{V_{res}^n - Ws_k^n * C_k^n}{A_s d}\right)A_s \quad 3.39$$

and,

$$\bar{C_{cell}} = \left(\frac{C_{cell}^{n+1}}{2} + \frac{C_{cell}^{n-1}}{2}\right) \quad 3.40$$

which has the form

$$u = AC + D \quad 3.41$$

with

$$u_1 = -\left(\frac{Q_{div}}{Ad} + \frac{w_s}{d}\right)C_1 + \left(\frac{V_{res}}{d} + \frac{Q_{div}C_{in}}{Ad}\right) \quad 3.42$$

$$A = -\left(\frac{Q_{div}}{Ad} + \frac{w_s}{d}\right) \quad 3.43$$

$$D = \left(\frac{V_{res}}{d} + \frac{Q_{div}C_{in}}{Ad}\right) \quad 3.44$$

Differentiating equation 3.41,

$$du = AdC \quad 3.45$$

$$C = \frac{u - D}{A} \quad 3.46$$

$$\left(\frac{1}{A}\right)\left(\frac{du}{dt}\right) = u \quad 3.47$$

$$\int_{u1}^{u2} \frac{du}{u} = \int_0^{\Delta t} A dt \quad 3.48$$

$$\ln(u)\,|_{u1}^{u2} = A\Delta t \quad (3.49)$$

$$\ln\left(\frac{u2}{21}\right) = A\Delta t \quad (3.50)$$

Solving for u_2,

$$u_2 = u_1 e^{A\Delta t} \quad (3.51)$$

and a new concentration, C2, can be determined:

$$C_2 = \frac{-A_1C_1 + D_1 e^{A_1\Delta t} - D_2}{-A_2} \quad (3.52)$$

$$C_2 = \frac{-\left(\frac{Q_{div_1}}{Ad} + \frac{w_s}{d}\right)C_1 + \left(\frac{q_{s_1}}{d} + \frac{Q_{div_1}C_{in}}{Ad}\right) - \left(\frac{q_{s_2}}{d} + \frac{Q_{div_2}C_{in}}{Ad}\right)}{-\left(\frac{Q_{div_2}}{Ad} + \frac{w_s}{d}\right)} \quad (3.53)$$

Chapter 4: Model Setup

4.1: Variables and Constants

Defined below are the default variables and constants within the model.

General:

- g: because all formulations in this model are in metric, the gravitational constant is taken to be 9.81m/s^2
- D_{50}: the median particle diameter for each class of sediment is given in table 4.1.
- ρ_s: the particle density for each sediment class is 2650 kg/m^3
- ρ_w: the density of water varies as salinity and temperature concentration varies. But for simplicity's sake, the general density of water is taken as 1000 kg/m^3.
- ν: the kinematic viscosity of water varies as function of temperature (Figure 3.1) but to minimize the inputs from the main program, the general kinematic viscosity is taken as 0.000001 m^2/s

Sand	Silt	Clay, Floc	Clay, Particulate
0.18mm	0.03125mm	0.002mm	0.006mm

Table 4. 1. Median Particle Diameter of each class of sediment

Temperature, C	Ws Sand (m/s)	Ws Silt (m/s)	Ws Clay Particulate (m/s)
10	0.0221	0.0001	2.46E-05
15	0.0253	0.0008	2.81E-05
20	0.0286	0.0009	3.19E-05
25	0.0322	0.0010	3.58E-05
30	0.0359	0.0010	4.00E-05

Table 4. 2. Settling Velocities versus Temperature

Equations 3.5-3.6 describe how the flocculation process is considered in the model.

- $P_{floc,max}$: The maximum percentage of clay able to flocculate is 0.6, or 60%
- C_{sal}: the average salinity concentration will vary from 0.2 parts per thousand (ppt) to 5ppt, to be defined.
- $C_{sal,max}$: The maximum salinity concentration is 5ppt.
- C_{floc}: in general, the percentage of clay that will be in flocculated form will be 60%, so $C_{floc} = 0.6 * C_{clay\ total}$
- a=33.38
- b=2.537
- n=1.83
- m=1.89
- C_1=0.1kg/m^3
- C_3=4.83 kg/m^3

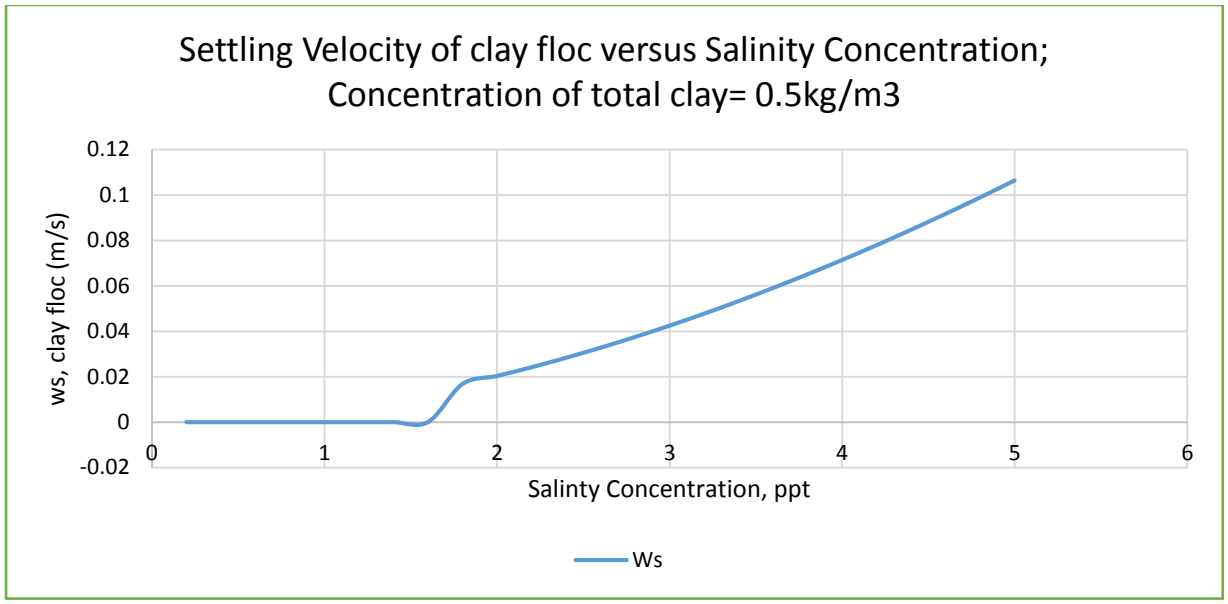

Figure 4. 1. Clay floc settling velocity and salinity.

To reduce the complications in the model calculations, a constant settling velocity for clay floc is taken as 0.004 m/s.

Equations 3.8-3.32 describes the processes of resuspension for each class of sediment.

- a_c: throughout test trials, it was found a value of 35,000 best complimented this model.
- T_{res}= the response time of the bed is taken to be 1 hour, or 60 seconds.
- T_{con}=the time since deposition of sediment can vary from 1 day to over 2 weeks. If the bed shear is considered slightly greater than the critical, e.g. $\tau_{bed} = 0.15$ and $\tau_{cr} = 0.1\ Pa$, sediment resuspension varying with T_{con} is show in figure 4.2. Unless otherwise stated, the default consolidation time since deposition will be 6 days.
- m=1
- τ_{cr}: Table 3.1 show typical values for critical shear stress. 0.1 N/m^2 is the default for all sediments besides sand.
- n: this coefficient can vary from 1.5 to 3. The default here is 3.
- C_f=0.0025
- k_a: this coefficient can vary from 0.023 to 0.032. It is taken to be 0.0275 by default
- n=1.74
- m-0.37
- α_s: this coefficient can range from 0.008 to 0.012. It is taken to be 0.01 by default
- γ: this coefficient is either 0.4 for irregular waves or 0.8 for regular waves. Because waves being dealt with here are shallow, only irregular parameters are considered, thus 0.4 is the default value here.
- D_{90}=0.0003m

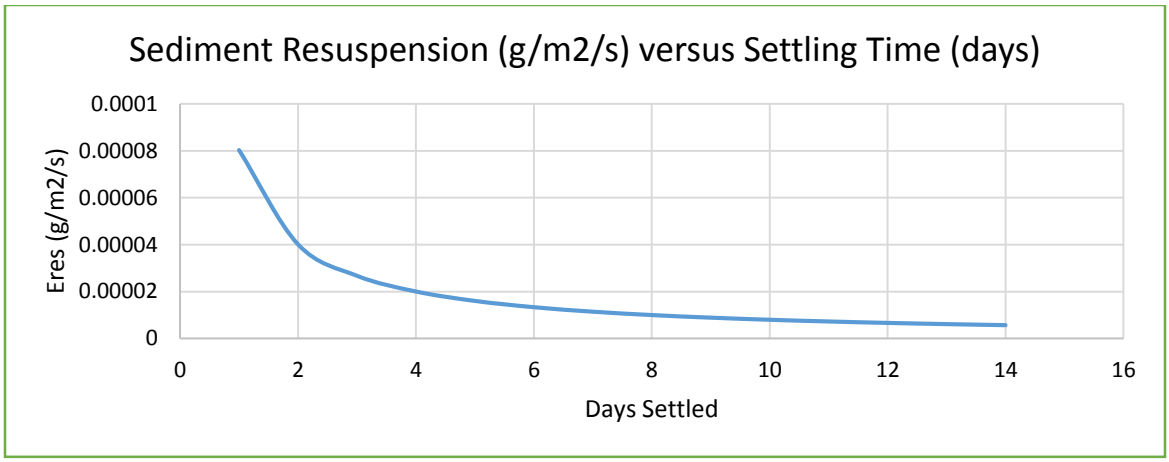

- *Figure 4. 2. Eres as a function of Tcon*

4.2: Data Sample

As mentioned in Chapter 3, the south-west quadrant of Lake Pontchartrain was chosen as an example to use with this model because. Its sediment characteristics and behaviors have been previously studied, and offers a solid reference to validate the model. The examples presented will use recorded data acquired from the New Orleans Airport containing the average wind speed and direction per day. This data set was applied to the model to represent real changes in ambient conditions.

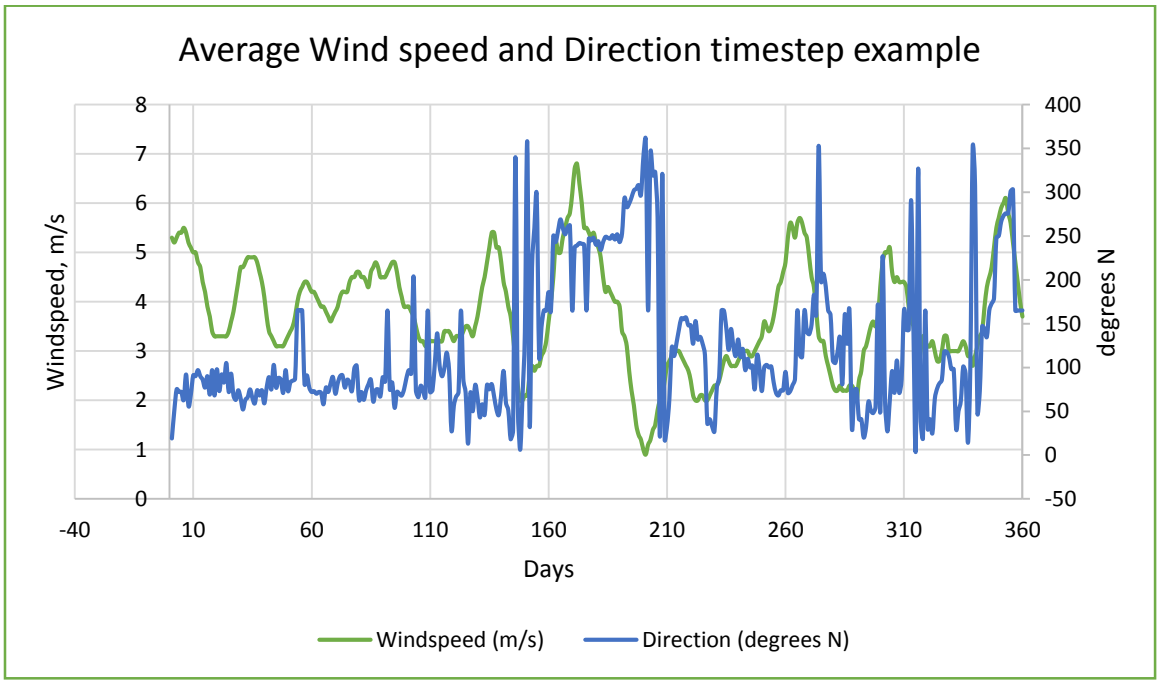

Figure 4. 3. Input data example: Wind speed and direction

5.1: Sediment Behavior in Open Water

Many variables work together in the above equations, so changing one or two can lead to very different results.

The three main inputs from the master program are depth, wind speed, and fetch (a function of the direction of the wind).

Using an example array of wind speeds and the corresponding direction (Figure 3.12) and matching the direction to a corresponding fetch (Figure 3.11), equation 3.35 can be applied to a 1m by 1m by 3.4m water column representative of the quadrant of Lake Pontchartrain in Figure 3.10.

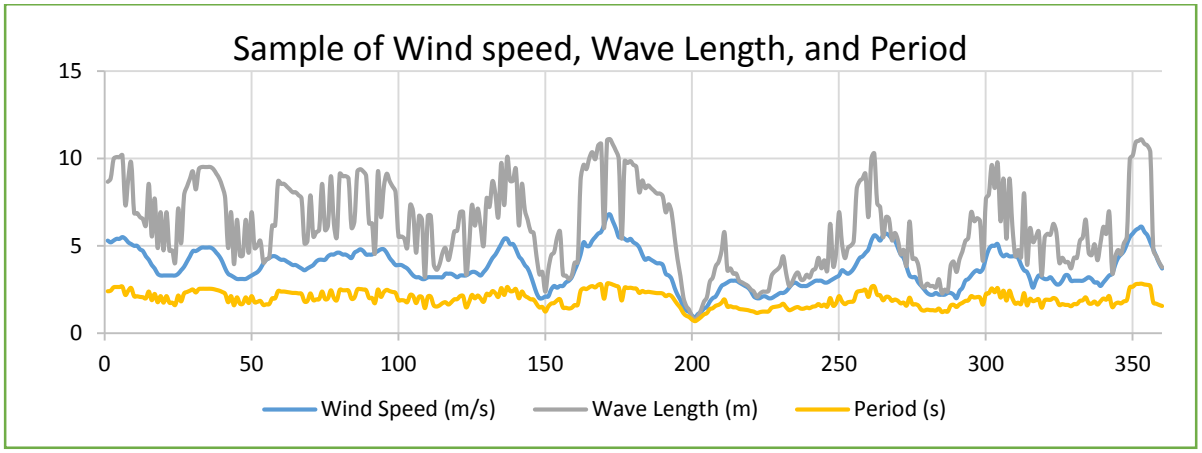

Figure 5. 1. A 5,000 point sample of wind speeds was taken from the USGS. 360 points are shown, with the wave length and period calculated according to the formulations of Young and Verhagen

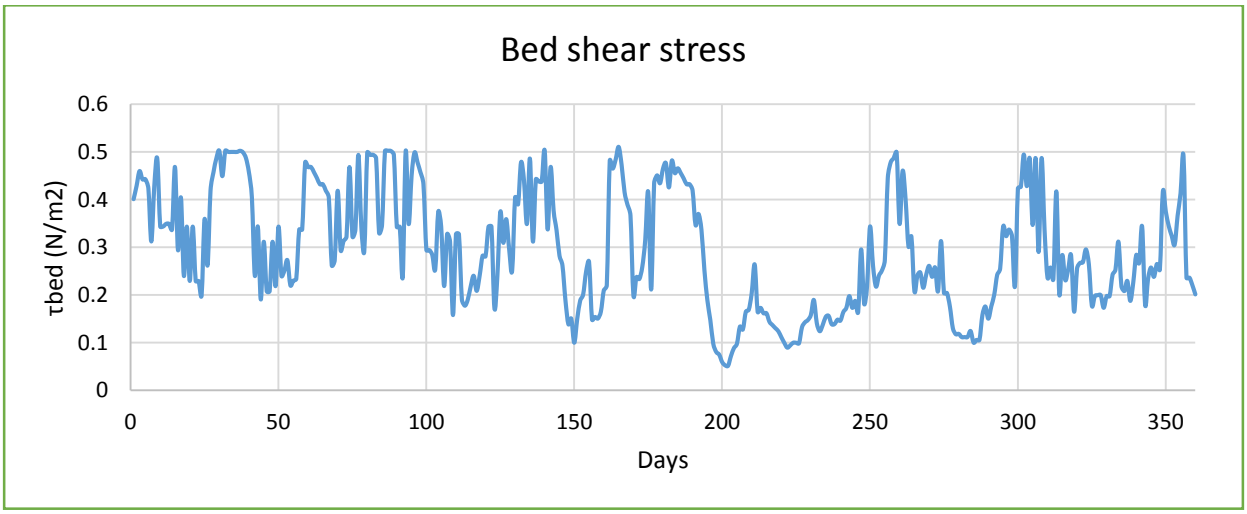

Figure 5. 2. The corresponding bed shear stress, a driving factor of resuspension, is calculated from the results of the sample array (Figure 5.1). Bed shear above the critical shear results in resuspension

With the inputs shown in Figures 5.1 and 5.2, the resuspension factor, in $g/m^2/s$, can be calculated for silt and clay particles, using equation 3.8.

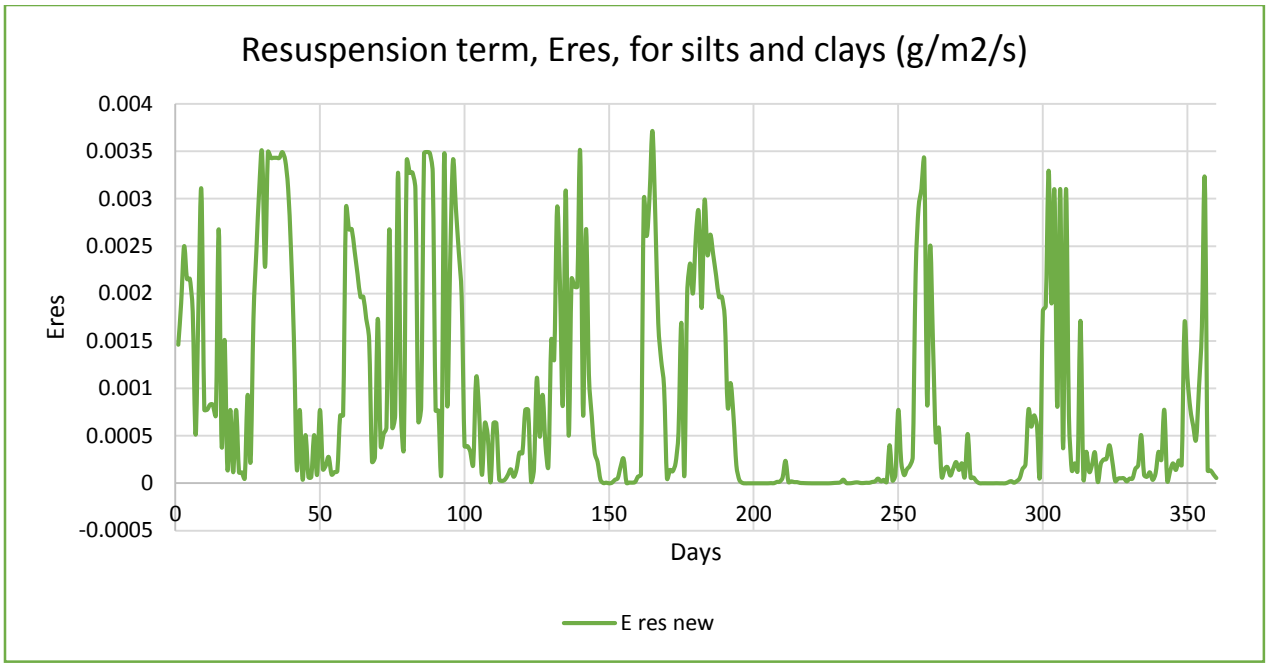

Figure 5. 3. Resuspension of silts and clays with respect to 360 point example sample

Using the resuspension term from figure 5.3 and applying it to 3 classes of sediments, each taking a percentage of the total suspended solids (silt:20%, Clay floc: 60%, clay particulate: 20%; the water column activity can be simulated as shown in Figure 5.4.

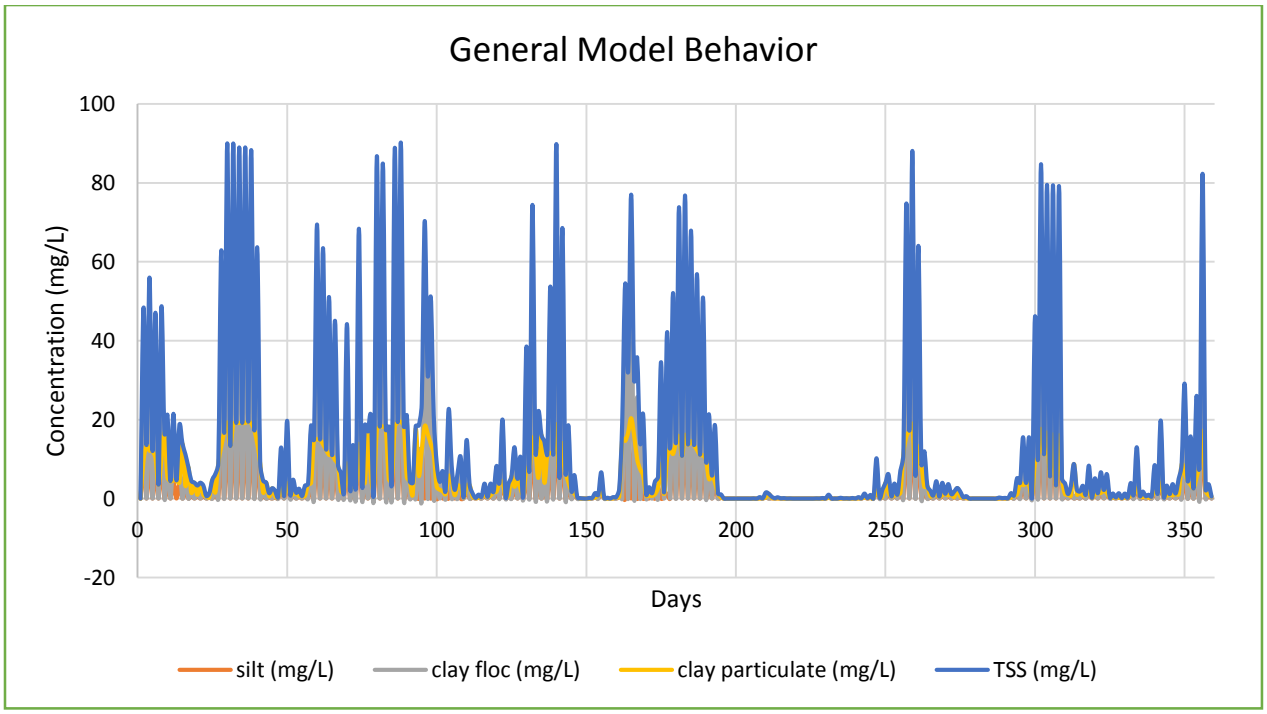

Figure 5. 4. Illustrates the general sediment behavior under default conditions of chapter 4.

Sand is not included in Figure 5.4 because its resuspension term was never strong enough to invoke a reaction more than a few micrograms per liter, but it is included in the TSS portion of Figure 5.4. It is important to note here how the calculation for bed velocity can play a huge role in the bed shear stress. The compartment's flow velocity, $(\mathrm{U} + U_{tide})$, is very low (0.1m/s) because this example is taken to be on the lake where there is not much compartment flow in or out. Changing this even a small bit has a huge effect on bed shear, and in turn, on resuspension. Setting the flow velocity to 0.25m/s results in concentrations almost 8 times higher. Haralampides (2000) presents a survey of tidal flow in Lake Pontchartrain (Haralampides K. , 2000) (see Section 2.5).

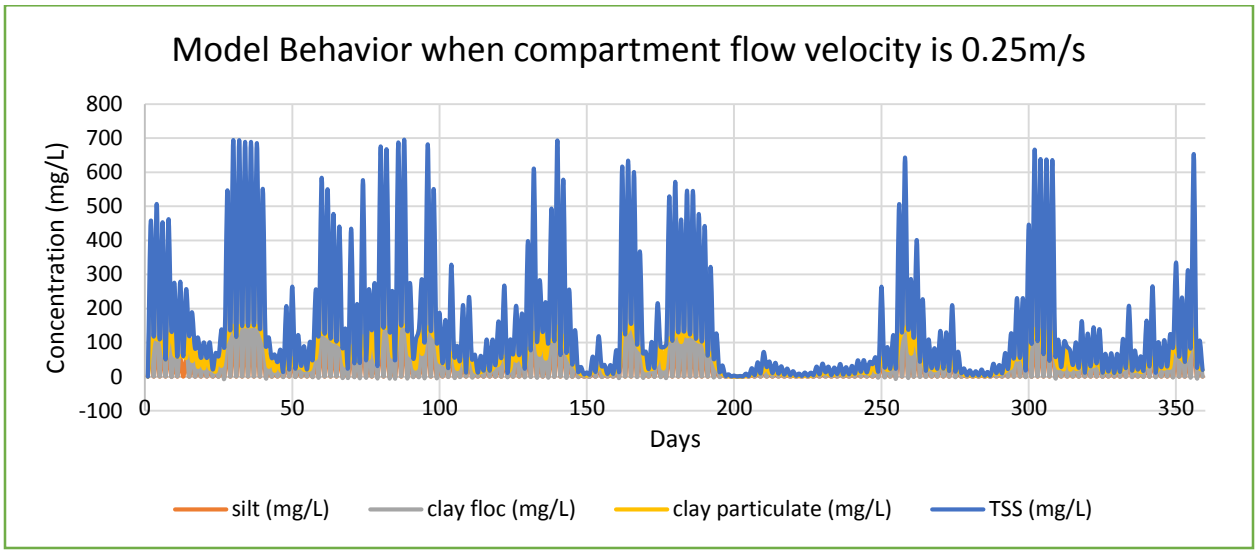

Figure 5. 5. Compartment flow velocity plays an important role by influencing the bed shear stress. Here is an example when the velocity is 0.25m/s, as opposed to 0.1 m/s in Figure 5.4.

Notice how the time step, Δt, in Figures 5.1-5.5 is 1 day (86,400 seconds). The sediment reaction can be observed if we take Δt to be one minute. The wind speed and direction array is the same 360 steps as above.

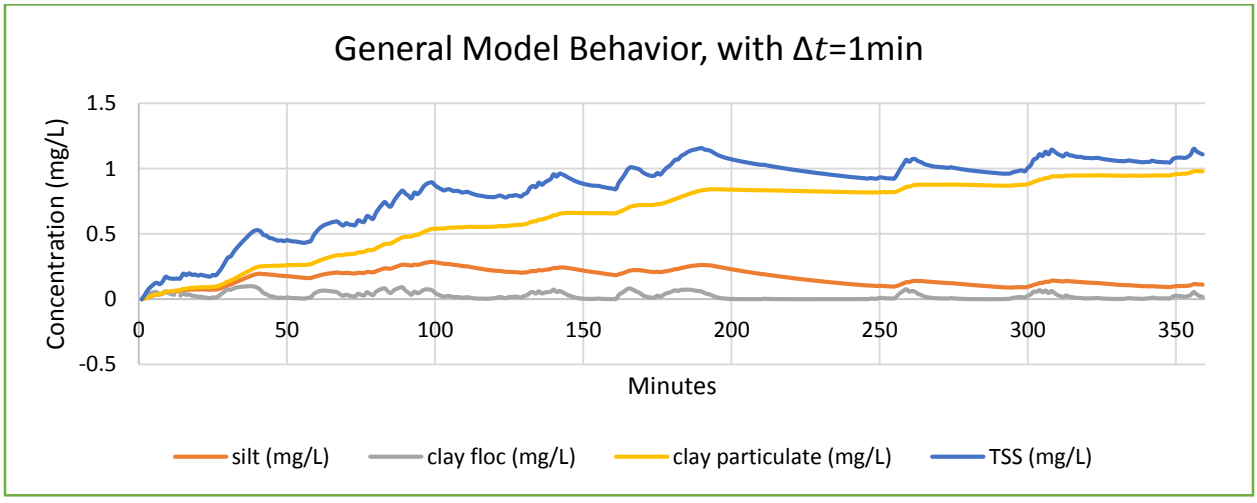

Figure 5. 6. Instead of running the model by days, it can be taken by minutes. Each time step represents a change in wind speed and fetch, minute by minute.

Consolidation time, T_{con}, is an interesting factor that also plays an important role in the model. Setting calculations back to default with a time step of 1 day, T_{con} can be changed from 6 days of undisturbed consolidation time:

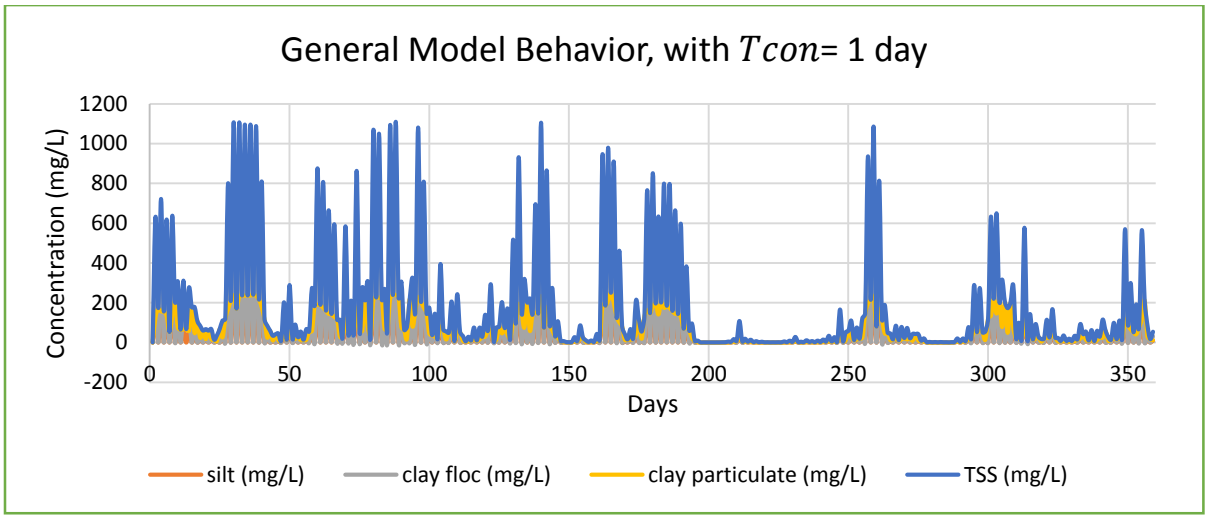

Figure 5. 7. Here the model is run with the sediment consolidation time equal to 1 day. This means the sediments are not packed tightly together and more prone to resuspension

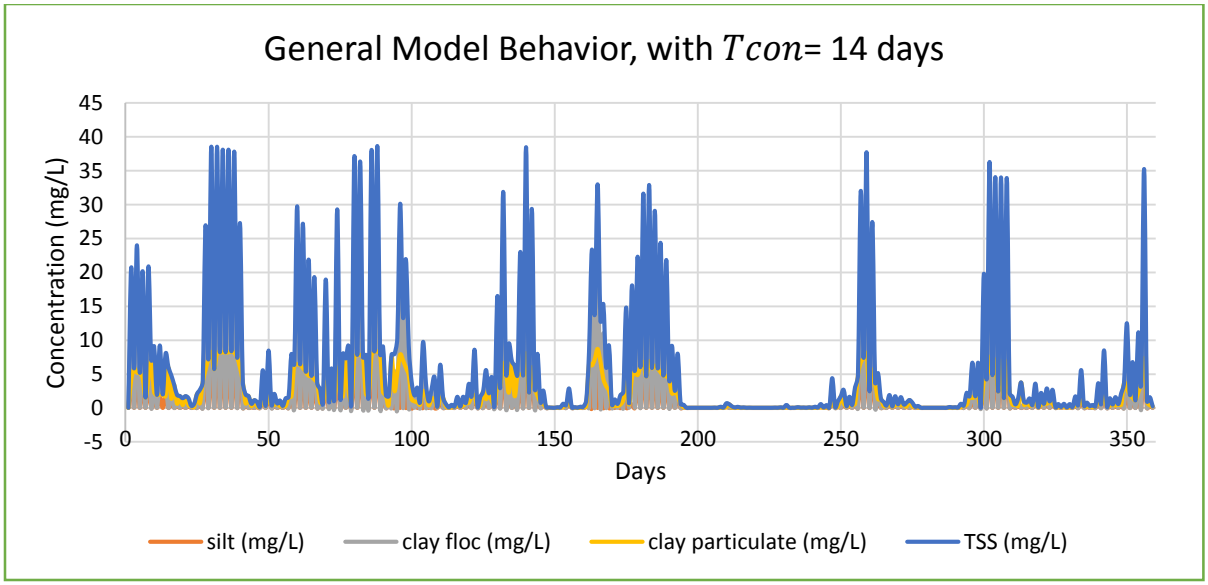

Figure 5. 8. Time of consolidation is two weeks in this example. The sediment has been sitting on the bed being packed tightly by water pressure and is less prone to resuspension

Following the results of (Ghose-Hajra, McCorquodale, Mattson, Jerolleman, & Filostrat, 2014), critical bed shear stress, τ_{cr}, can be set to 0.06 N/m2 and $Tcon$ to 3 days:

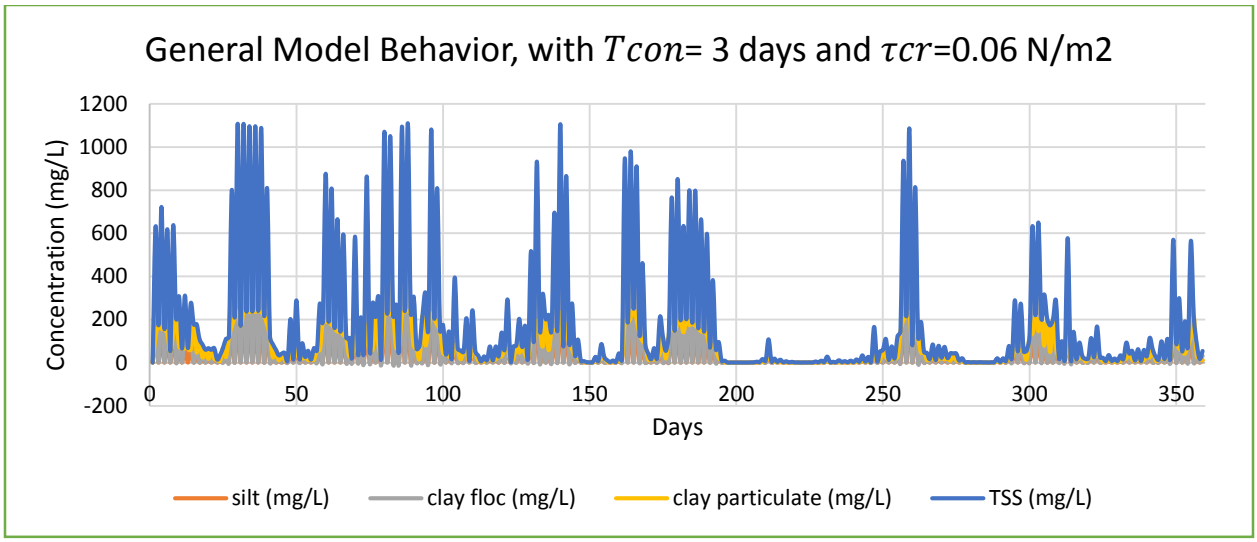

Figure 5. 9. Here we kept all other variables default but changed the critical shear and time of consolidation to 0.06N/m2 and 3 days, respectively, to match the study of (Ghose-Hajra, McCorquodale, Mattson, Jerolleman, & Filostrat, 2014)

Depth determines how easily the wind forces can reach the bed through the orbital velocity. Resuspension of a shallow water column verses a deep is more susceptible to the winds.

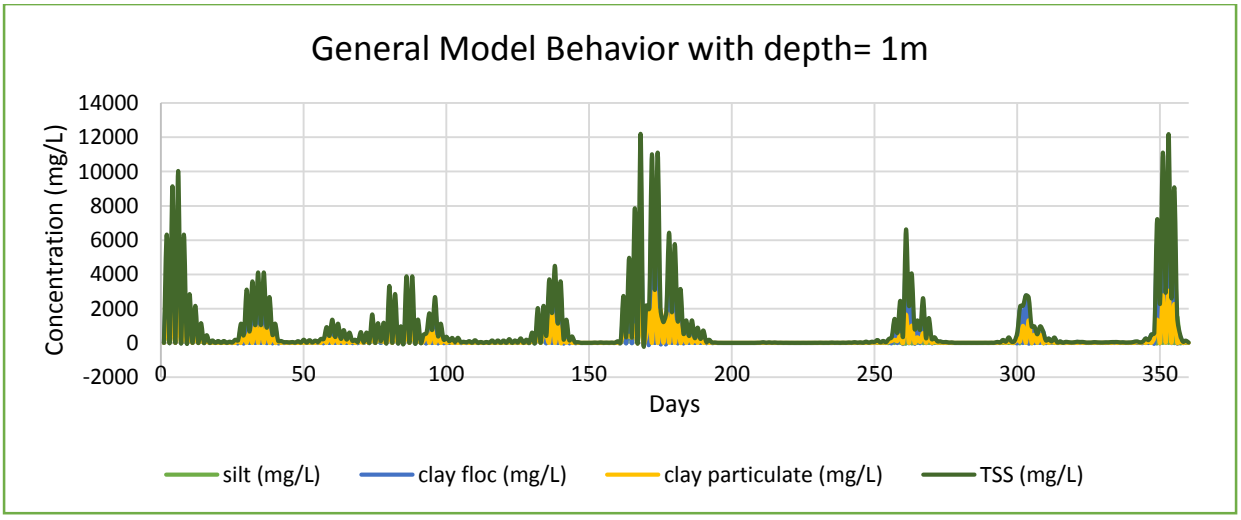

Figure 5. 10. Here the model is the same as default except for the average depth, which is taken to be 1m.

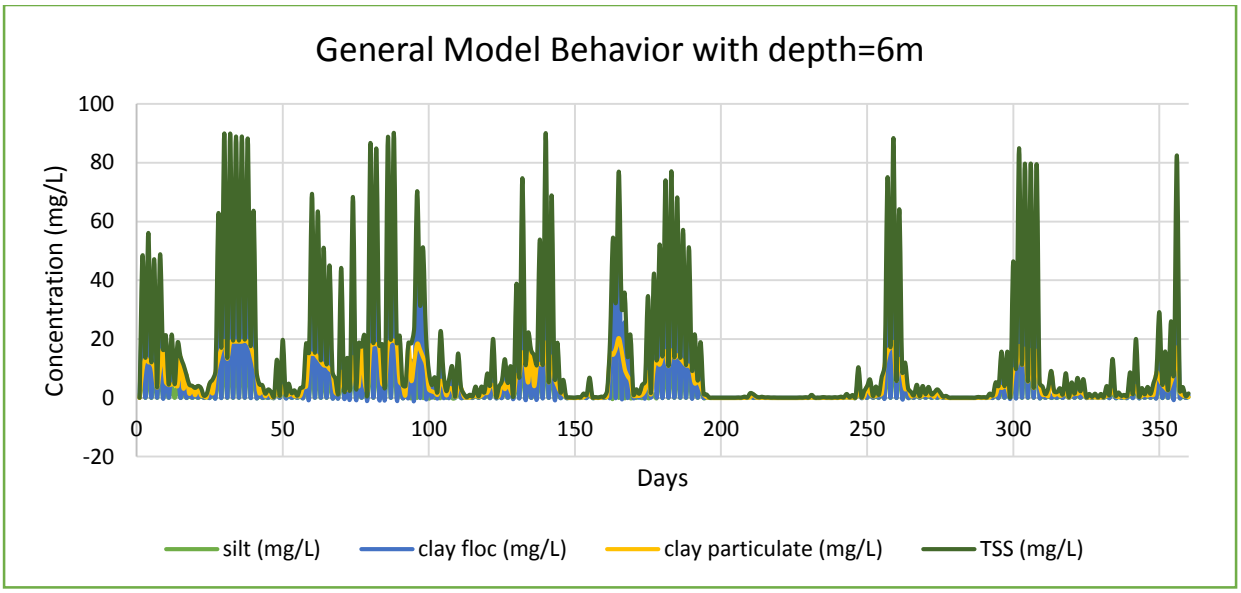

Figure 5. 11. With 6 meters of average depth, the example plot shows a significantly less amount of resuspension.

Figure 5.12 shows how 5,000 point array of wind speeds and directions relate to TSS concentration. Figure 5.13 does the same with bed shear stress and wind speed.

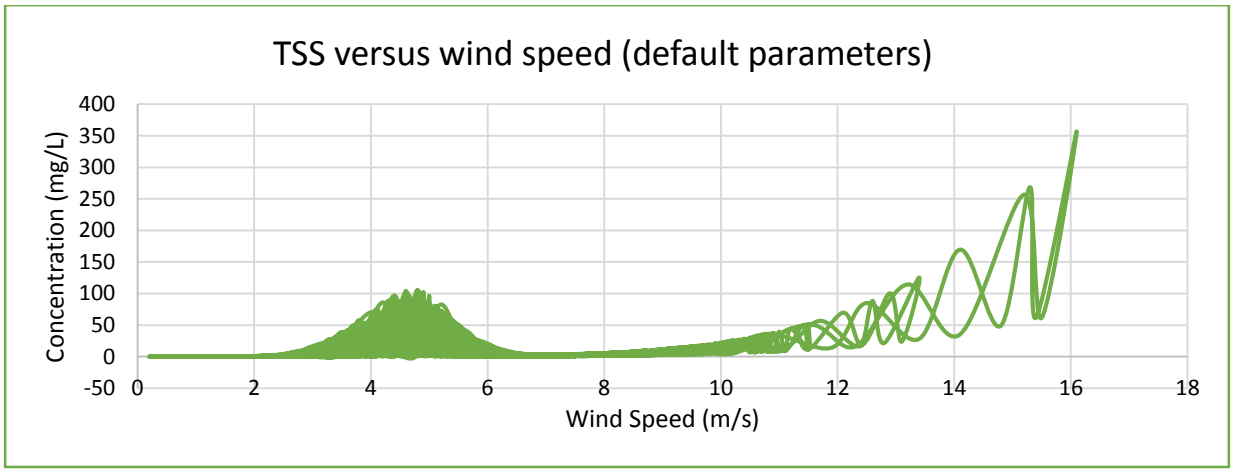

Figure 5. 12. Here the wind speeds with corresponding directions of a 5,000 point sample are matched to the total suspended solid concentrations they cause. Outliers are towards the right.

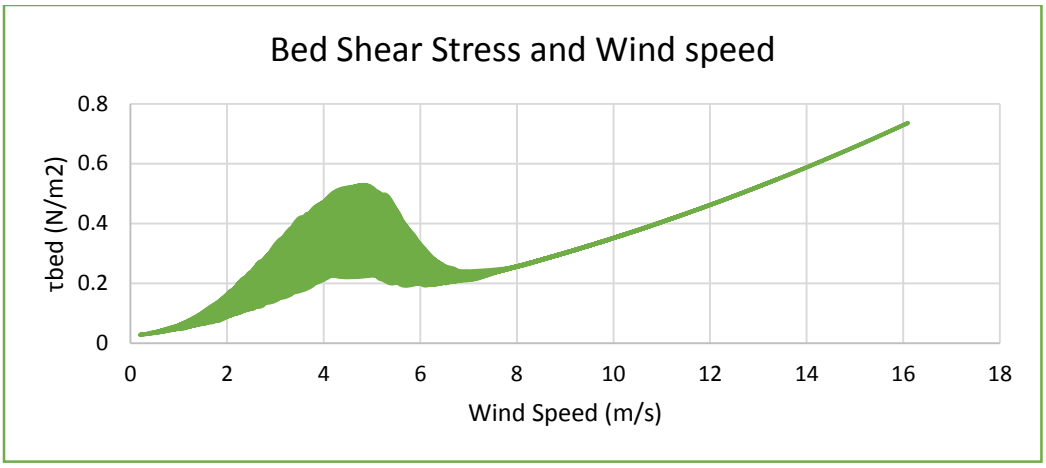

Figure 5. 13. Bed shear stress is compared to wind speed with 5,000 points

5.2: Sediment Behavior with respect to Diversions

Because the compartment velocity of the cell is higher in river and diversion areas, not only does resuspension of silts and clays increase, but sands come into play with a greater impact. Consider a river with the following daily discharge:

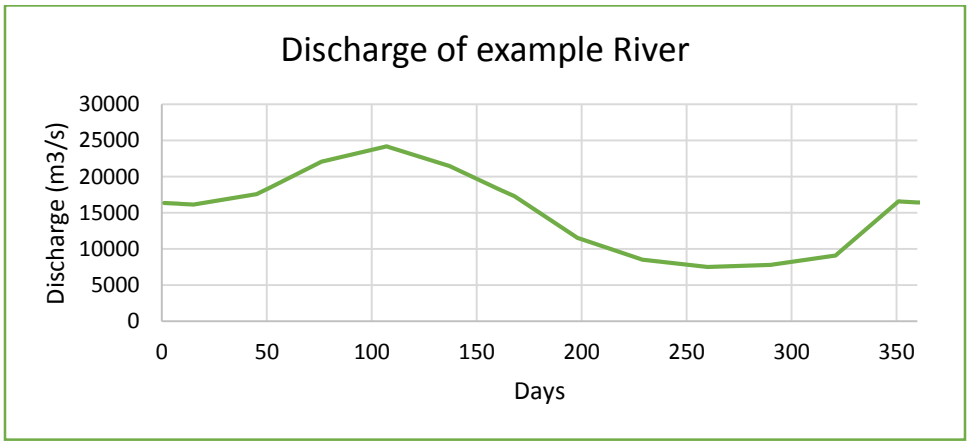

Figure 5. 14. Example of daily discharge of the Mississippi River, borrowed from the State Master Plan model (CPRA, 2012)

Connected to this river at some point is a diversion, 5,000 meters in length, a top width of 3,000 meters, and depth of 3m. Water from the river will become a flow in the diversion according to the following table.

Q_{river}	$Q_{diversion}$
0-17,000m^3/s	$0m^3/s$
17,001-18,200m^3/s	Q_{river}-17,000m^3/s
>18,201m^3/s	1,200m^3/s

Table 5. 1. Example behavior of diversion flow

Using the discharge from Figure 5.14 and the behavior from Table 5.1, the diversion flow is presented in Figure 5.16.

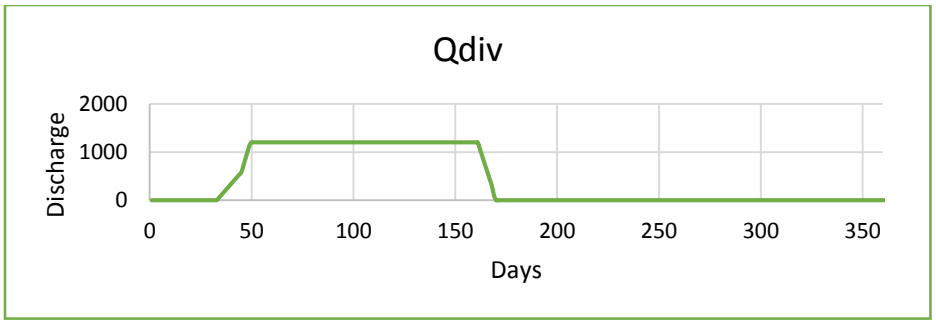

Figure 5. 15. Discharge of Diversion, flow extraction

Using equation 3.36 as the governing formula, the south east Lake Pontchartrain fetch array, and setting the concentration of suspended sand in the river water to 10 mg/L, deposition (positive) and erosion (negative) is plotted for 360 days below. The strong wind and significant fetch of the recorded input data keep the potential rate of sediment transport, q_s, high. This causes sand transport and erosion. If the diversion with a width b, is made narrower, from 3000 m, 971 m, and 300 m, erosion is even greater (Figure 5.16-18). With a full width of 3000m, there is more deposition, with a net of about 3 kg at the end of the year. When the width is equal to 971 m, the net is zero. With a width of 300 m, the net erosion is 560 kg total at the end of the year.

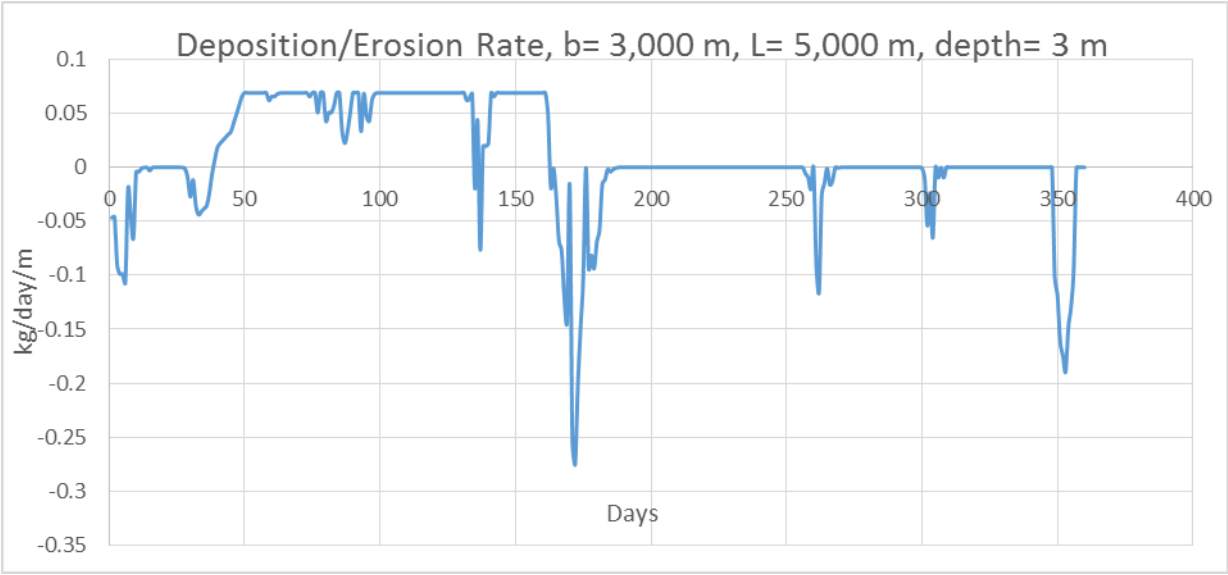

Figure 5. 16. Deposition and Erosion of sand in a diversion, width=3000 m

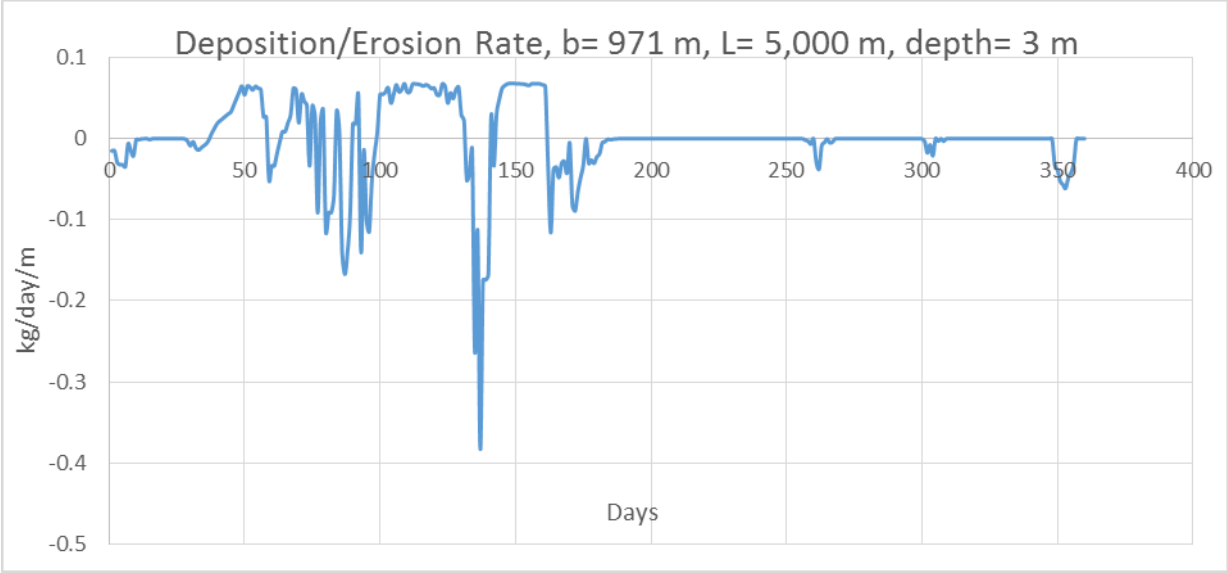

Figure 5. 17. Deposition and Erosion of sand in a diversion, width=971 m

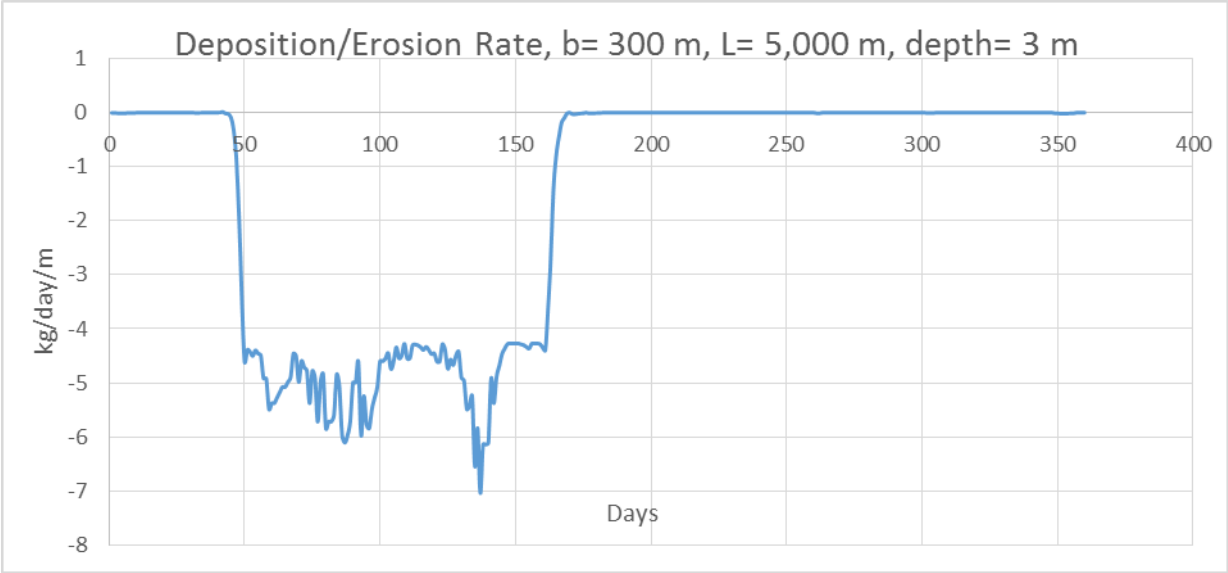

Figure 5. 18. Deposition and Erosion of sand in a diversion, width= 300 m

Silt and Clay also get deposited in diversions, as shown in Figures 5.22-5.25. Silt and Clay particulate both had a concentration in of 5 mg/L and Clay floc had 10 m/L. High erosion is observed when the diversion inflow produces high compartment currents.

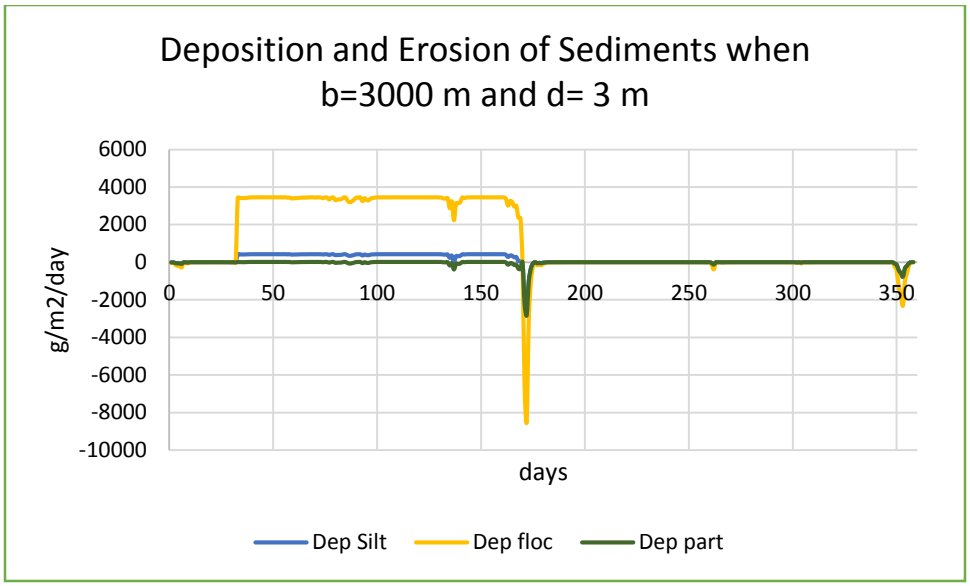

Figure 5. 19. Deposition and Erosion of sediments when the width of the diversion is 3000 m and the depth is 3 m

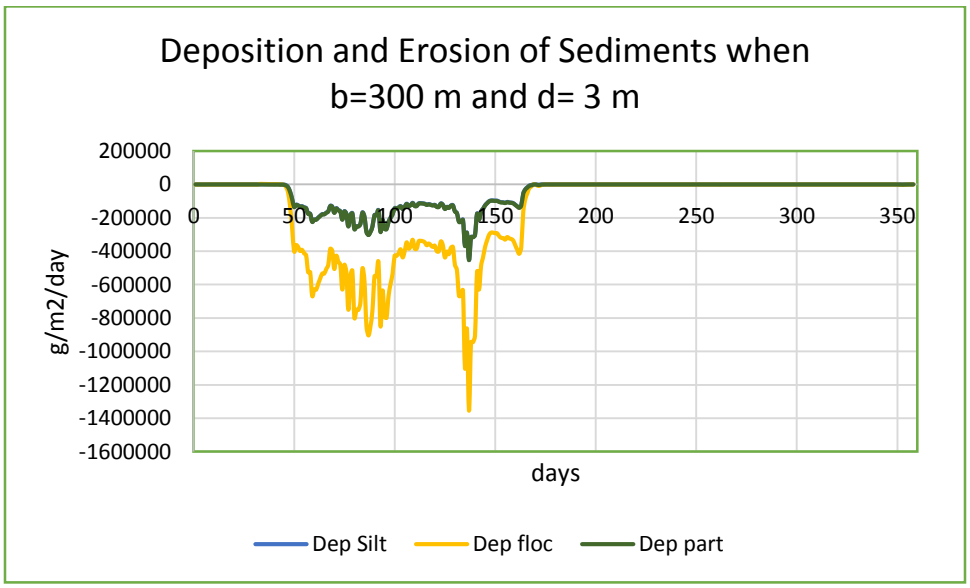

Figure 5. 20. Deposition of Clay Particulate in a Diversion in g/m2 over one year

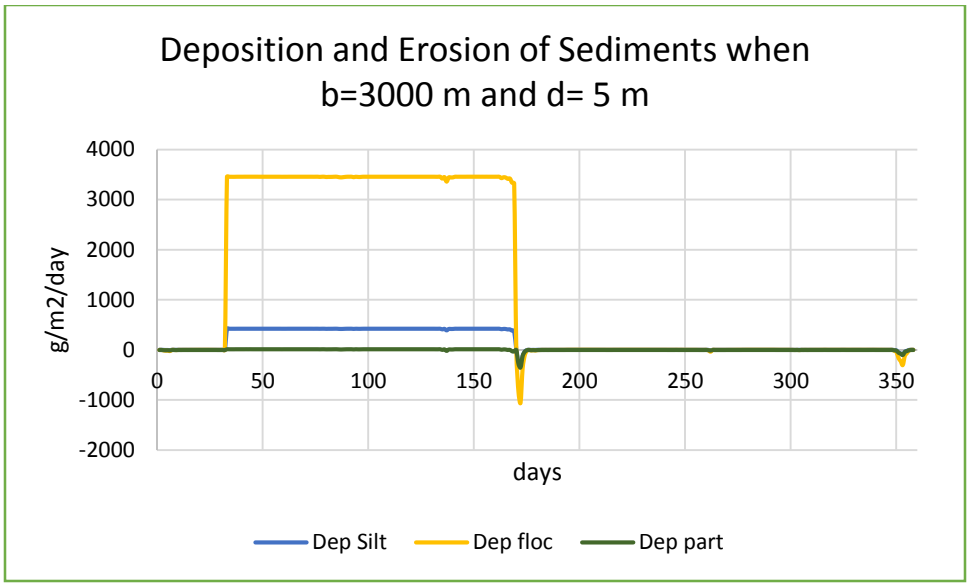

Figure 5. 21. Deposition of Clay Floc in a Diversion in g/m2 over one year

Table 5.2 illustrates the cumulative deposition or erosion over the year for each scenario.

Table 5. 2. A cumulative deposition (positive) or erosion (negative) for each class of sediment.

	Cumulative silt (g/m2/year)	Cumulative floc (g/m2/year)	Cumulative particulate (g/m2/year)
b=3000 m,d=3 m	44350.44	434019.1	-11031.2
b=300 m,d=3 m	-2E+07	-5.9E+07	-2E+07
b=3000 m,d=5 m	56199.6	469566.6	817.9331

5.3: Conclusion and Recommendations

This thesis was focused on integrating wind currents, flow, and orbital velocity to determine bed shear and transport with waves using methods developed by van Rijn and Young and Verhagen for sand transport and the ECOMSED and Krone procedures for silt and clay. A fetch array of 16 bins was applied to a cell of water and a multi-year dataset of daily wind speed and direction was used to simulate resuspension forces.

The wind directions were mapped into the 16-bins of the fetch array for the computation of the significant wave heights and periods.

It was found that the Young and Verhagen wave model have wave characteristic that were consistent with the USACE wave model in the Shore Protection Manual.

The results of critical shear stress tests at the University of New Orleans allowed the models to consider critical shear stresses that were a function of consolidation time, i.e. the inter-storm period. The model showed that very high resuspension occurred if the inter-storm period approached one day.

Under non-diversion scenarios, the wind shear tends to result in bed erosion that could lead to a net degradation of the bed.

The derived procedures were written into EXCEL and a FORTRAN code that will be integrated into the 2012 Louisiana State Master Plan for the update in 2017.

Using the simulation, the model's sensitivity to wind speed, fetch, depth, and consolidation time can be seen. The effective width of an open water cell that is subject to a diversion also plays an important role in sediment deposition, erosion, and transport through the cell.

The width of the cell was assumed to decrease as the cell filled with sediment. Additional sensitivity studies are recommended to determine more appropriate calibration constants. For more intricate calculations, more species of sediment can be added to the existing four in this study. Different sediment composition percentages could be used to better characterize the makeup of individual cells. Better methods to determine settling velocities can also be applied to better characterize sediments.

This model should be applied to the transfer of sediment to the adjacent marshes. The marsh edge erosion contribution should be included with respect to change in the surface area of the water cell and as a source of sediment in the mass balance.

Hurricane driven resuspension, deposition, and transport should be considered in the model.

The settling velocities of clay can vary throughout each region, or cell, and should be addressed case by case. Salinity plays a large role on whether the clay flocculates or not.

References

Abril, G., Riou, S. A., Etcheber, H., Frankignoulle, M., de Wit, R., Hedges, J. I., & Keil, R. (1999). Organic geochemical perspectives on estuarine processes: Sorption reactions and consequences. *Mar. Chem, 65*, 55-65.

Aller, R. C., Blair, N. E., Xia, Q., & Rude, P. D. (1996). Remineralization rates, recycling, and storage of carbon in amazon shelf sediments. *Cont. Shelf Res., 16*, 753-786.

Allison, M. A., Nittrouer, C. A., & Kineke, G. C. (1995). Season sediment storage on mudflats adjacent to the Amazon River. *Mar. Geol, 125*, 303-328.

Anderson, F. E. (1970). The periodic cycle of particulate matter in a shallow, temperate estuary. *Sediment Petrology, 40*, 1128-1135.

Anderson, F. E. (1972, September). Resuspension of Estuarine Sediments by Small Amplitude Waves. *Sedimentary Petrology, 42, 3*, 602-607.

Bachmann, R. W., Hoyer, M. V., & Canfield, D. E. (2000). Internal heterotrophy following the switch from macrophytes to algae in Lake Apopka, Fla. *Hydrobiologia, 418*, 217-227.

Bacon, M. P. (1994). Pb balance and implications for particle transport on the continental shelf, US Middle Atlantic Bright. *Deep Sea Research, 41*(Part II), 511-535.

Biscaye, P. E. (1988). Fluxes of particles and constituents to the eastern US continental slope and rise: SEEP-I. *Cont. Shelf Research, 8*, 855-904.

Blatt, M. M. (1980, January). Origin of sedimentary rocks (second edn). *Earth Surface Processes and Landforms*, p. 97.

Blom, G., & Aalderink, R. H. (1998). Calibration of three resuspension/sedimentation models. *Water Science Tech, 37*(3), 41-49.

Booth, J. G., Miller, R. L., McKee, B. A., & Leathers, R. A. (2000). Wind induced sediment resuspension in a microtidal estuary. *Continental Shelf Research, 20*(7), 785-806.

Cauwet, G., & Mackenzie, F. T. (1993). Carbon inputs and distribution in estuaries of turbid rivers: the Yangtze and Yellow Rivers. *Mar. Chem, 43*, 235-246.

Chang, G. C., Dickey, T. D., & Williams, A. J. (2001, May). Sediment resuspension over a continental shelf during Hurricanes Edoouard and Hortense. *Journal of Geophysical Research, 106*(C5), 9517-9531.

Deltares. (2013). Ch. 11: Sediment Transport and Morphology. *Delft 3D-Flow-Simulation of multidimensional hydrodynamic flows and transport phenomena, including sediments, 3.15.30059*. (H.-M. User Manual, Ed.)

Demirbilek, Z., & Vincent, C. L. (2002). Multispectral remote sensing of turbidity among Nebraska Sand Hills lakes. *International Journal of Remote Sensing*, 3011-3016. Wave Water Mechanics.

deWit, K. a. (1994). Liquefaction and Erosion of mud due to waves and current. *International Conference on Coastal Engineering, 115*, 278-279. Kobe.

Ekman, V. W. (1905). On the influence of Earth's rotation on ocean currents. *Ark. F. Mat. Astr. Och. Fysik, 2, 11*, 1-52. Stockholm.

Ekman, V. W. (1905). On the influence of Earth's rotation on ocean currents. *Ark. F. Mat. Astr. Och. Fysik, 2, 11*, 1-52. Stockholm.

Erm, A., Alari, V., & Kask, J. (2011, March). Resuspension of sediment in a semi-sheltered bay due to wind waves and fast ferry wakes. *Boreal Environmental Research, 16, Suppl A*, pp. 149-163.

Feng, J. (1992). Laboratory experiments on cohesive soil bed fluidization by water waves. *MS thesis*. Gainsville, Florida: University of Florida.

Foda, M. A., Tzang, S. Y., & Maeno, Y. (1991). Resonant soil liquefaction by water waves. *Proc. of Geo-Coast*. Yokohama, Japan: Port and Harbor Research Institute.

Friedman, C. T., & Sanders, J. E. (1978). Gravity-driven sediment transport on the continental shelf: Implications for equilibrium profiles near river mouths. *Principles of sedimentology*, 792. New York: Wiley.

Galvin, C. J. (1979). Relation Between Immersed Weight and Volume Rates of Longshore Transport. *Coastal Engineering Research Center*. VA: For Belvoir.

Ghose-Hajra, M., McCorquodale, A., Mattson, G., Jerolleman, D., & Filostrat, J. (2014). Effects of Salinity and Particle concentration on Sediment Hydrodynamics and critical Bed-Shear-Stress for Erosion of Fine Grained Sediments used in Wetland Restoration Projects. *Sediment Dynamics from the Summit to the Sea*. New Orleans, Louisiana: University of New Orleans.

Glenn, S. M. (1987). A suspended sediment stratification correction for combined wave and current flows. *Geophys Research, 92*, 8244-8264.

Granboulan, J., Feral, A., & Villerot, M. (1989). Study of sedimentological and rheological properties of fluid mud in the fluvio-estuarine system of the Gironde estuary. *Ocean Shoreline Management, 12*, 23-46.

Grant, W. D. (1979). Combined wave and current interaction with a rough bottom. *Geophys Res., 84*, 1797-1808.

Haralampides, K. (2000). A study of the hydrodynamics and salinity regimes of the Lake Pontchartrain system. *A Dissertation for the Doctor of Philosophy in Engineering and Applied Science in the Department of Civil and Environmental Enginnering*. New Orleans, Louisiana: University of New Orleans.

Haralampides, K. (2000). A Study of the Hydrodynamics and Salinity Regimes of the Lake Pontchartrain System. *Graduate Faculty of UNO*. New Orleans, Louisiana.

Havens, K. E., James, R. T., East, T. L., & Smith, V. H. (2003). "N:P ratios, light limitation, and cyanobacterial dominance in a subtropical lake impacted by nonpoint source nutrient pollution. *Environ. Pollut, 122*, 379-390.

Hedges, J. L., & Keil, R. G. (1999). Organic geochemical perspectives on estuarine processes: Sorption reactions and consequences. *Mar. Chem, 65*, 20951-10957.

HydroQual. (2002). A primer for ECOMSED. *User's Manual, 1.3*. Mahwah, New Jersey: HydroQual Inc.

Inman, C. a. (1992). Field Observations of the Fluid-Granular Boundary Layer Under Near-Breaking Waves. *Journal of Geophysical Research, 97, C6*, 9631-9643.

Kajiura, R. a. (1957, October). On the Damping of Gravity Waves Over a Permeable Sea Bed. *Tran. America, 38, 5*, 662-666. Union.

Kelderman, P., De Rozari, P., Mukhopadhyay, S., & Ang'weya, R. O. (2012). Sediment dynamics in shallow Lake Markermeer, The Netherlands: field/laboratory surveys and first results for a 3-D suspended solids model. *Water Science and Technology, 66*(9), 1984-1990.

Keulegan, G. H. (1951). Wind Tides in Small Closed Channels. *J. Res. National Bureau of Standards, 46*, 358-381.

Kineke, G. C., Sternberg, R. W., Trowbridge, J. H., & Geyer, W. R. (1996). Fluid mud processes on the Amazon continental shelf. *Cont. Shelf Res., 16*, 667-696.

Kirby, R. (1986). Suspended fine cohesive sediment in the Severn Estuary and inner Bristol Channel. *Rep. No. ESTU-STP-4042*, 242. Harwell, U.K.: Dept. of Atomic Energy.

Kirk, M. a. (1969). Relationship Between Grain Size, Size-Sorting, and Foreshore Slope on Mixed Sandy-Shingle Beaches. *N. Z. J. Geol and Geophys, 12*, 128-155.

Kotylar, L. S., Sparks, B. D., & Schutte, R. (1996). Effect of Salt on the Flocculation Behavior of Nano Particles in Oil Sands Fines Railings. *Clays and Clay Minerals, 4, 1*, 121-131.

Kraft, A. B. (1979). Processes and Morphologic Evolution of an Estuarine and Coastal Barrier System. *Barrier Islands*, 149-183. New York: S.P. Leatherman, Academic Press.

Krone, R. B. (1962). Flume studies of the transport of sediment in estuarial shoaling processes. *Hydr. Engrg Lab*. Berkeley, CA: University of California.

Krone, R. B. (1966). Predicted suspended sediment inflows to the San Francisco bay system. *Central Pacific River Basins Comprehensive Water Pollution Project*, 133. Federal Water Pollution Control Admin, Southwest Region.

Krone, R. B. (1966). Predicted suspended sediment inflows to the San Francisco bay system. *Central Pacific River Basins Comprehensive Water Pollution Project*, 133. Federal Water Pollution Control Administration, Southwest Region.

Krone, R. B., & Mehta, A. J. (n.d.). The significance of aggregate properties to transport. *Estuarine cohesive transport Dynamics*. Berlin, Germany: Springer-Verlag.

Krumbein, S. (1963). Stratigraphy and Sedimentation. 660. San Francisco: W.H. Freeman and Company.

Laenen, A., & LeTourneau, A. P. (1996). Upper Klamath Basin Nutrient-Loading Study: Estimate of WInd-Induced Resuspension of Bed Sediment during Periods of Low Lake Elevation. *USGS, Open File Report*. Portland, Oregon.

Lambe, W. (1969). *Soil Mechanics.* Wiley.

Lee, C., Schwab, D. J., & Hawley, N. (2005). Sensitivity analysis of sediment resuspension parameters in coastal area of southern Lake Michigan. *Geophysical Research, 110*.

Leithold, E. L., & Hope, R. S. (1999). Deposition and modification of a flood layer on the northern California shelf: Lessons from and about the fate of terrestrial particulate organic carbon. *Mar. Geol, 154*, 183-195.

Lo, E. L., Bentley, S. J., & Xu, K. (2014). Consolidation properites of mud from Lake Lery and relevance to wetland restoration. *State of the Coast Conference* (p. 246). New Orleans: CPRA.

Lowe, D. R. (1975). Grain flow and grain flow deposits. *J. Sedimentary Petrology, 46*, 188-199.

Lowe, D. R. (1975). Water escape structures in coarse-grained sediments. *Sedimentology, 46*, 157-204.

Lynn, V. D. (1990). Sediment movement along the US east coast continental shelf, I, Estimates of Bottom stress using the Grant-Madsen model and near-bottom wave and current measurements. *Cont. Shelf Research, 10*, 397-428.

McAnally, W. H., Friedrichs, Hamilton, Hayter, Shrestha, Rodriquez, & Teeter. (2007, January). Management of Fluid Mud in Estuaries, Bays, and Lakes. 1: Present State of Understanding on Character and Behavior. *Journal of Hydraulic Engineering, 133, 1*, 9-22. ASCE.

McCorquodale, J. A. (2014). Internal memo on sand balance.

McCorquodale, J. A., Roblin, R., Georgiou, I. Y., & Haralampides, K. (2009). Salinity, Nutrient and Sediment Dynamics in the Pontchartrain Estuary. *Journal Of Coastal Research, Special Volume 54 (1)*.

Mehta, A. J. (1991). Understanding fluid mud in a dynamic environment. *Geo-Mar Lett., 11*, 113-118.

Mehta, A. J., & Li, Y. (1996). Fine-grained sediment transport engineering. *Proc., Coastal and Oceanographic Engineering Dept. Course*. Gainesville, Florida: University of Florida.

Mehta, A. J., & McAnally, W. H. (2002). Fine-grained cohesive sediment transport. *Sedimentation engineering, ASCE manual 54, 2*, Ch. 4. New York: ASCE.

Mehta, A. J., & Partheniades, E. (1975, Dec). An Investigation of the Depositional properties of flocculated fine sediments. *Journal of hydraulic research, 12(4)*, 1037-1057.

Mehta, A. J., Parchure, T. M., Dixit, J. G., & Ariaturai, R. (1982). Re-suspension potential of deposited cohesive sediment beds. *Estuarine Comparisons*, 591-609. New York: Academic Press.

Mehta, A., Lee, S.-C., & Li, Y. (1994). Fluid mud and water waves: a brief review of interactive processes and simple modeling approaches. *WES Contract Rep. No. DRP-94-4*. Vicksburg, Mississippi: U.S. Army Corps of Engineers Waterways Experiment Station.

Miller, M. C., McCave, I. N., & Komar, P. D. (1977). Threshold of sediment motion under unidirectional current. *Sedimentology, 24*, 504-527.

Miller, R. L., McKee, B. A., & D'Sa, E. J. (2005). Monitoring bottom sediment resuspension and suspended sediments in shallow coastal waters. *Remote Sensing of Coastal Aquatic Environments*, 259-276.

Nichos, M. A., & Thompson, G. S. (1978). A field study of fluid mud dredged material: Its physical nature and dispersal. *Rep. No. D-78-40*. Vicksburg, Miss: U.S. Army Engineer Waterways Experiment Station.

Packwood. (1983). The Influence of Beach Porosity on Wave Uprush and Backwash. *Coastal Engineering, 7*, 29-40.

Parker, K. a. (1977). The Physical Characteristics and Environmental Significance Fine Sediment Suspensions in Estuaries. *Estuaries, Geophysics, and the Environment*. Washington D. C.: National Research Council Academy.

Partheniades, E. (1965). Erosion and deposition of cohesive soils. *Journal of the Hydraulic Division, 91*. ASCE.

Peregrine, P. a. (1980). The Propagation of Solitary Waves and Bores over a Porous Bed. *Coastal Engineering, 3*, 221-242.

Pettijohn. (1957). Sedimentary Rocks. *Harper's Geoscience Series*. Harper.

Philips, O. M. (1966). The dynamics of the upper ocean. *Cambridge University Press*.

Roblin, R. (2008). Water quality modeling of freshwater diversions in the Pontchartrain Estuary. *A Thesis Submitted to UNO*. New Orleans, Louisiana: University of New Orleans.

Rossby, C. G., & Montgomery, D. B. (1935). The Layer of Frictional Influence in Wind and Ocean Currents. *Paper Phys Oceanography, 4, 3*, 1-30.

Savage. (1958). Wave Run-Up on Roughened and Permeable Slopes. *Journal of the Waterways and Harbors Division, 84(1640), WW3*. American Society of Civil Engineers.

Schelske, C. L., & Kenney, W. F. (2001). Model erroneously predicts failure for restoration of Lake Apopka, a hypereutrophic, subtropical lake. *Hydrobiologia, 448*, 1-5.

Schubel, J. R. (1968b). Suspended sediment of the northern chesapeake bay. *Chesapeake Bay Institue Tech, 35*, 264.

Shen, I. a. (1994). Mud Transport and Muddy Bottom Deformation Due to Waves. *International Conference on Coastal Engineering, 30*, 106-107. Kobe.

Sheng, Y. P., & Lick, W. (1979). The transport and resuspension of sediments in a shallow lake. *Geophysical Res, 84*, 1809-1826.

Sheng, Y. P., & Lick, W. (1979). The Transport and Resuspension of sediments in a shallow lake. *Geophysical Res, 84*, 1809-1826.

Shields, A. (1936). Anwendung der Ahnlichkeitsmechanik under der Turbulenz Forschung auf die Geschiebebewegung. *Heft 26*. Berlin.

Teeter. (1992). The Viscous Characteristics of Channel-Bottom Muds. *Technical Note*. Vicksburg, Mississippi: U.S. Army Engineer Waterways Experiment Station.

Tolhurst, T. J., Gust, G., & Patterson, D. M. (2002). The influence of an extracellular polymeric substance (EPS) on cohesive sediment stability. *Fine sediment*

dynamics in the marine environment, 425-429. Amersterdam, The Netherlands: J. C. Winterwerp and C. Kranenburg.

Trzaska, J. R., Miller, B., McKee, & Powell, R. (2002). Monitoring Sediment Resuspension events in Shallow Aquatic Systems using remote sensing and numerical models. *Seventh Thematic Conference, Remote Sensing for Marine and Coastal Environments.* Miami, FL.

Twichell, D. C. (1987). Shallow structure, surficial geoplogy, and the processes currently shaping the bank, in Georges Bank. (R. H. Backus, Ed.) *MIT Press*, 31-37.

USACE. (2002, April 30). Coastal Engineering Manual- Part 3. *EM 1110-2-1100*. Louisiana, United States: CECW-EW.

USGS. (2014).

van Rijn, L. C. (1984b). Sediment transport. Part 2: Suspended load transport. *Journal of Hydraulic Engineering, 110, 11*, 1613-1641.

van Rijn, L. C. (1993). Principles of sediment transport in rivers, estuaries, and coastal seas. *Aqua Publications*. Blokzijl, The Netherlands.

van Rijn, L. C. (2007a). Unified View of Sediment Transport by currents and waves. 1: Initiation of Motion, Bed Roughness, and Bed-Load Transport. *Journal of Hydraulic Engineering, 133, 6*, 668-689.

van Rijn, L. C. (2013). Simple General Formulae for Sand Transport in Rivers, Estuaries and Coastal Waters. Retrieved Feb 4, 2014, from www.leovanrijn-sediment.com

Vanoni, V. A. (1975). Sedimentation Engineering. *The Society*. New York.

White, M. C. (1978). Sediment Transport: An Appraisal of Available Methods, Report # IT 119. *Hydraulic Research Station, 2nd*. Wallingfod, U.K.

Young, I. R., & Verhagen, L. A. (1996a). The growth of Fetch Limited Waves in Water of Finite Depth, Part 1: Total Energy and Peak Frequency. *Coastal Engineering, 29*, 47-78.

Zabawa, C. F. (1978). Flocculation in the turbidity maximum of Northern Chesapeake Bay. *Ph. D. Thesis*. Columbia: Univ. of South Carolina.

Zanke, U. C. (2003). On the influence of turbulence on the initiation of sediment motion. *Int. J. Sediment Research, 18, 1*, 1-15.

Zhao, J. a. (1989). Viscous Damping of Solitary Waves over Fluid-Mud Seabeds. *Journal Waterway, Port, Coastal, and Ocean Engineering, 115, 3*, 345-362. American Society of Civil Engineers.

Zhou, S., & McCorquodale, J. A. (1992). Influence of Skirt Radius on Performance of Circular Clarifier with Density Stratification. *Int. Journal for Numberical Methods in Fluids, 14*, 919-934. Ontario, Canada: University of Windsor.

Appendix 1: FORTRAN

A1.1: FORTRAN Main Code

The following code was used to produce the outputs using listed inputs. Two arrays, *wind5000* and *deg5000* contain an average wind speed and direction in degrees acquired from the New Orleans airport that are used in the main program. *Fetchbin* takes each line as a degree, from 0 to 360 and assigns it a bin ranging 1 to 16. *Actualfetch* is an array of 16 lines, each one corresponding with *fetchbin*.

```
!YandVer.f
!
!       AUTHOR: John E. D. Filostrat
!
!               Spring 2014 Master's Degree; For Thesis
!
!*************************************************************
*******
!
!       PROGRAM: YandVer
!
!       PURPOSE: To estimate the resuspension of sediments in a
!                       water column using formulas developed from Delft3D
!                       and Young and Verhagen
!
!*************************************************************
*******
!
!Variables:
!
!Main Inputs:
!g=gravity (m/s2)
!depth=depth of water body (m)
!U10=wind speed (m/s)
!wind5000=array of wind speeds, to be called U10
!F=Fetch (m)
!fetchbin(361)=assigns 361 degrees into bins
!deg(5000)=array of wind directions from 0-360
!actualfetch(16)=16 bins each with an assigned fetch, F, in m
!
!Intermediate Variables:
!Tres=bed response time, 3600s here (s)
!Tcon=time since deposition of sediments (inter-storm period) 6 days here (s)
!tcr=critical shear stress of bed for small sediments, 0.1 here (N/m2)
!Cf=calibration coefficient (.0025 here)
!ac=calibration coefficient (100-100,000)
```

```
!delta=a function of g, depth, and wind speed
!X=a function of g, fetch, and wind speed
!A1,A2,A3,A4=sub functions of Young and Verhagen equations
!sub and sub1=substitute functions of Young and Verhagen to simplify equations
!epsi=dimensionless energy formula
!nu=dimensionless frequency formula
!ka=wind speed coefficient (can range from .023-.032)
!Uw=adjusted windspeed (m/s)
!m=calibration coefficient (equaled to 1 here)
!n=calibration coefficient (equaled to 1.5 here)
!L0=wavelength, deepwater waves (m)
!L1=first wavelength correction (m)
!Me=intermediate variable
!Utide=velocity due to tide (max=0.1, moving as spring tide here) (m/s)
!Uinflo=compartment velocity near bed (m/s)
!D50=median diameter of grain .00018 here(m)
!D90=90th percentile particle diameter of grain 0.00030 here(m)
!wsCF=settling velocity of clay floc (m/s)
!wsil=settling velocity of silt (m/s)
!wsCP=settling velocity of clay particulate (m/s)
!CFmas=mass of clay floc according to time step (g)
!silmas=mass of silt according to time step (g)
!CPmas=mass of clay particulate according to time step (g)
!
!Main Outputs:
!Energy=wave Energy
!FreqPK=wave peak frequency (s^-1)
!Period=wave Period (s)
!Hrms=root mean squared wave height (m)
!sight=significant wave height (m)
!L2=final wavelength (m)
!Uorb=orbital velocity (m/s)
!Eres=fine sediment resuspension term (g/m2/s)
!qs=rate of potential sand resuspension (kg/m/s)
!CFcon=clay floc concentration (g/m3)
!silcon=silt concentration (g/m3)
!CPcon=clay particulate concentration (g/m3)
!
!**********************************************************************
*******

      program YandVer
      real::g
      real::sub1
      real::delta
      real::X
```

```
real::A1
real::A2
real::B1
real::B2
real::sub
real::epsi
real::nu
real::Energy
real::freqPK
real::Period
real::Hrms
real::sight
real::ka
real::m
real::n
real::L0
real::L1
real::L2
real::Me
real::Utide

real::wsil
real::silmas
real::silcon

real::wsCF
real::CFmas
real::CFcon

real::wsCP
real::CPmas
real::CPcon

real::fetchbin(361)
real::deg5000(5000)
real::actualfetch(16)
real::wind5000(5000)

open(unit=1,file='fetchbin.prn')
open(unit=2,file='output1.txt')
open(unit=3,file='deg5000.prn')
open(unit=4,file='actualfetch.prn')
open(unit=5,file='wind5000.prn')
open(unit=6,file='output2.txt')

!Begin computing Period and Significant Waveheight using Young and Verhagen
```

```
DO I=1,5000
read(5,*) wind5000(i)
wind5000(i)=max(.2,wind5000(i))
enddo

DO I=1,5000
read(3,*)deg5000(i)
deg5000(i)=deg5000(i)+1
end do

DO I=1,361
read(1,*) fetchbin(i)
enddo

DO I=1,16
read(4,*)actualfetch(i)
enddo

do I=1,5000

U10=wind5000(i)
F=(ifix(actualfetch(ifix(fetchbin(ifix(deg5000(i)))))))

g=9.81
row=1000.
gamma=9810.
pi=3.14159265359

depth=3.4
U10=U10
F=F

delta=(g*depth)/(U10*U10)
X=(g*F)/(U10*U10)
A1=.493*delta**.75
A2=.331*delta**1.01
B1=.00313*X**.57
B2=.0005215*X**.73
 sub=B1/(tanh(A1))
epsi=.00364*(tanh(A1)*tanh(sub))**1.74
nu=.133*(tanh(A2)*tanh((B2)/(tanh(A2))))**-.37
Energy=(epsi*U10**4)/(g*g)
freqPK=nu*g/U10
Period=freqPK**-1

SigHt=3.8*(Energy**.5)
```

```
!Begin Computing resuspension, Eres
        ac=35000.
        Tres=3600.
        tcon=518400.
        tcr=.1
        m=1.
        n=3.
        Cf=.0025
        ka=.0275
        Uw=U10*ka
        L0=(g*Period*period)/(2*pi)
        L1=L0*tanh((2.*pi*depth)/L0)
        L2=L1*tanh((2.*pi*depth)/L1)
        Uorb=(g*SigHt*Period)/(2.*L2*cosh((2.*pi*depth)/L2))
        Utide=0.1*sin(i*2*3.14/14.)
        Uinflo=.1
        Ubed=Utide+Uinflo+Uw+Uorb
        taubed=Cf*row*Ubed*Ubed
        Eres=(ac/(Tres*Tcon**m))*(taubed/tcr-1.)**n   !Resuspension of silts and clays
!Begin computing resuspension using van Rijn
        D50=.00018
        D90=.00030
        Ucritw=.24*((2.65-1)*g)**.66*D50**.33*Period**.33
        Ucritc=.19*D50**.1*log10((12.*depth)/(3.*D90))
        Ucrit=((Uinflo)/(Uinflo+Uorb))*Ucritc+((Uinflo)/(Uinflo+Uorb)-1.)*Uc
    &ritw
     ygam=.4
        Ue=uinflo+ygam*Uorb
        Me=(Ue-Ucrit)/(sqrt(g*D50*(2.65-1.)))
        alphas=.01
        Dstar=D50*((g*(2.65-1.))/(.000001*.000001))**(1./3.)
        qs=alphas*2650.*uinflo*D50*Me**2.4*Dstar**-.6 !Resuspension of sand

!Begin computing concentration in 1m x 1m water column
        wsCF=.020334
        CFmas=max(.0001,CFmas+(.7*Eres-wsCF*(CFmas/depth))*(86400.))
        CFcon=CFmas/depth
        wsil=.00097157
        silmas=max(.0001,silmas+(.2*Eres-wsil*(silmas/depth))*(86400.))
        silcon=silmas/depth
        wsCP=.000035816
        CPmas=max(.0001,CPmas+(.1*Eres-wsCP*(CPmas/depth))*(86400.))
        CPcon=CPmas/depth

!Use write command to pick what outputs to be displayed
```

```
    write(2,*)i,CFcon,silcon,CPcon
    enddo
end
```

Vita

John Edgar Dimitri Filostrat (called Jed by friends and family) was born on May 22nd, 1988 in Baton Rouge, Louisiana. After grammar school in Metairie at St. Ann Elementary, he continued the tradition of his father and graduated from Brother Martin High School in 2006. Inspired by his favorite childhood movie, *Jurassic Park,* he graduated from Louisiana State University in May of 2012 with a bachelor's degree in Biological Engineering. After completing one year of engineering master's coursework at UNO and an internship with NASA's Michoud Assembly Facility in New Orleans east, he scored a research assistantship with Dr. Alex McCorquodale, studying the Gulf Coast. In May of 2014 he is anticipated to fulfill his requirements for a master's degree in Civil and Environmental Engineering at the University of New Orleans.